

**WP2 & WP3 – EXPERIMENTAL AND NUMERICAL
INVESTIGATION OF CLASS 4 BEAMS, SIMPLE
DESIGN RULES AND APPLICATION EXAMPLES**

Table of contents

1	Fire tests.....	3
1.1	Beams subjected to simple bending.....	3
1.1.1	Set-up of experimental tests.....	4
1.1.2	Development of numerical models and correlation with experimental results.....	14
1.2	Beams subjected to lateral torsional buckling.....	20
1.2.1	Set-up of experimental tests.....	22
1.2.2	Development of numerical models and correlation with experimental results.....	31
2	Description of the parametric studies and comparisons with simple design rules.....	43
2.1	Numerical parametric study for class 4 cross-sections subjected to simple bending.....	43
2.1.1	Presentation of chosen parameters.....	43
2.1.2	Detailed list of results of the parametric study and comparisons with simple design rules	47
2.2	Numerical parametric study for class 4 beams subjected to lateral torsional buckling	66
2.2.1	Presentation of chosen parameters.....	66
2.2.2	Detailed results of the parametric study and comparisons with current EC3 design rules .	70
3	Application examples	82
3.1	Cross-sectional resistance of a beam subjected to pure bending following new design rule	82
3.1.1	Classification of the cross-section	82
3.1.2	Evaluation of the effective section modulus (major axis).....	84
3.1.3	Calculation of the cross-sectional resistance	88
3.2	Lateral torsional buckling of a beam subjected to bending	89
3.2.1	Evaluation of the non-dimensional slenderness.....	89
3.2.2	Calculation of the reduction factor for LTB	89
3.2.3	Evaluation of the lateral torsional buckling resistance	90
4	List of references	91

1 Fire tests

The fire tests concern simply supported steel beams. Four beams subjected to simple bending and four beams subjected to lateral torsional buckling are tested. The eight beams are constituted of different steel plates which are described in the next part. Then the test set-up and records of the experiments are explained in the following parts.

1.1 Beams subjected to simple bending

The focus of the project is to carry out experiments with I shape beams with slender class 4 cross-sections. The load capacity of these sections is not directly affected by the yield strength of the steel, but by deformations and buckling of the compressed areas of the cross-section, i.e. the upper wall and the upper flange. To reach this way of deformation of the samples during the planned experiments, it is necessary to choose the appropriate cross-section shape, thickness, beam load form and intensity of the load. Four tests with two types of cross-section loaded by four-point bending are carried out (see Figure 1). Beams incurred a variable load and they are heated with a constant temperature by an electric resistance mat until exhaustion of the load capacity. Each section is heated to a temperature of 450 °C and 650 °C:

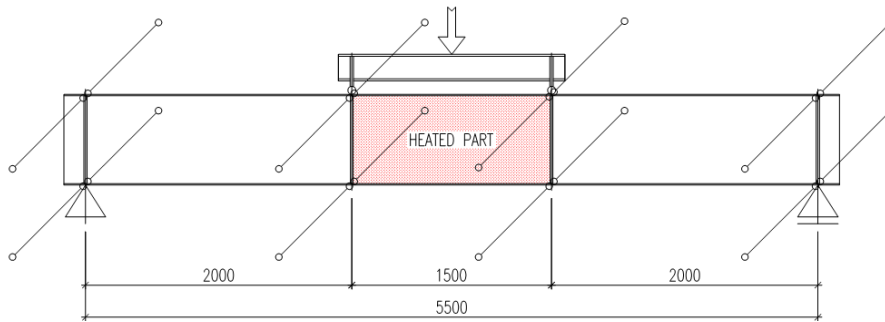


Figure 1: Static scheme of the experiment

For these experiments, two types of welded cross-sections have been chosen. They represent cross-sections of the 4th class and they are sufficiently burdened by the problematic of local stability of the walls:

- The cross-section A (IS 680/250/12/4) has a vertical strut in the class 4 ($\bar{\lambda}_p = 1.439$) and the flanges are in class 3 ($\bar{\lambda}_p = 0.661$)
- The cross-section B (IS 846/300/8/5) has a vertical strut in the class 4 ($\bar{\lambda}_p = 1.454$) and the flanges are in class 4 ($\bar{\lambda}_p = 1.182$)

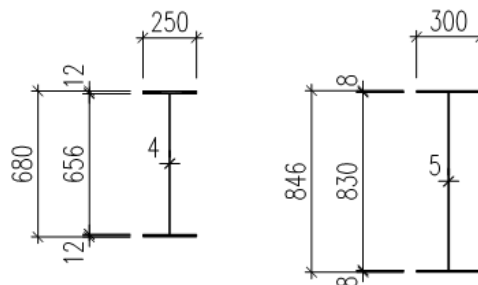


Figure 2: Cross-sections designed for the experiment – *left*) Cross-section A, *right*) Cross-section B

There were four beams produced for the experiments, with different lengths of the heated middle part. Due to thermal expansion and to maintain the static scheme (see Figure 1), the middle heated part was shortened depending on the operating temperature. When heated to a prescribed temperature, the middle

part of the beam will have a length of approximately 1 500 mm. The A1 beam (cross-section 680/250/12/4 IS) and B1 beam (cross-section 846/300/8/5 IS) for temperature 450 °C were made with the middle part length of 1 492 mm. The beams A2 (cross-section 680/250/12/4 IS) and B2 (cross-section 846/300/8/5 IS) designated for a temperature of 650 °C were made with the middle part length of 1 488 mm. For the manufacturers of steel beams (LINDAB - Luxemburg) production documentation in the required range was developed.

1.1.1 Set-up of experimental tests

Material tests were performed at normal temperature in accordance with EN 10002-1. Each beam was made of different steel plates welded together. There were exactly six different steels which have all been accurately tested in terms of stress-strain relationship at room temperature and at high temperature. Only room temperature tests results are described in this report. These steels are named from steel S1 to steel S6. The following figure shows which steel composed the four tested beams:

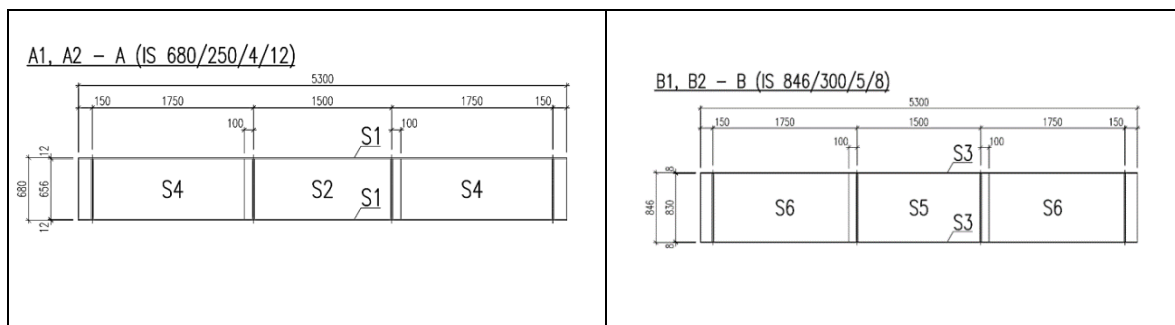


Figure 3: A1, A2 and B1, B2 schemes of layout samples

The following Figure 4 is an illustration of the sample of S1 steel used for material testing at room temperature and also illustrates S2 to S6 steel samples:

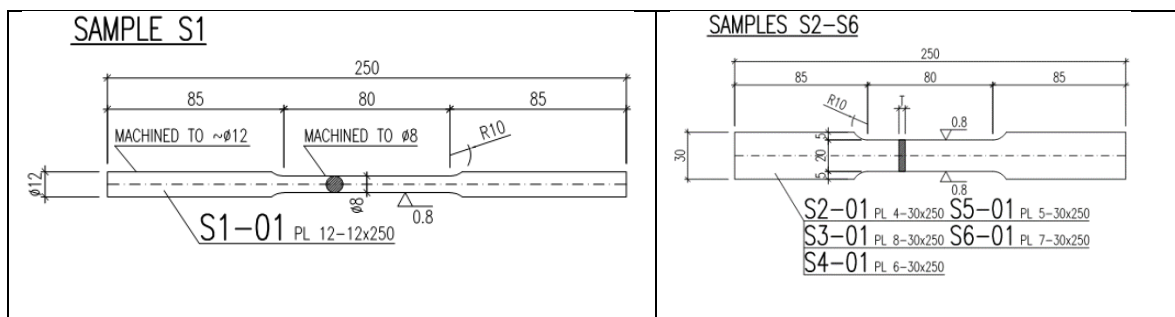


Figure 4: a) Sample test S1, b) Sample test S2 to S6

Figure 5 a) and b) respectively illustrate the samples for high temperature material testing used for S1 steel and S2 to S6 steel:

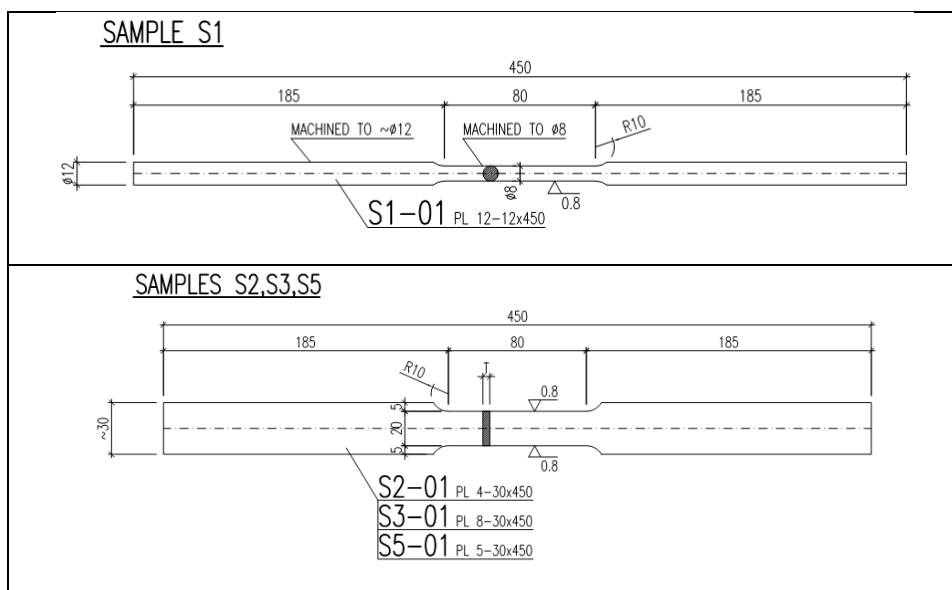


Figure 5: a) Sample test S1, b) Sample test S2 to S6

The material tests let have the information about yield strength and elastic modulus for each steel plate at room temperature. These results are summarized in the following table:

Sample	(MPa)	S1	S2	S3	S4	S5	S6
Upper Yield strength	R_{eH}	430	394	341	376	382	435
Bottom yield strength	R_{eL}	424	392	338	361	378	408
Elastic modulus	E	178399	176897	194375	199200	209988	208900

Table 1: Material properties of the six studied steels at 20 °C

For the smooth running of the experiment and to take into account all the boundary conditions according to the static scheme (Figure 1), steel tools were designed and manufactured. The scheme of the tools layout, including the location of the test beam is shown in the following figure:

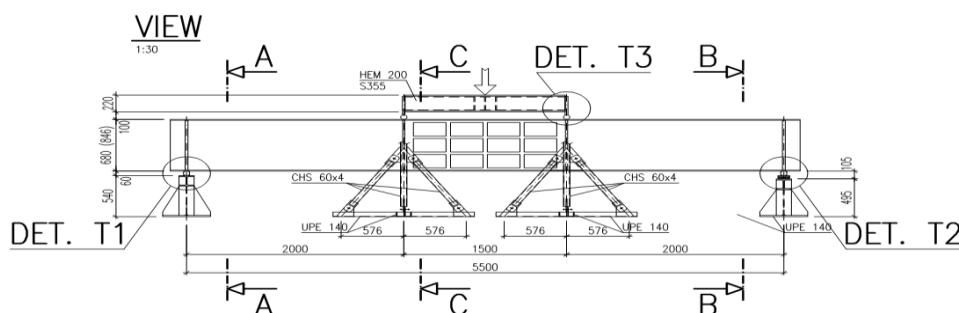


Figure 6: Scheme of the tools layout

The following diagrams show the stress-strain relationship for steels S1, S2 and S3 at room temperature:

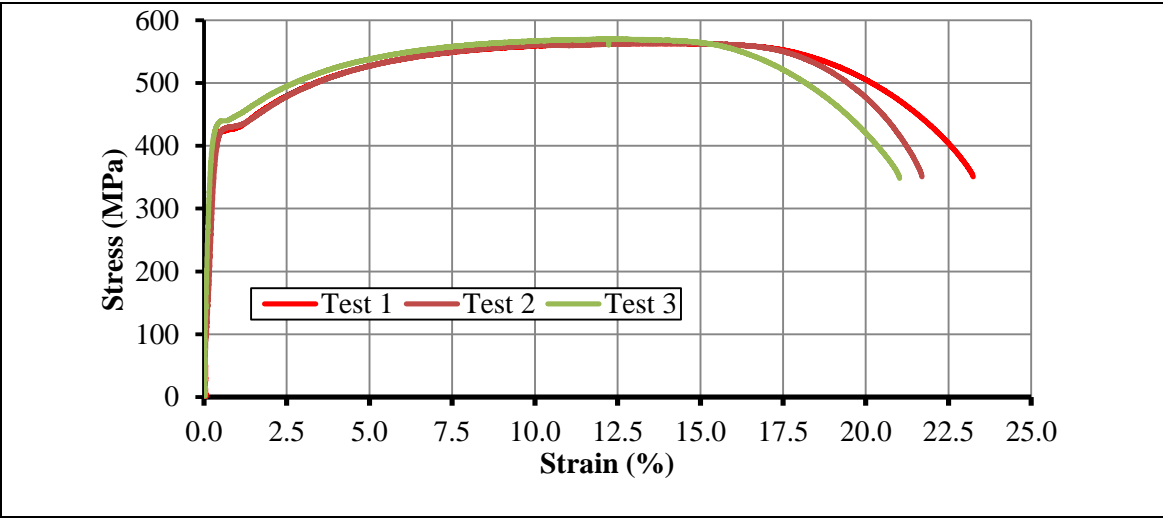


Figure 7: Stress-strain relationship for S1 steel

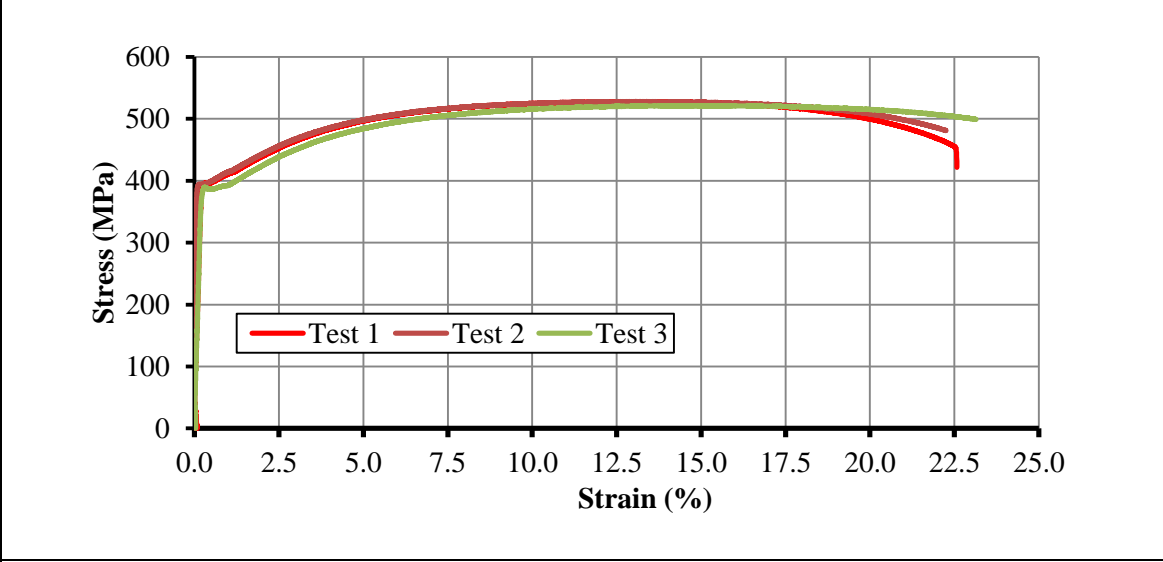


Figure 8: Stress-strain relationship for S2 steel

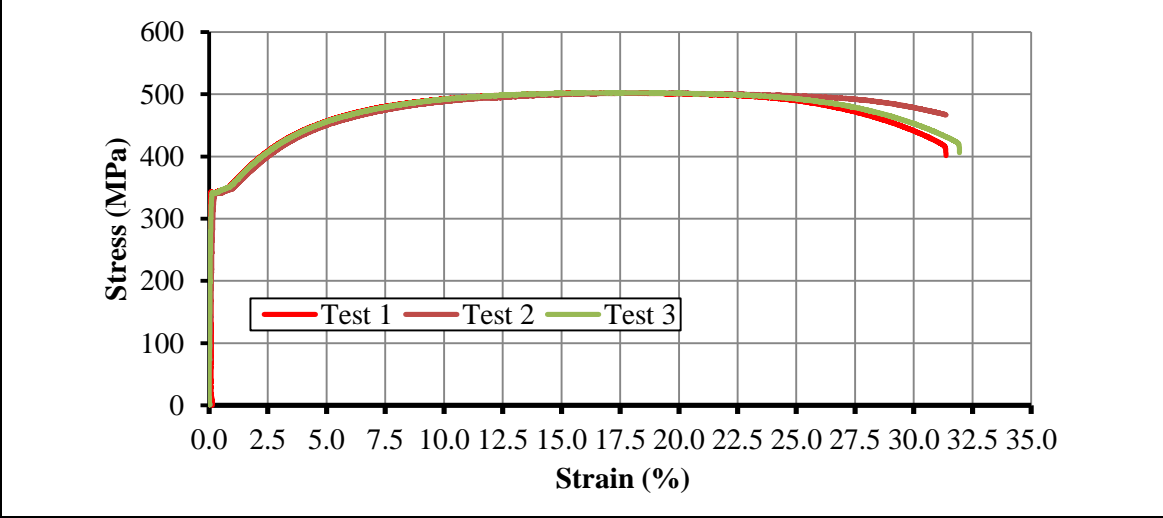


Figure 9: Stress-strain relationship for S3 steel

The principle of the tools for ensuring the torsional stability at the support points and at the point of the load input is shown in cross sectional views A-A, B-B and C-C (see Figure 10):

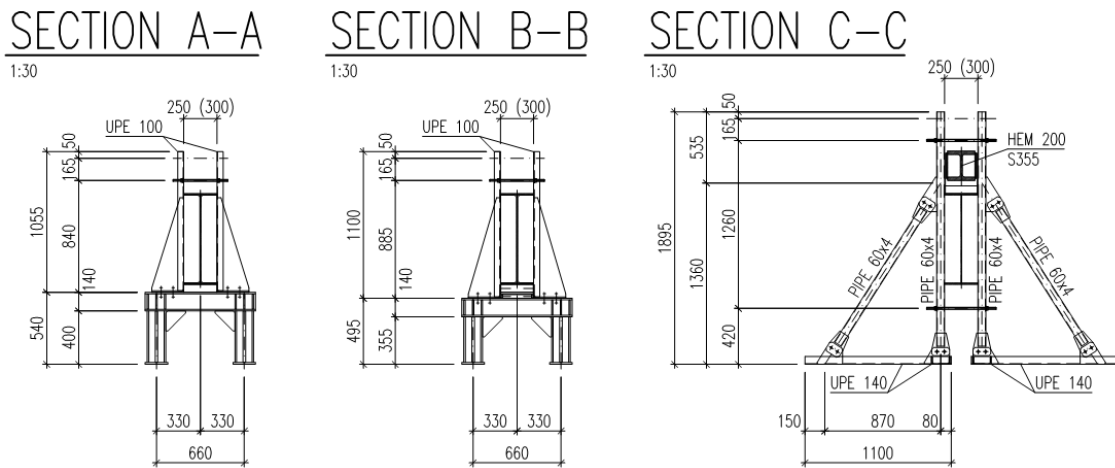


Figure 10: A-A- at the point of the firm joint support, B-B- at the point of the sliding joint support, C-C- at the point of the load input

According to the previous scheme, the tested beam is set on the fixed articulated support from the left side (T1 detail – see Figure 11) and on the sliding joint support (T2 detail – see Figure 12) from the right side. The sliding articulated support is designed as a rolling bearing:



Figure 11: fixed articulation support: left) construction detail, right) side view of the finished support



Figure 12: sliding articulation support: left) construction detail, right) side view of the finished support

Another important parameter of these specimens is the initial imperfections which are measured using two different methods. The first one is a laser scanning of the shape of the beams. This method ensures a good accuracy of the amplitudes, which easily meets the requirements of the numerical simulations. It provides both the global curvature of the beam and the local imperfections of the flanges and of the web in the compressed part. The second method is a manual measurement of these imperfections to check the accuracy of the previous laser scanning. It is found that the results of above two methods are very

close. The following Figure 14 shows the amplitude of imperfections in different points of the compressive part of the web of the beam A1 tested at 450 °C and the location of these measurement points is illustrated in the following figure:

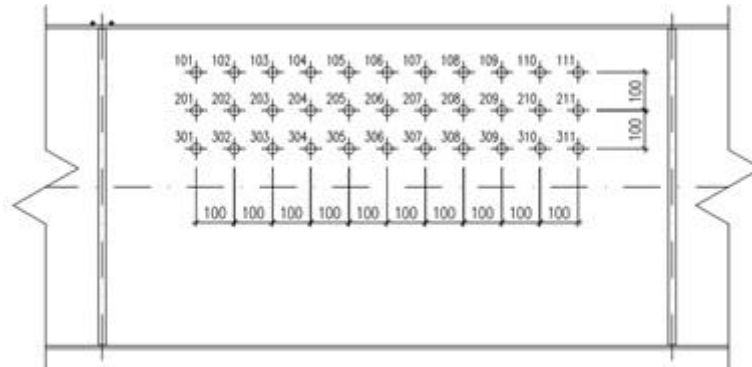


Figure 13: Localization of measurement points on web

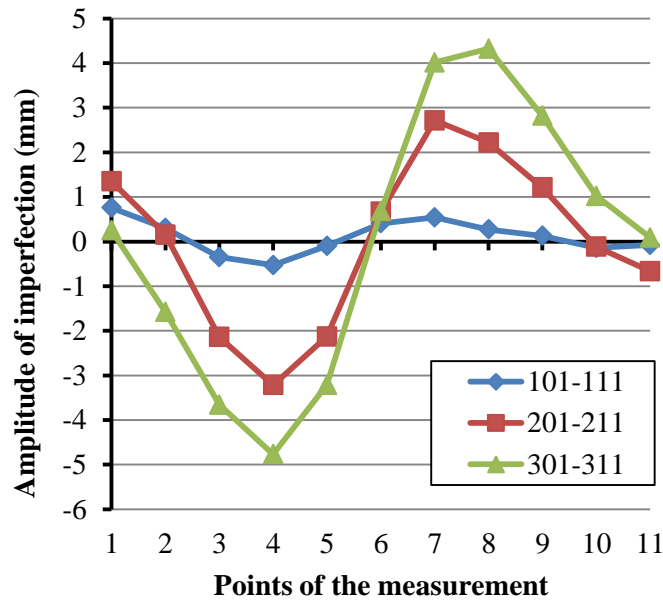


Figure 14: Amplitude of imperfections for web of beam A1 (cross-section IS 680/250/12/4)

The following figure shows the measured amplitude of imperfections in different points of the compressive flange of beam B. The location of these points of measurement is given in the same figure:

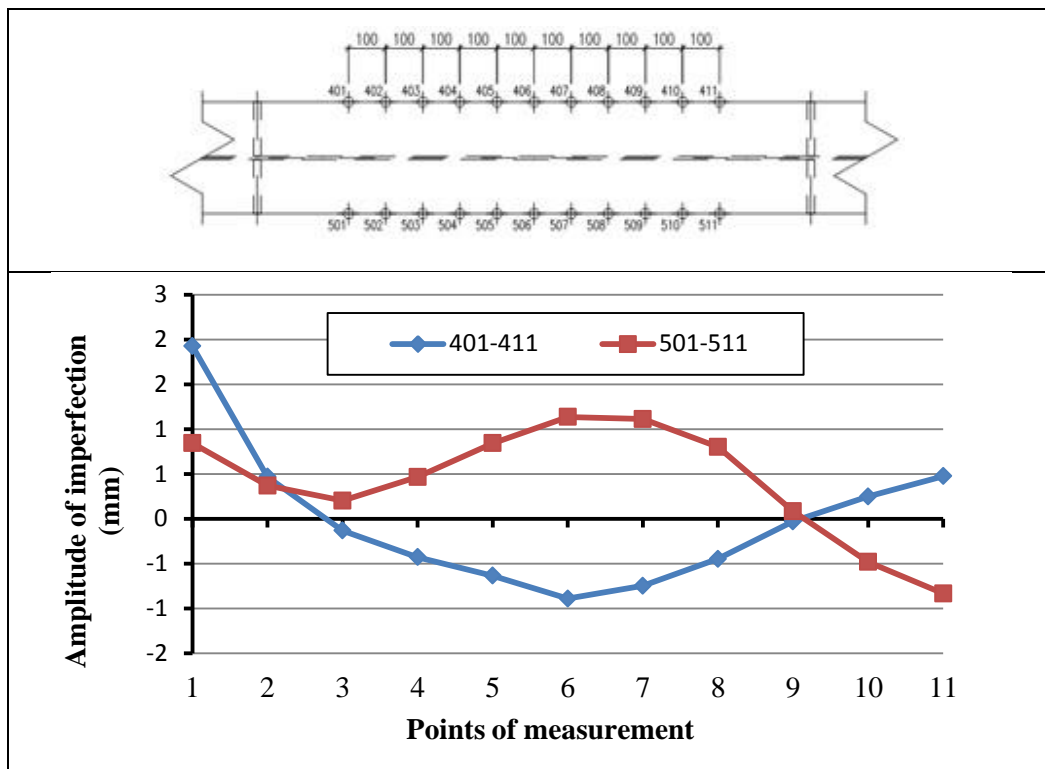


Figure 15: Measured imperfections of compressive flange of beam B

According to the measured results, the maximum amplitudes of the initial imperfections are given in following table:

Beam	Cross-section	Web (mm)	Flange (mm)
A1	680/4+250/12	4.765	0.400
A2		1.340	1.975
B1	846/5+300/8	2.364	1.924
B2		1.595	0.685

Table 2: Initial imperfections of tested beams

The distribution of ceramic heating pads, thermocouples, strain gauges and potentiometers was carried out according to the scheme (see Figure 16):

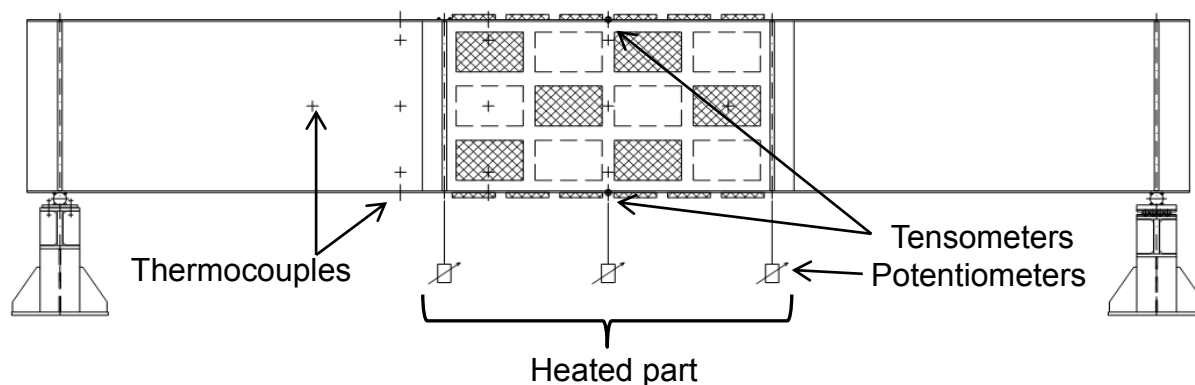


Figure 16: Scheme of heating pads and sensing devices distribution

Heating mats 195×305 mm are placed on the strut and the flange of the test beam according to the diagram (see Figure 17). Alternately distributed mats were fastened to the strut using a steel wire grate, which was then fastened by a paper tape. The mats were placed on the flanges only from the outside. The mats on the top flange were loosely laid, and the mats on the bottom flange were fastened by bent wires. The distributed heating mats are seen on these photographs (Figure 17). The heating mats are able to reach a maximum temperature of $1\ 200\ ^\circ\text{C}$ at a heating rate of $10\ ^\circ\text{C}/\text{min}$:



Figure 17: Photo of the distributed heating mats: *left) on the web, right) on the flange*

To record the temperature in different parts of the test beam, 17 pieces of MC10 (type J) thermocouples with the diameter of 2 mm and the length of $N = 1\ 000$ mm (see Figure 18) were used. The placement of thermocouples was performed according to the scheme (see Figure 16).

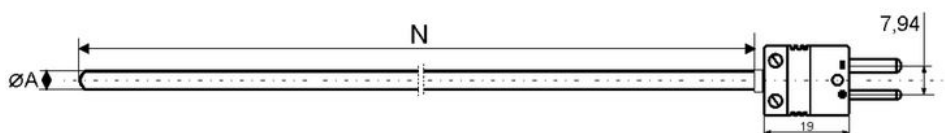


Figure 18: Thermocouple scheme

To determine the position of the neutral axis, two resistive tensiometers for high temperatures were used. The tensiometers were placed on the axis of the upper and lower flange in the centre of the heated section. The surface was treated prior to bonding and bonding of the tensiometers themselves was carried out according to manufacturers recommended. The vertical deformation (deflection) of the test beam was measured at three points (see Figure 16). The deflection was measured at the point of the load input and in the middle of the heated part of the beam.

The entire heated middle part of the test beam was wrapped by ROCKWOOL Airrock HD thermal insulation boards. The space between the flanges was filled by the insulation boards and strips of thermal insulation were then placed on both flanges. Thus insulated beam was then tied by a wire. The insulation procedure of the test beam is shown in Figure 19. Finally, the whole middle part was wrapped by SIBRAL insulating strip.

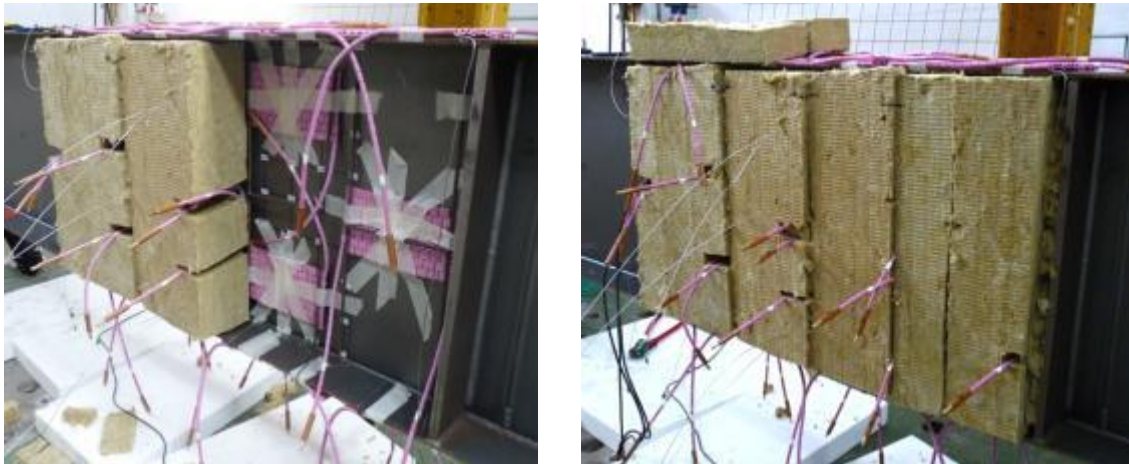


Figure 19: Insulation procedure of the test beam

After connecting all sensing devices (thermocouples, tensiometers, potentiometers, dynamometer in a hydraulic press) to the central measuring equipment and after connection the heating mats to the transformer, the beam was ready for the experiment:

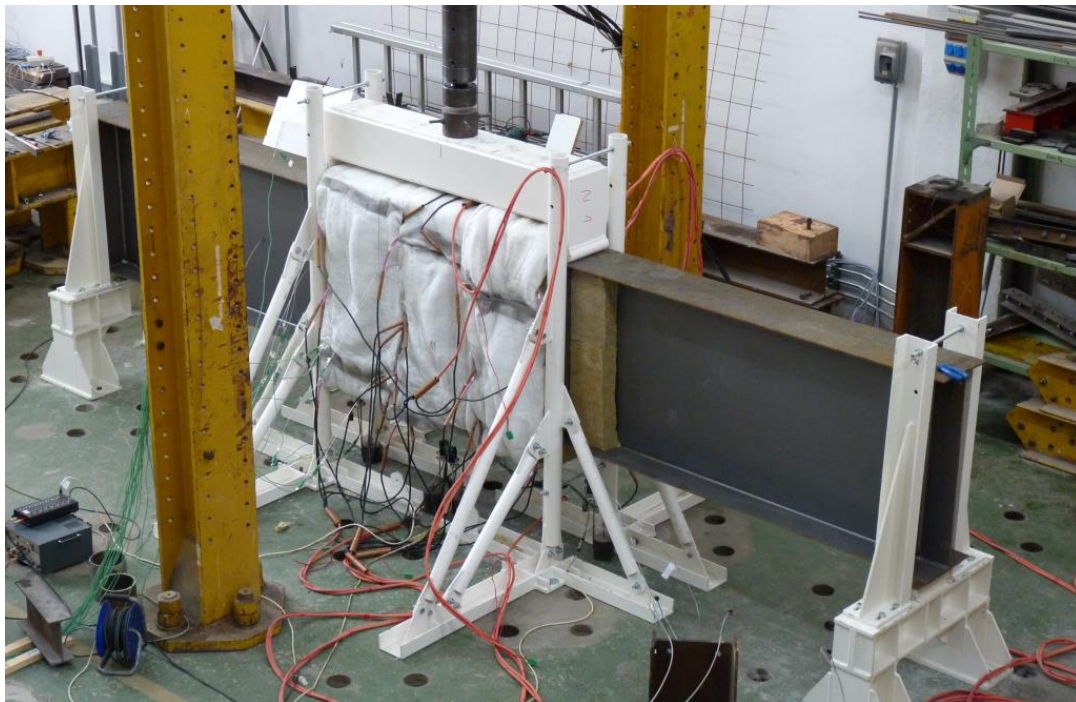


Figure 20: Prepared test beam prior to the experiment

The heating rate was controlled manually on the basis of the data provided by thermocouples. The two predicted heating levels of 450 °C and 650 °C were reached respectively after 45 minutes and 65 minutes. It is necessary to point out that the real heating was not fully uniform in the beams but the difference is very small. The following figure shows the temperature evolution during loading phase of beam A (target temperature level: 650 °C).

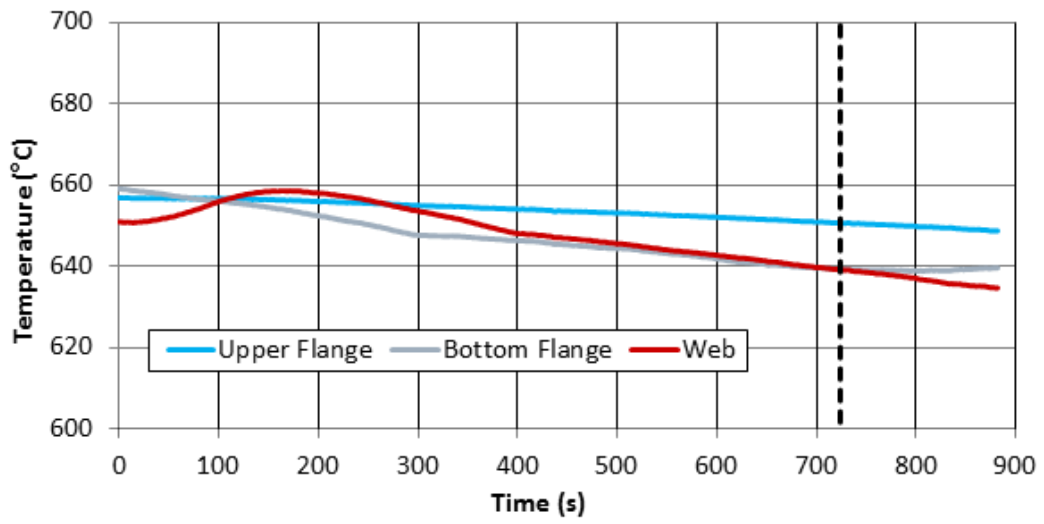


Figure 21 : Temperature evolution as a function of time during loading phase of beam A

The recorded load-deflection curves of all above beam tests are shown together in Figure 22 and the failure modes of these beams are shown later on. The following observations can be formulated from experimental results:

- Beam A (cross-section: 680/4+250/12) reaches the maximum load-bearing capacity under more important deflection than Beam B (cross-section: 846/5+300/8) due to the fact that Beam A with its smaller cross-section size is much less stiff than Beam B;
- After reaching the maximum strength, the load-bearing capacity decreases slightly for all these beams without any sharp strength fall;
- All the beams failed with local buckling occurred in both upper flange and web. However, the local buckling of Beam A is less developed than Beam B, certainly due to the fact that the flanges of Beam B are much slender than Beam A;
- The temperature level of the beam seems to have small influence on the amplitude of its local buckling but the maximum load-bearing capacity of the beams is reached at higher deflection if the heating of the beam is more important.

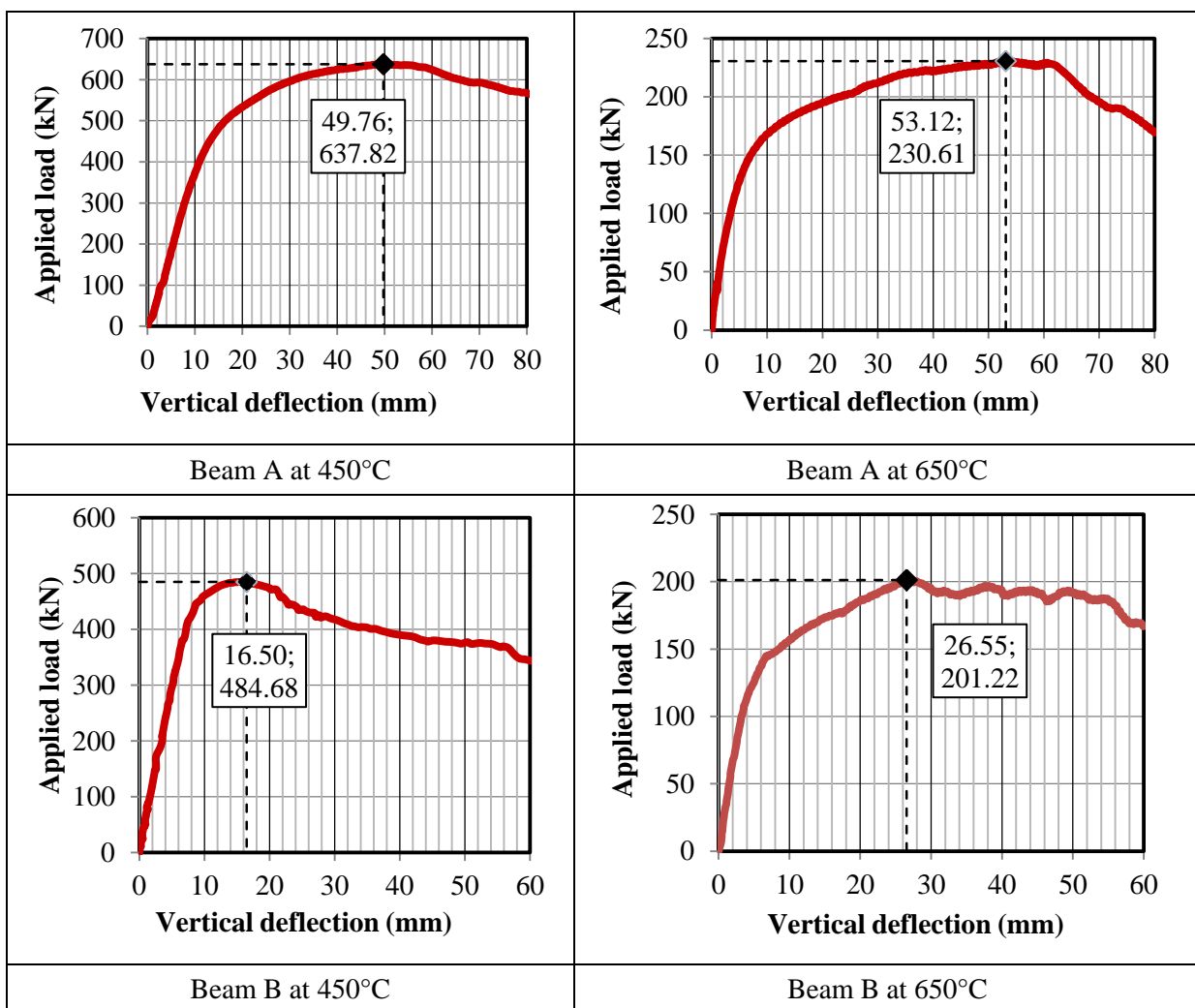


Figure 22 : Recorded load-deflection curves of four tested beams

1.1.2 Development of numerical models and correlation with experimental results

The four tests with class 4 cross-section steel beams subjected to elevated temperatures are conducted with specific test set-up which is quite far from real construction configuration. In fact, the main purpose of these tests is to establish an experimental database from which the relevant numerical models can be created and used thereafter to investigate the fire behaviour of I or H shape class 4 cross-section steel beams under simple bending in extended manner. In the scope of this project, the numerical models are developed with help of different finite element computer codes, in particular ABAQUS and ANSYS. In order to deal with the local buckling in case of class 4 cross-section members, these numerical models are specifically based on shell elements capable of taking account of both material and geometric nonlinearities. However, two different types of shell elements are used under the computer codes ABAQUS and ANSYS which are respectively quadrilateral four nodes linear shell element and quadrilateral eight nodes (with mid-side nodes) quadratic shell element. The advantage of eight nodes quadratic shell element under the computer code ANSYS is both its efficiency (larger mesh size and higher accuracy) and numerical robustness (easy convergence under instability behaviour). The other parameters of these numerical models to simulate the tests at elevated temperatures are:

- five integration points through the thickness of all shell elements
- density of mesh used in each model remains constant which leads to about 100 000 degrees of freedom (see Figure 23)
- initial imperfections of the numerical model for tested beam based on eigenvalue analysis with the amplitude measured from the test specimens (see Figure 24)
- average temperature values measured in each part of the beam (flanges and web) affected to numerical model (Figure 24)
- thermal expansion of steel in accordance to EN 1993-1-2
- stress-strain relationships of steel with its yield stress at room temperature taken from the tensile tests according to EN 1993-1-2

A typical example of the numerical model created to simulate the tests at elevated temperatures is shown in Figure 23, in which the applied boundary and loading conditions are also illustrated. In Figure 24, the initial imperfection and the temperature field used for the same numerical model are provided.

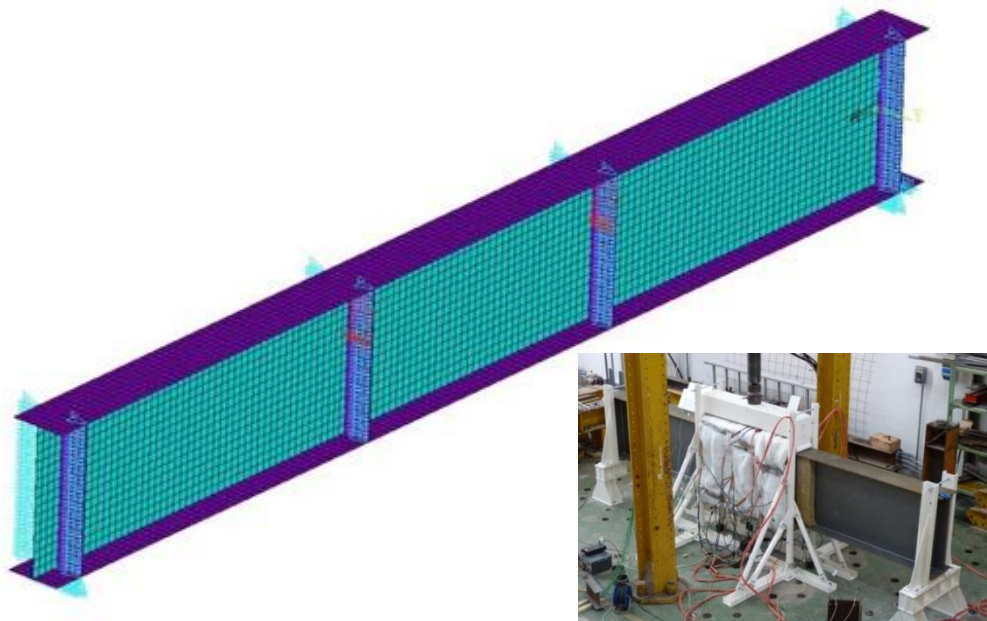


Figure 23 : Boundary and loading conditions applied to the numerical model

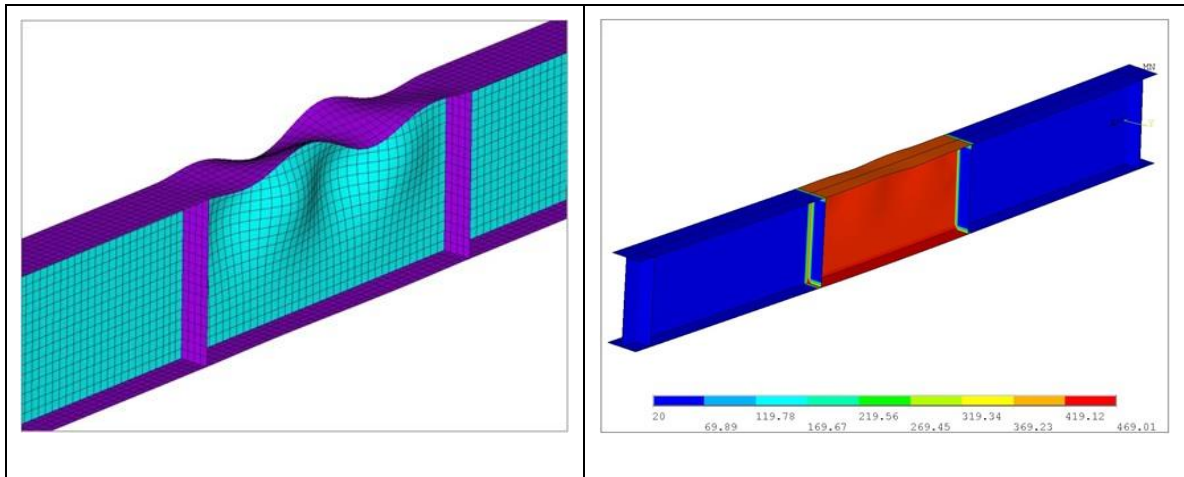


Figure 24 : Shape of implemented initial imperfections and temperature field of the beam in the numerical model

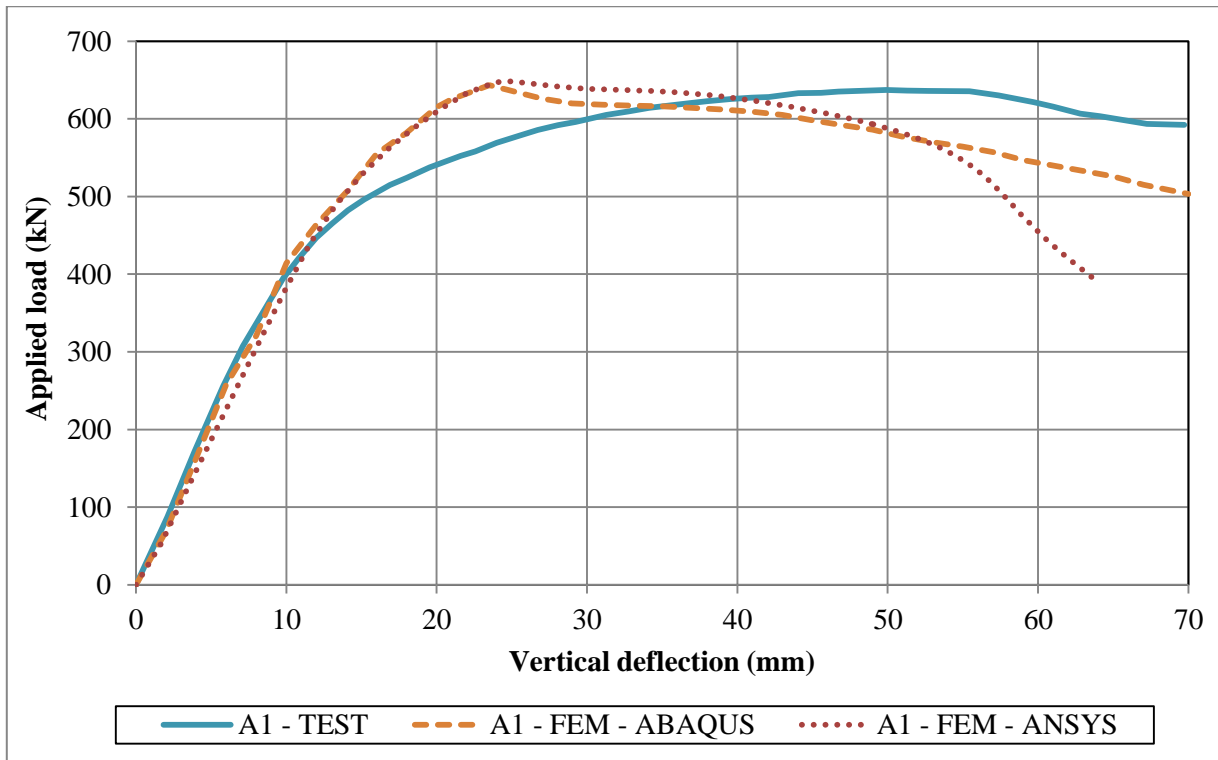
For the numerical models in ABAQUS and ANSYS the loads were applied through displacement-controlled method in order to follow the discharging state after buckling. The results from numerical simulations were compared systematically to the experimental ones recorded during the tests (see Figure 25). From these comparisons, one can find that:

- the numerical results from the two computer codes are close to each other up to the ultimate load-bearing capacity of the beams
- the load-bearing capacity predicted by the numerical models is very similar to that obtained by means of the tests
- the numerical initial stiffness of Beam A is slightly lower than the experimental stiffness but the real initial stiffness of Beam B is accurately simulated in the numerical models

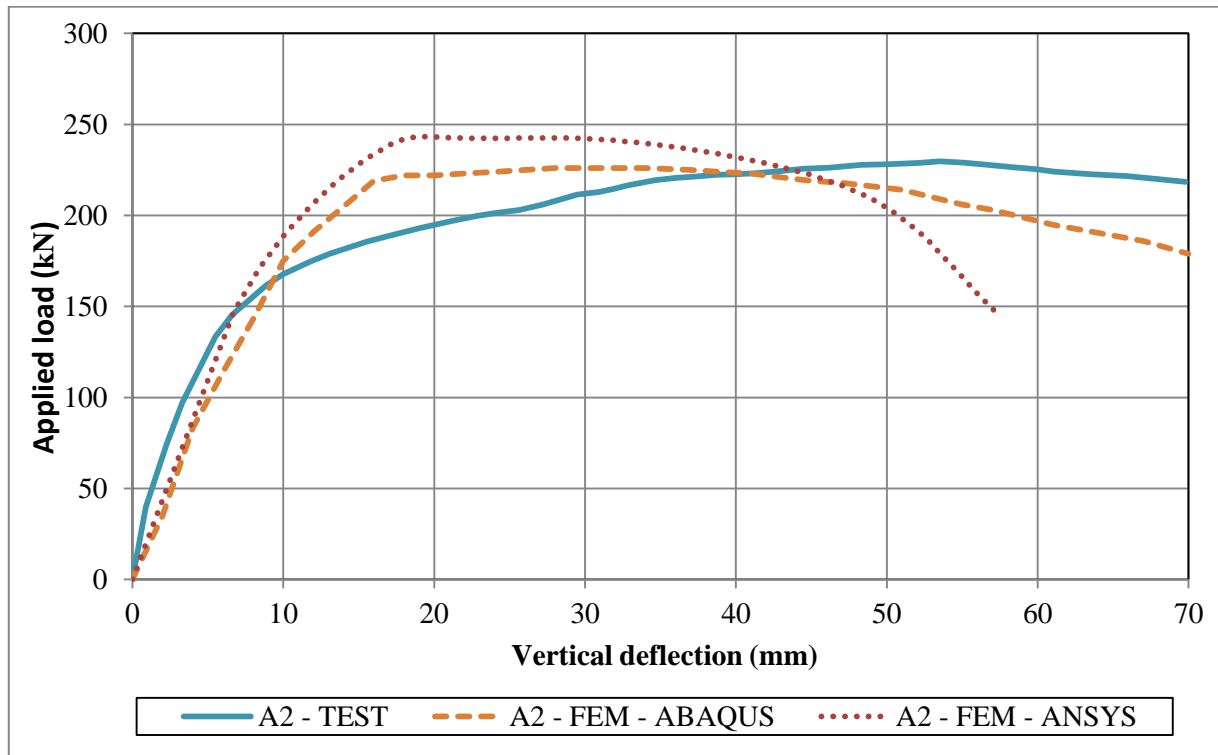
The difference between the numerical simulations and tests may be due to the fact that:

- the imperfections are not exactly the same though their amplitude remains the same
- the temperature fields are also slightly different
- initial residual stresses are not taken into account in the model

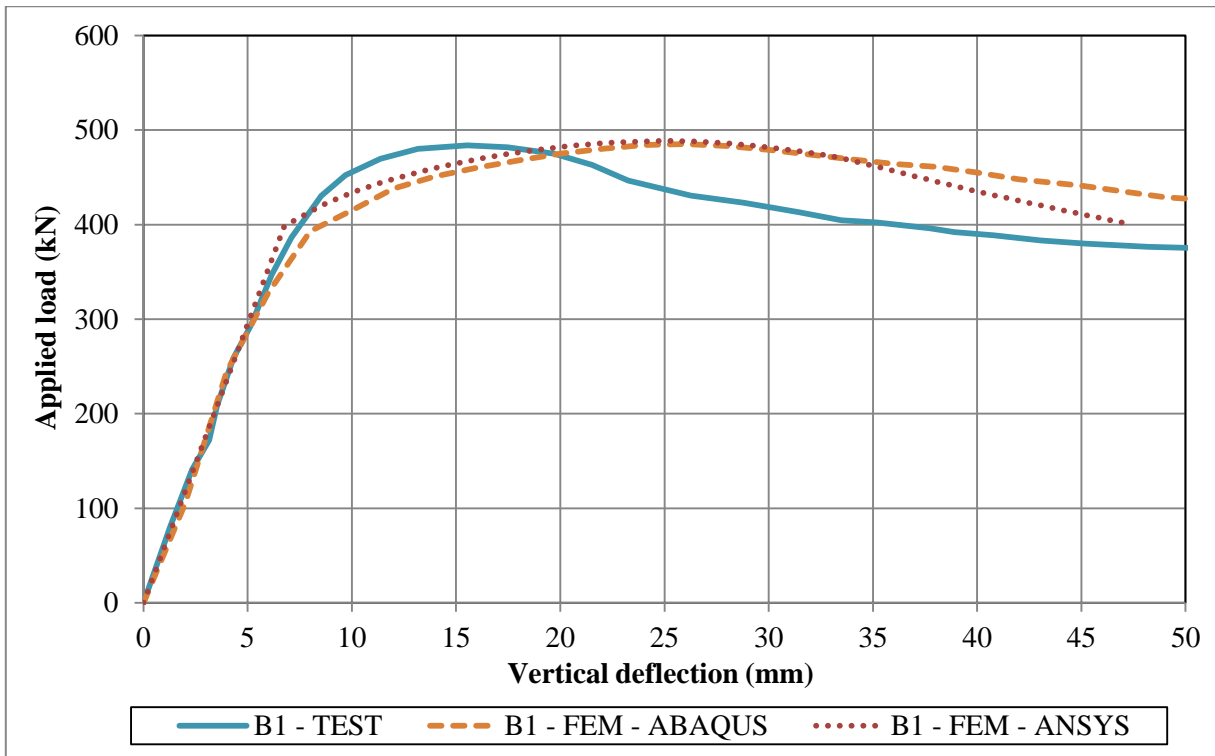
However, with respect to the key parameter of tested beams, that is the ultimate load-bearing capacity, the numerical models are accurate enough because the scatter between the numerical and experimental results is less than 6% and can be considered as satisfactory (see Table 3).



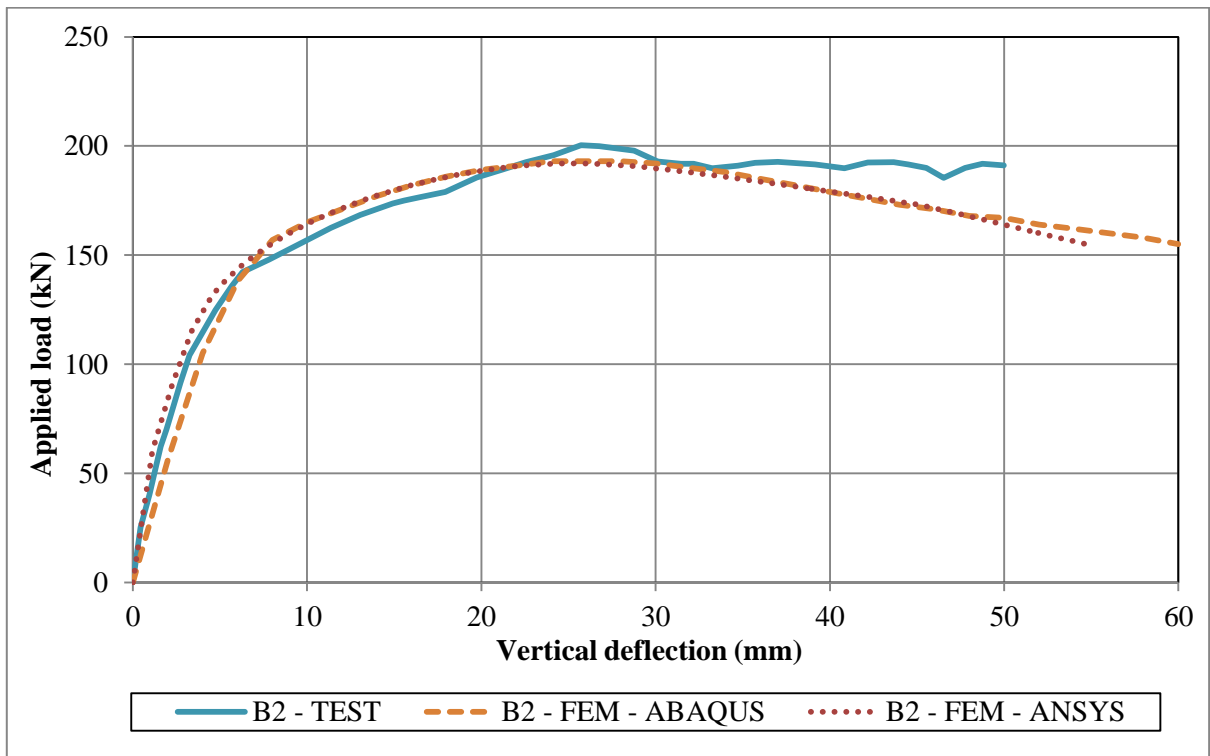
TEST A1: cross-section A – 450 °C



TEST A2: cross-section A – 650 °C



TEST B1: cross-section B – 450 °C



Cross-section B – 650 °C

Figure 25 : Applied load (kN) in function of the vertical deflection (mm) for each tested beam – comparison between fire tests and simulations

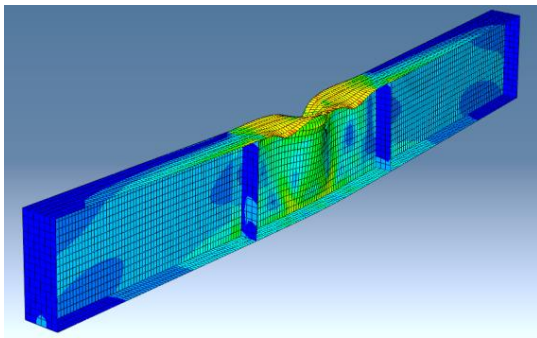
Test number	Failure load (kN) and relative difference (%)				
	TEST	ABAQUS	Difference	ANSYS	Difference
A1	637.82	643.27	0.85	648.27	1.61
A2	230.61	226.36	1.84	243.32	5.22
B1	484.68	484.58	0.02	488.37	0.76
B2	201.22	193.29	3.94	192.02	4.57

Table 3 : Comparison between numerical and experimental results

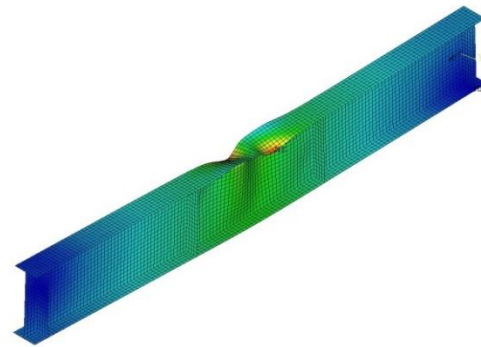
Another feature to be checked with the numerical models is the failure mode because the validity of the numerical models is also in relation to their capability of predicting correctly the local buckling. In order to do so, the deformed shapes of the four beams from both tests and the numerical simulations are shown together in figures Figure 26 to Figure 29 **Erreur ! Source du renvoi introuvable..**



TEST



ABAQUS

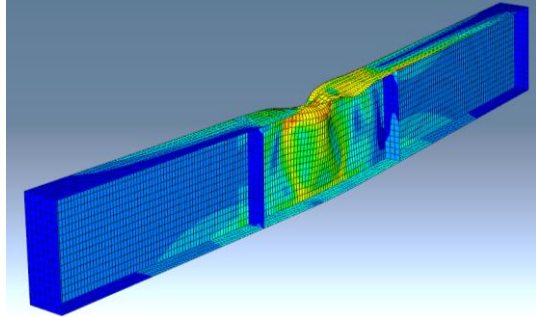


ANSYS

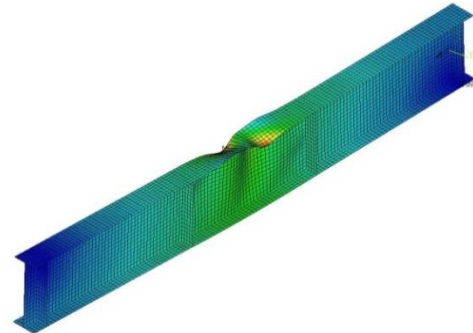
Figure 26 : Beam A at 450 °C - deformed shape of beam for both test and simulation



TEST



ABAQUS

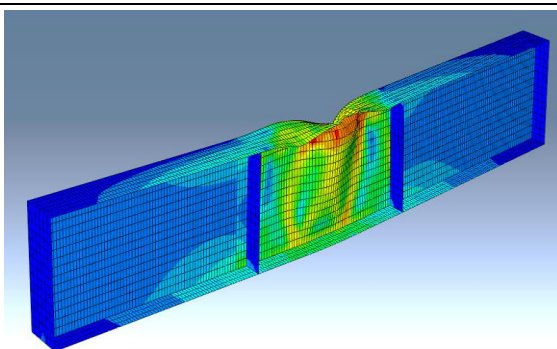


ANSYS

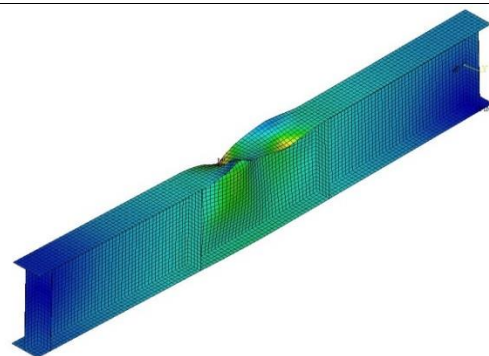
Figure 27 : Beam A at 650 °C - deformed shape of beam for both test and simulation



TEST



ABAQUS

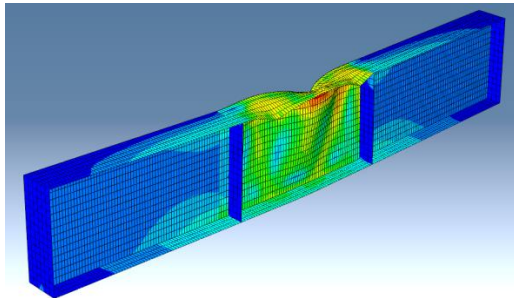


ANSYS

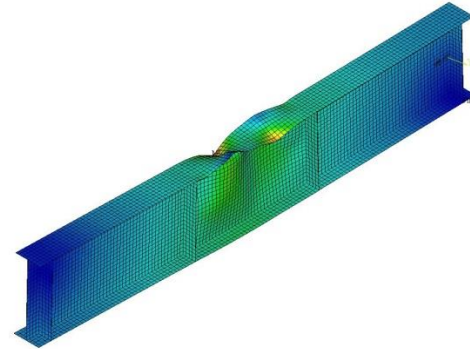
Figure 28 : Beam B at 450 °C - deformed shape of beam for both test and simulation



TEST



ABAQUS



ANSYS

Figure 29 : Beam B at 650 °C - deformed shape of beam for both test and simulation

It can be found easily that, for both numerical simulations and fire tests, the collapse of the beams is due to the local buckling of the upper flange and the web, both of them submitted to compression. Furthermore, the buckling modes predicted by means of the numerical models are all close to those of tested beams. From this point of view, the reliability of the numerical models is convincing.

The comparison between the numerical and experimental results has provided a very good idea about the validity of the numerical models as well as the assumptions adopted for various parameters. In fact, the difference between tests and the numerical simulations remains lower than 6 % in terms of load-bearing capacity. Furthermore, the initial stiffness is quite well established by the numerical analysis and the failure modes are precisely predicted. As a conclusion, the developed numerical modelling is validated and can be used with confidence in the numerical parametric studies to enlarge the investigation field of the fire behaviour of I or H shape class 4 cross-section steel beams under simple bending.

1.2 Beams subjected to lateral torsional buckling

The four tests differ in the cross-sections dimensions and in the considered temperature. The following table describes the main parameters of each test. Three beams with constant cross-section and one with variable cross-section (height of the web varies linearly from one end to another) are considered. The temperature is chosen based on the most significant changes of plate slenderness calculated using the elevated temperature reduction factors. The classification and plate slenderness is done according to Eurocode 3 Part 1-2.

Test number	Web	Flange	Temperature (°C)
Test 1 / Test 2 IW460/150/4/5	Class 4 $\bar{\lambda}_p = 1.33$	Class 4 $\bar{\lambda}_p = 1.13$	450 / 650
Test 3 IW460/150/4/7	Class 4 $\bar{\lambda}_p = 1.23$	Class 3 $\bar{\lambda}_p = 0.81$	450
Test 4 IW585-495/150/4/5	Class 4 $\bar{\lambda}_p \in [1.45 ; 1.76]$	Class 4 $\bar{\lambda}_p = 1.13$	650

Table 4: Tested cross-sections

The tested cross-sections are illustrated in the following figure:

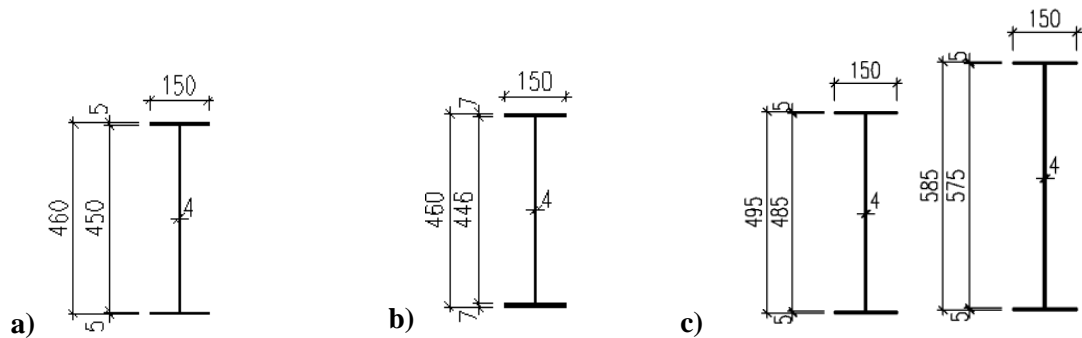
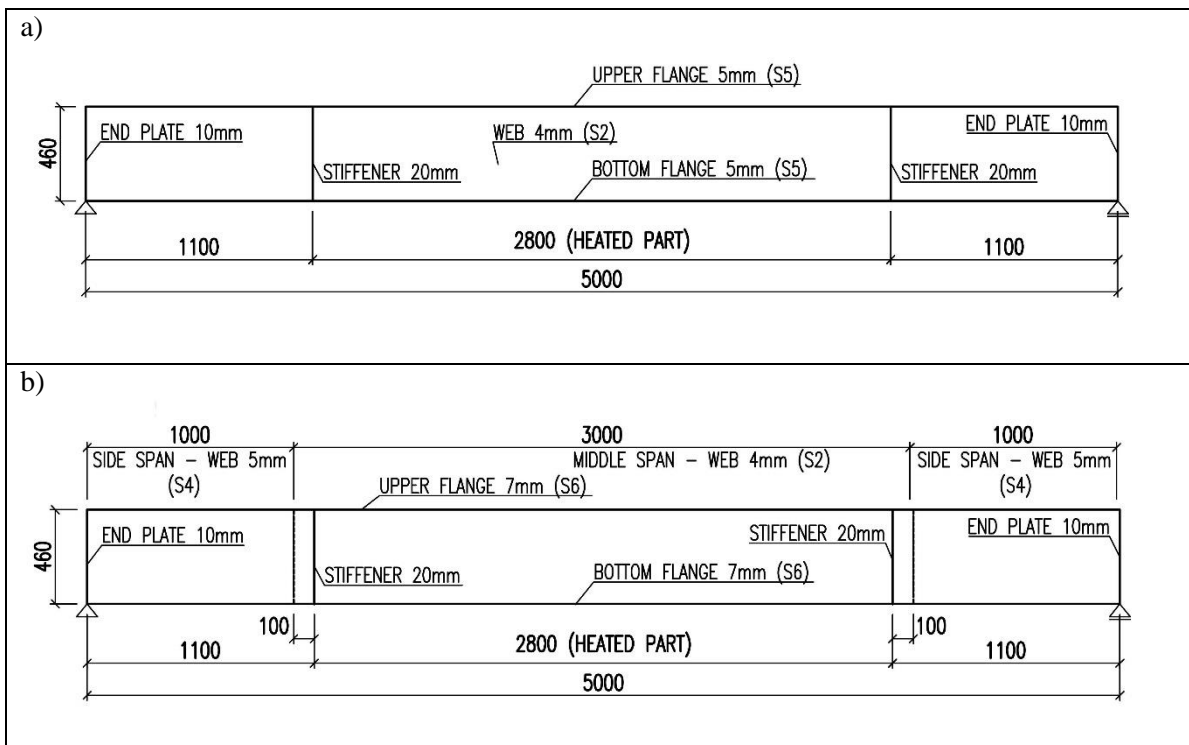


Figure 30: Cross-section: a) Tests 1 & 2, b) Test 3, c) Test 4

The following figure illustrates experimentally all tested beams:



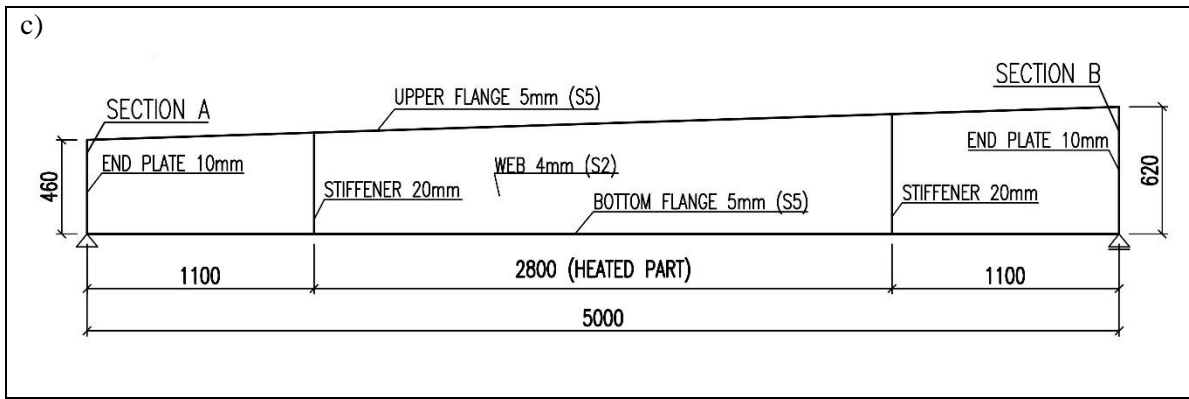


Figure 31: Tested beams: a) tests 1 & 2, b) test 3, c) test 4

1.2.1 Set-up of experimental tests

Material tests were performed at normal temperature and at high temperature. Each beam was made of different steel plates welded together. There were exactly six different steels which have all been accurately tested in terms of stress-strain relationship at room temperature and at high temperature.

The material tests let have the information about yield strength and elastic modulus for each steel plate at room temperature. The tensile coupon tests are conducted in accordance with EN ISO 6892-1 to determine the basic engineering stress-strain response of the material. These results are summarized in the following table:

Sample	(MPa)	S1	S2	S3	S4	S5	S6
Upper Yield strength	R_{eH}	430	394	341	376	385	435
Bottom yield strength	R_{eL}	424	392	338	361	378	408
Elastic modulus	E	178399	176897	194375	199200	209988	208900

Table 5: Material properties of the six studied steels at 20 °C

The following figure shows which steel composed the four tested beams:

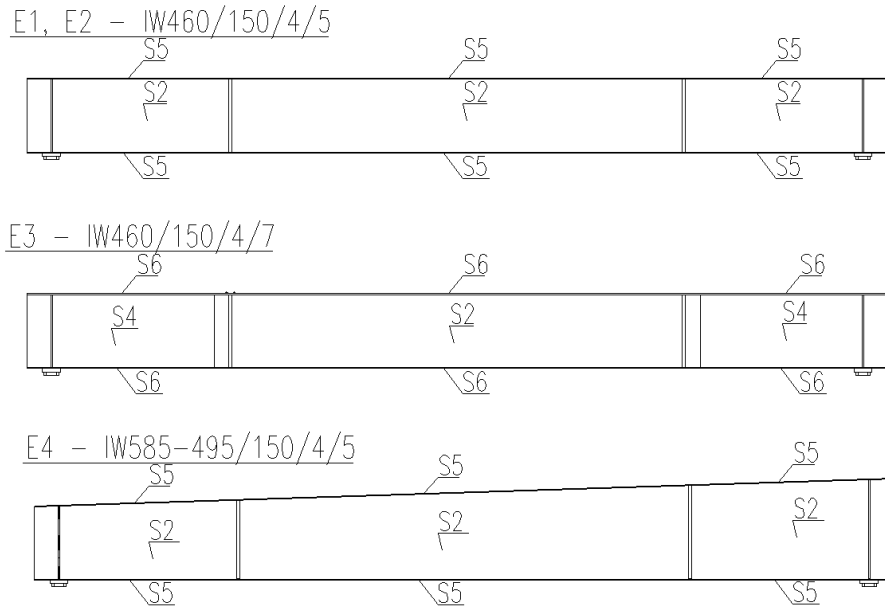


Figure 32: Composition of steel beams

During the experiments a simply supported beam with two equal concentrated point loads applied symmetrically is tested. The heated central part of beam where the temperature is aimed to be constant and uniform is therefore subjected to a uniform bending moment. The fire tests are performed on steady state, the beam is heated in a first time and then the loads are applied, until failure. The tests are controlled by deflection which is estimated as 3.5 mm per minute. Final deformation at the end of experiment is 50 mm at mid-span of the beam. This procedure is the same for all three beams. The following figure shows a scheme of experiment:

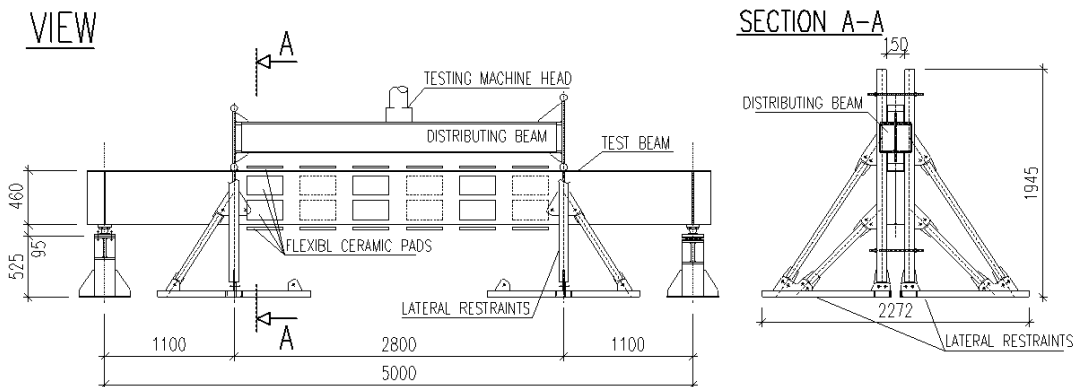


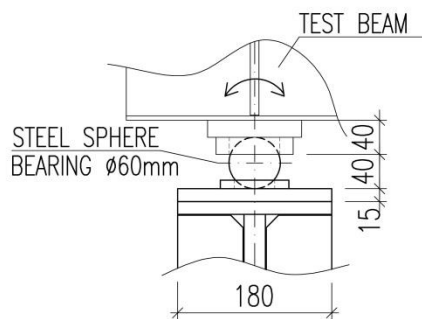
Figure 33: Scheme of the experiment and lateral restraints



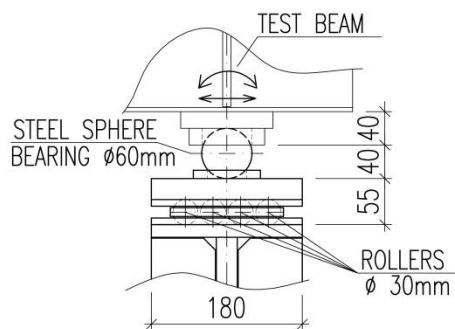
Figure 34: Lateral restraints

The end supports are considered just by one point support. It is made using a high-quality steel sphere bearing placed between two steel plates. Both end supports allow free torsion of the end cross-section. The first one restrains the displacement in all directions. The second allow also free horizontal displacement in the direction along the beam axis.

The load is introduced via a distributing beam at the edges of the heated (central) part. Free rotation and transverse deflection is allowed between these points. The load is applied by means of one hydraulic jack of 650 kN capacity.



a)



b)

Figure 35: Pinned point supports: a) fixed; b) free

Before the experiment, after placing the beam on the support, the initial geometry of the specimens was established using the two methods, namely manual measurements and laser scanning. The first method by manual measurement consists of the measurement of amplitude for global and local imperfection. Amplitude of global imperfection was measured as a deviation from a string spanned between the stiffeners. For measurements of local imperfection amplitude, a special device set with a centesimal displacement meter was used:



Figure 36: Manual measurement of imperfections

The following figure illustrates the points of measurement for uniform cross-sections (see Figure 37):

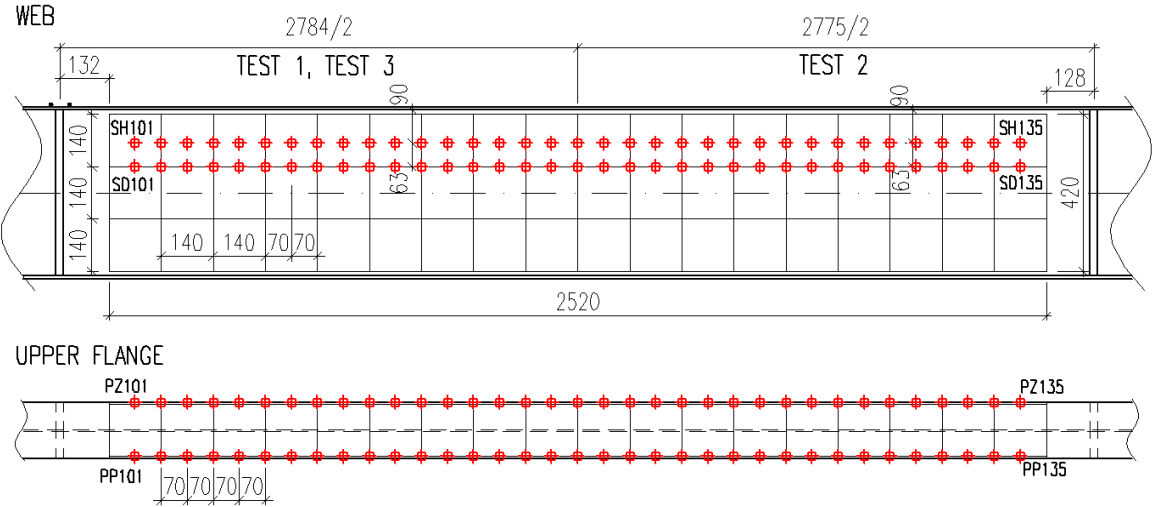


Figure 37: Points of measurement for uniform cross-sections

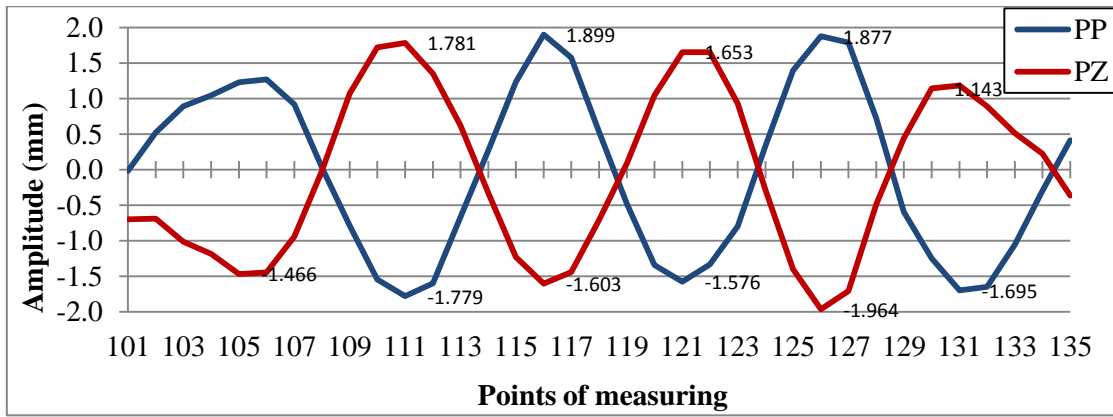


Figure 41: Local imperfections of upper flange

The maximum amplitudes of imperfections of all tested beams are summarized in the following table:

Test number	Local imperfection (mm)		Global imperfection (mm)
	Web	Flange	
Test 1 IW460/150/4/5	7.36	2.27	2.5
Test 2 IW460/150/4/5	6.24	1.96	1.0
Test 3 IW460/150/4/7	5.80	0.69	1.5
Test 4 IW585-495/150/4/5	7.59	2.13	1.5

Table 6: Amplitude of initial imperfections

Twenty-four thermocouples are used to measure the temperature of the beams. Twenty are localized in the middle span and four are placed in the side spans to monitor the temperature in not-heated sections. The thermocouples are distributed on the beam according to position of ceramic pads, as shown and numbered in the following figure. Beam temperatures are recorded from the beginning of heating to the end of experiment.

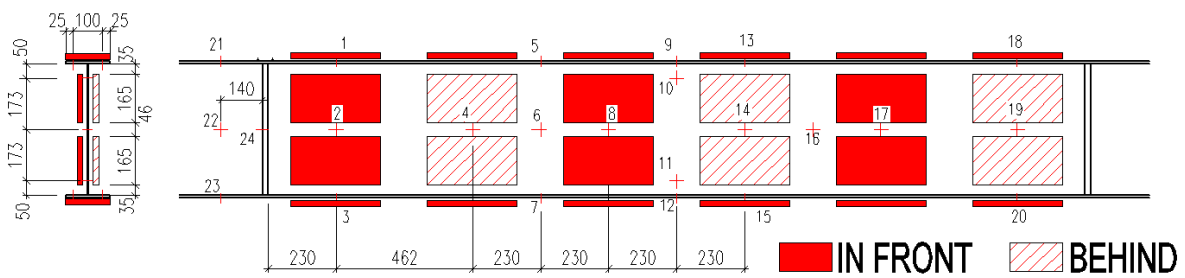


Figure 42: Layout of flexible ceramic pads and thermocouples

The displacements are measured by potentiometers. Two potentiometers are used to measure the displacement in the locations of load application. Vertical deflection (VD) and horizontal deflection (HD) of the bottom flange centre and lateral rotation (R) of the beam at mid-span are calculated, based on the measurement of the four potentiometers. Two of them measure relative vertical deflection and the rest of them measure relative horizontal deflection:

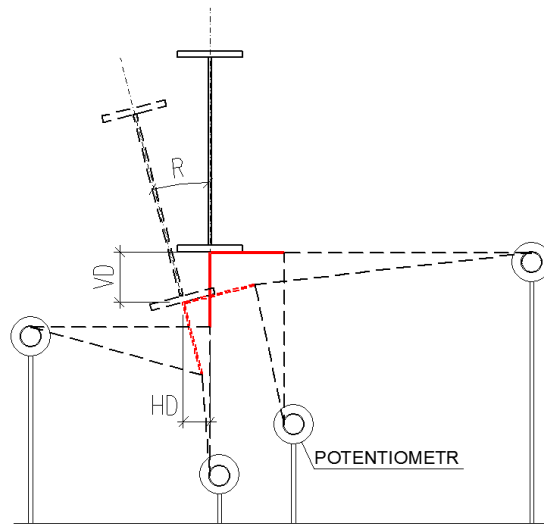


Figure 43: Measuring of displacement at mid-span

The following figure illustrates the test set-up of the beams subjected to lateral torsional buckling:

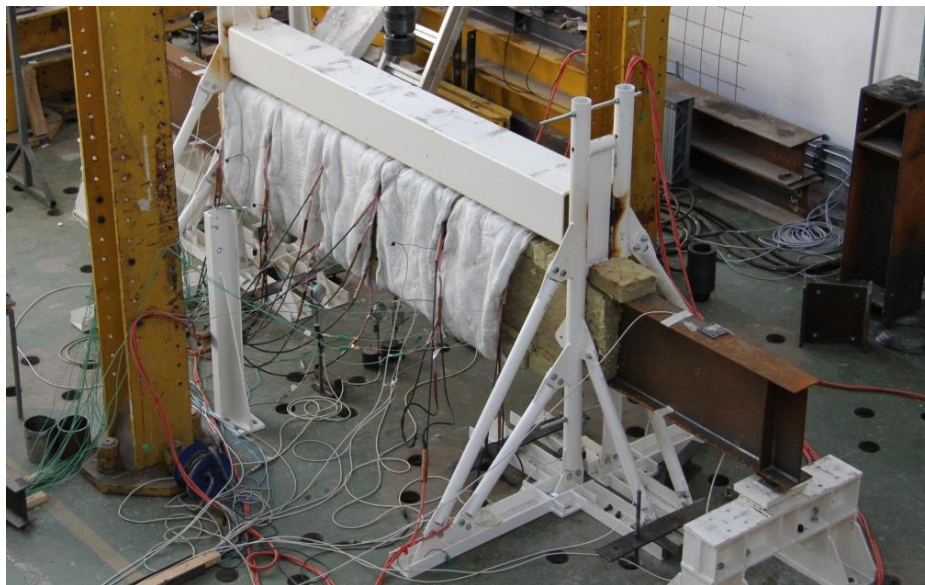


Figure 44: Test set-up of beams submitted to lateral torsional buckling

The following diagram shows, as an example, the temperature of beam of test 2 from the beginning of loading to the end of the experiment. Each line represents arithmetic mean temperature obtained from all thermocouples in the area:

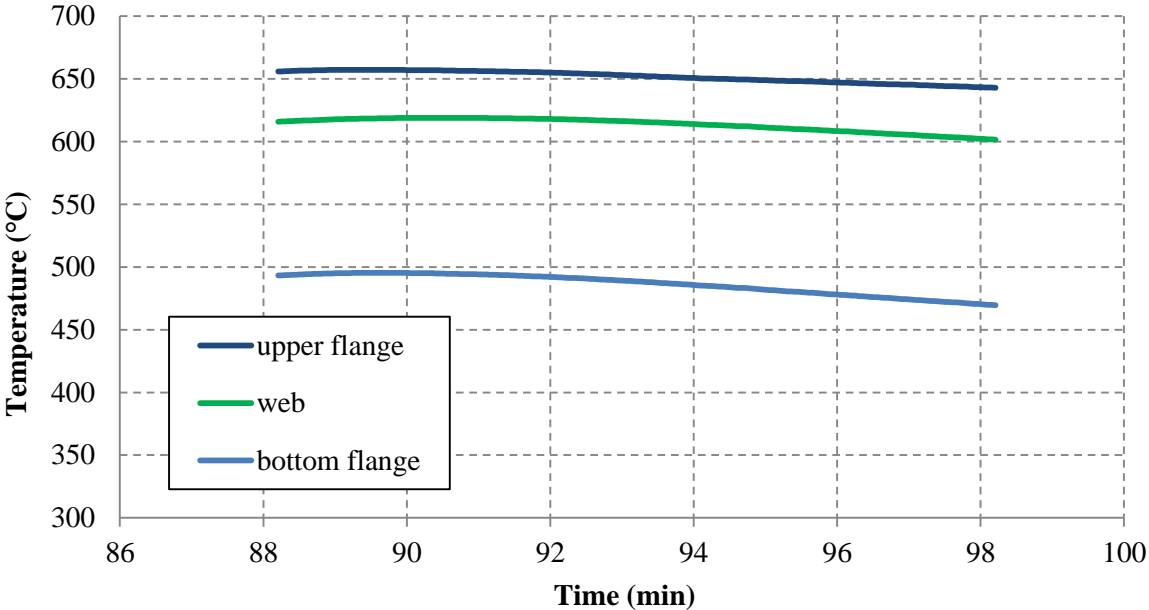


Figure 45: Evolution of the temperature as a function of time for test 2

The recorded load-deflection curves of all above beam tests are shown together from Figure 46 to Figure 49 and the failure modes of these beams are shown later in the next part:

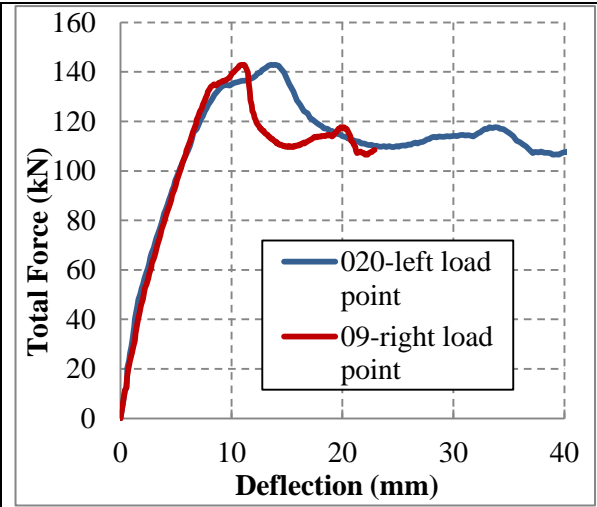


Figure 46: Vertical deflections of bottom flange at the load points (test 1)

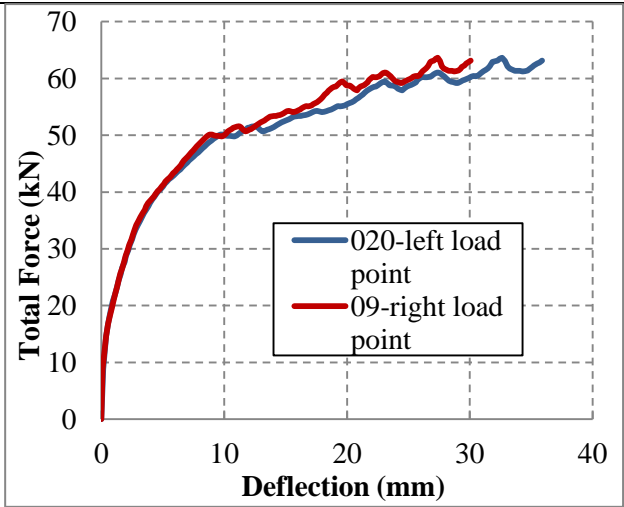


Figure 47: Vertical deflections of bottom flange at the load points (test 2)

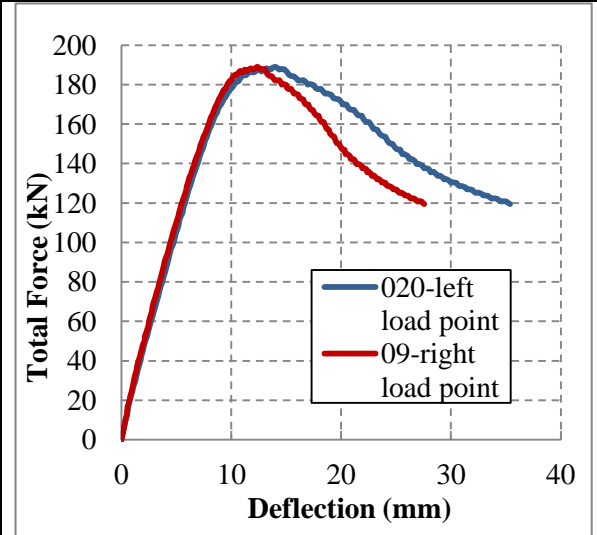


Figure 48: Vertical deflections of bottom flange at the load points (test 3)

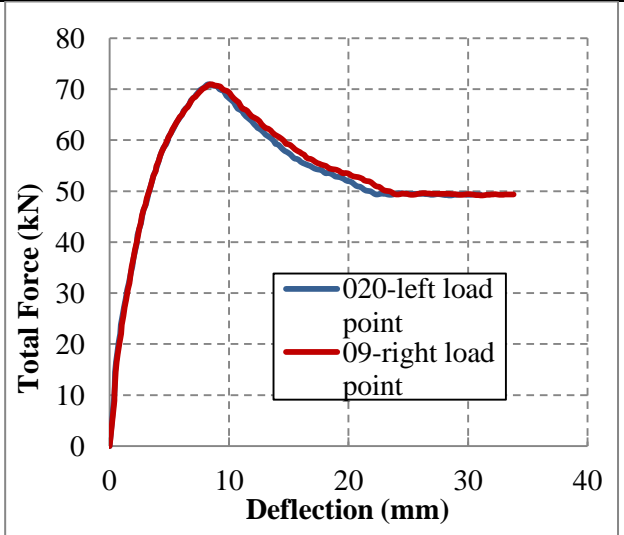


Figure 49: Vertical deflections of bottom flange at the load points (test 4)

1.2.2 Development of numerical models and correlation with experimental results

To consider the local buckling of thin walls in members with Class 4 cross-sections, shell finite elements are used instead of the beam finite elements, due to the fact that it is the primary failure mode. The tests are replicated by means of the finite element method programs ABAQUS and SAFIR.

SAFIR software (Franssen, 2005) is a geometrical and material non-linear finite element code especially developed, at the University of Liege, to model the behaviour of structures in case of fire.

The ABAQUS code is a general software for finite element analysis. It allows a complete solution for a large range of problems, including the analysis of structures under fire. Static calculation is used in this case. The same models as for preliminary numerical simulation are used. The beam is meshed using quadrilateral conventional shell elements (namely type S4). Conventional shell elements discretize a body by defining the geometry at a reference surface. In this case, the thickness is defined through the section property definition. Conventional shell elements have three displacements and three rotational degrees of freedom per node. Element type S4 is a fully integrated, general-purpose, finite-membrane-strain shell element. The element has four integration points. For definition of mesh size in ABAQUS model, six elements for flange width and twenty elements for web height are used. Along the beam, four elements each 100 mm are used. All experimental data are used to check the numerical model. The Eigen modes obtained from elastic buckling analysis are used as the initial geometric imperfection shape for the post-buckling analysis. Two imperfection shapes are considered: the beam first local buckling mode and first global buckling mode (lateral torsional buckling) shapes. The imperfection amplitudes are based on the initial geometry measurement. The material law is defined by elastic-plastic nonlinear stress-strain diagram. The true material stress-strain relationship is calculated from the static engineering stress-strain curves obtained from the coupon tests. The reductions of material properties as well as the material nonlinearity are based on EN 1993-1-2. The average measured temperatures from each heated part of the beams are introduced to the model. Adjacent parts of the beam and stiffeners are considered to be at room temperature (20 °C).

All experimental data have been used for verification of the numerical model. The Eigen modes obtained from elastic buckling analysis were used as the initial geometric imperfection shape for the post-buckling analysis. Two imperfection shapes are considered: the beam first local buckling mode and first global buckling mode (LTB) shapes. The imperfection amplitudes are based on the initial geometry measurement.

1.2.2.1 Test 1

The real material properties of steel which are obtained with the sample tests are given for the first tested beam in the following table:

Part of beam	Maximum Yield stress (MPa)	Young Modulus (MPa)
Web	393	176897
Flanges	382	209988
stiffeners	355	210000

Table 7: Material properties used for numerical model of test 1

The applied temperatures on beam of test 1 are listed in the following table:

Part of beam	Temperature (°C)
Web	444.4
Bottom flange	354.0
Upper flange	456.7

Table 8: Temperatures applied on numerical model of test 1

The amplitude of each imperfection taken into account is listed in the next table and the shape of each buckling mode used is illustrated in Figure 50:

Global imperfection (mm)	Local imperfection of upper flange (mm)	Global imperfection of flange (mm)
2.50	2.27	2.72

Table 9: Amplitude of imperfections

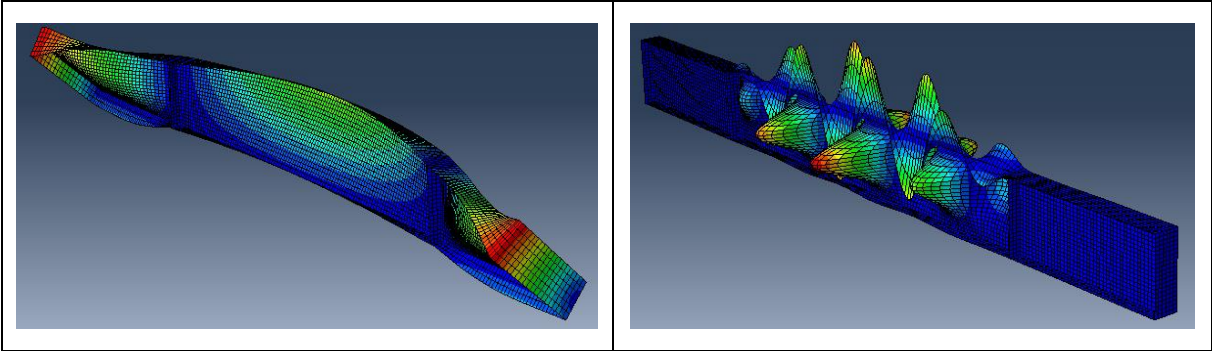


Figure 50: Mode shape from linear buckling analysis: left) lateral torsional buckling failure mode, right) local buckling failure mode

The next diagram shows the comparison in terms of total applied force in function of deflection for both fire test and numerical analysis:

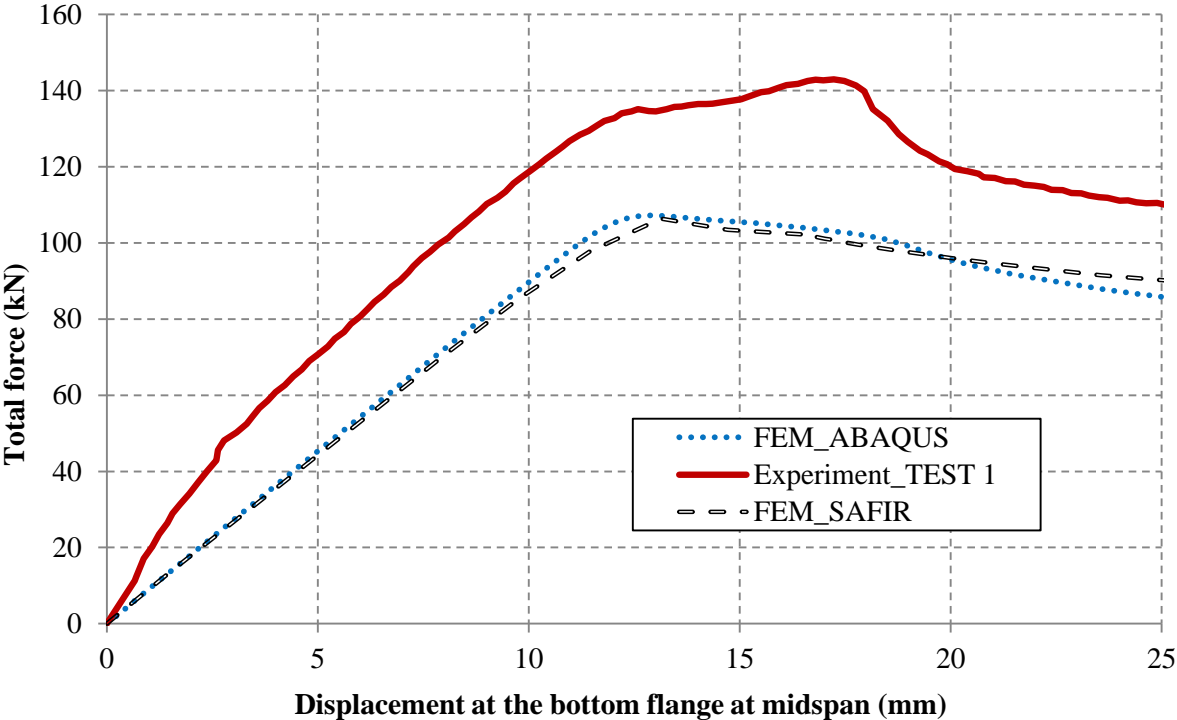


Figure 51: Numerical simulations against experimental fire test

The next table illustrates the comparison between the numerical simulation and experimental test in terms of ultimate load:

	Total force (kN)	Half-force (kN)	Ultimate bending moment (kN.m)
ABAQUS	107.2	53.6	58.80
SAFIR	106.3	53.15	58.42
Experiment	142.9	71.5	78.60

Table 10: Numerical simulation against experimental fire test

The next figure illustrates the failure mode for both numerical simulation and experimental test:

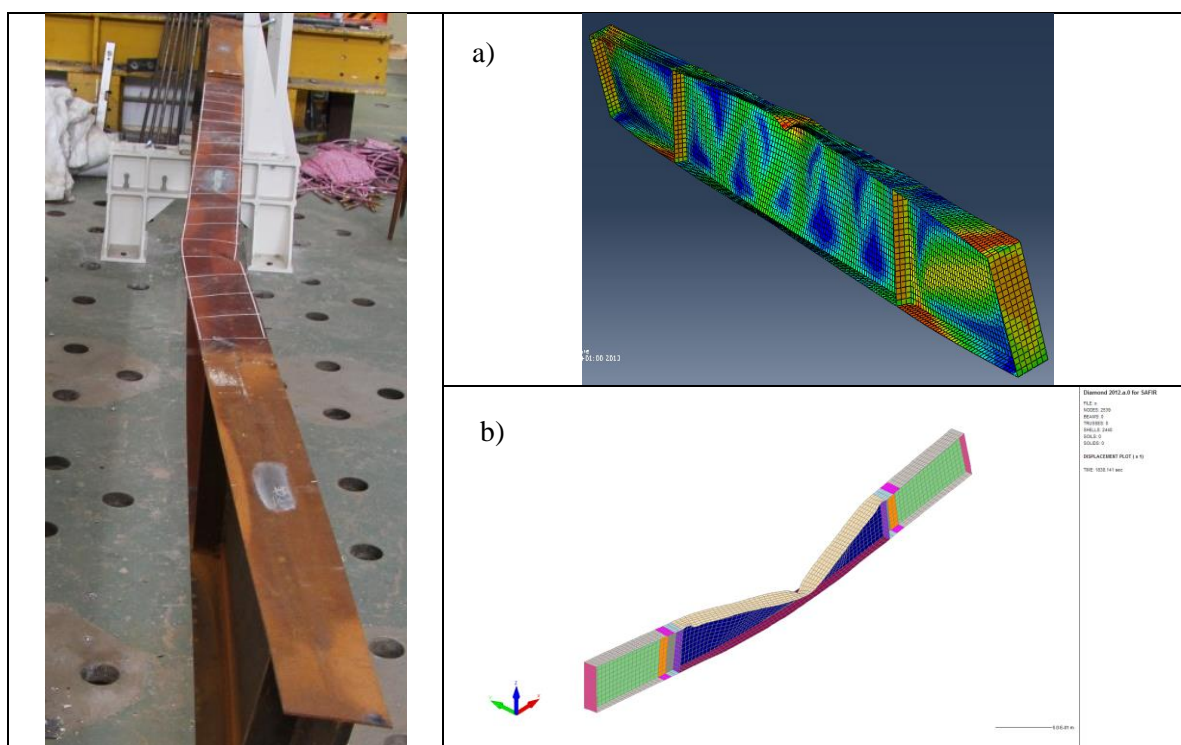


Figure 52: Failure mode shape for fire test and numerical simulation with: a) ABAQUS, b) SAFIR

1.2.2.2 Test 2

The real material properties of steel which are obtained with the sample tests are given for the second tested beam in the following table:

Part of beam	Maximum Yield stress (MPa)	Young Modulus (MPa)
Web	393	176897
Flanges	382	209988
stiffeners	355	210000

Table 11: Material properties used for numerical model of test 2

The applied temperatures on beam of test 2 are listed in the following table:

Part of beam	Temperature (°C)
Web	613.5
Bottom flange	486.3
Upper flange	651.7

Table 12: Temperatures applied on numerical model of test 2

The amplitude of the imperfections taken into account are listed in the next table and the shape of buckling modes used are illustrated in Figure 63:

Global imperfection (mm)	Local imperfection of upper flange (mm)	Global imperfection of flange (mm)
1.00	1.96	2.36

Table 13: Amplitude of imperfections

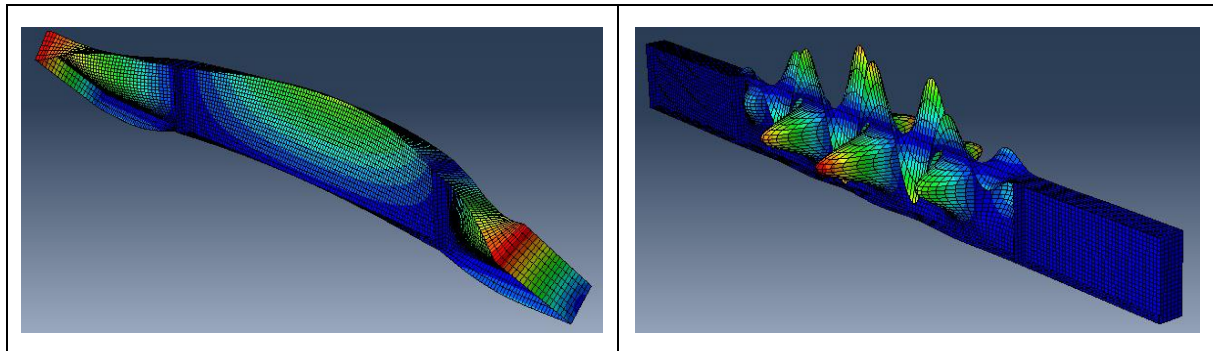


Figure 53: Mode shape from linear buckling analysis: *left) lateral torsional buckling failure mode, right) local buckling failure mode*

The next diagram shows the comparison in terms of total applied force in function of deflection for both fire test and numerical analysis:

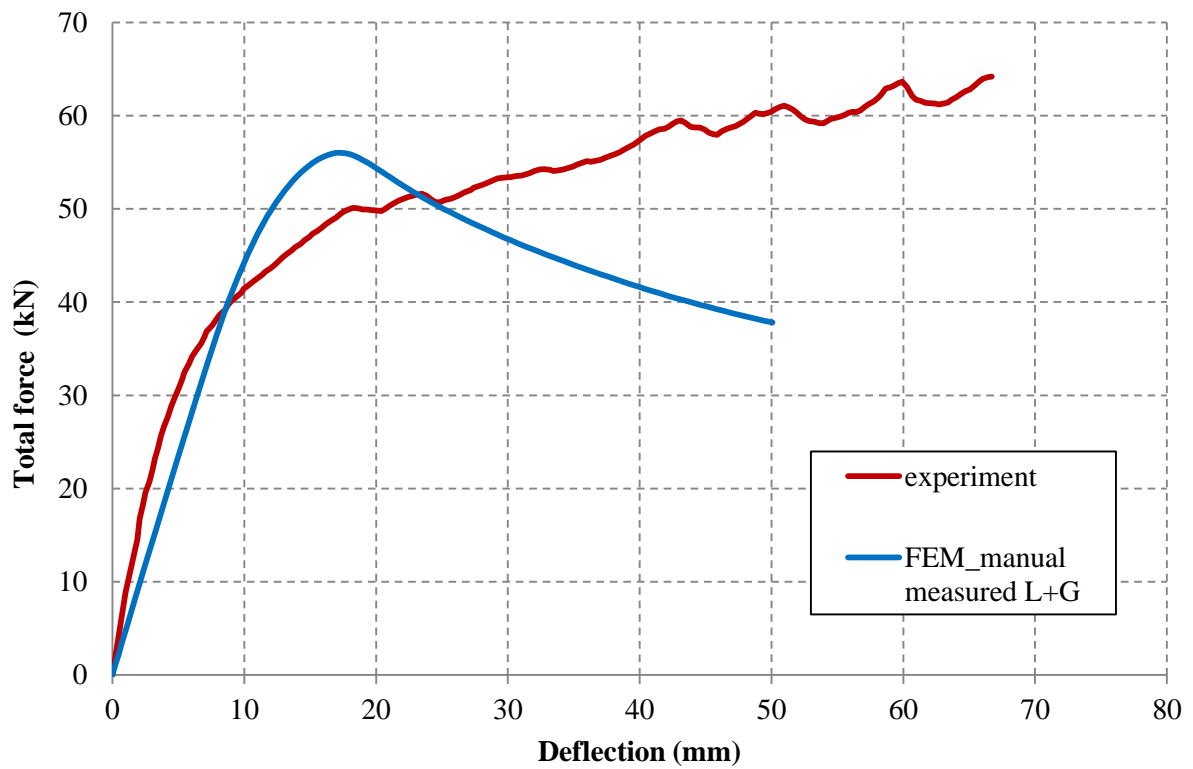


Figure 54: Numerical simulations against experimental fire test

The next table illustrates the comparison between the numerical simulation and experimental test in terms of ultimate load:

	Total force (kN)	Half-force (kN)	Ultimate bending moment (kN.m)
ABAQUS	56.02	28.01	30.81
Experiment	*	*	*

Table 14: Numerical simulation against experimental fire test

The next figure illustrates the failure mode obtained with the help of numerical simulations:

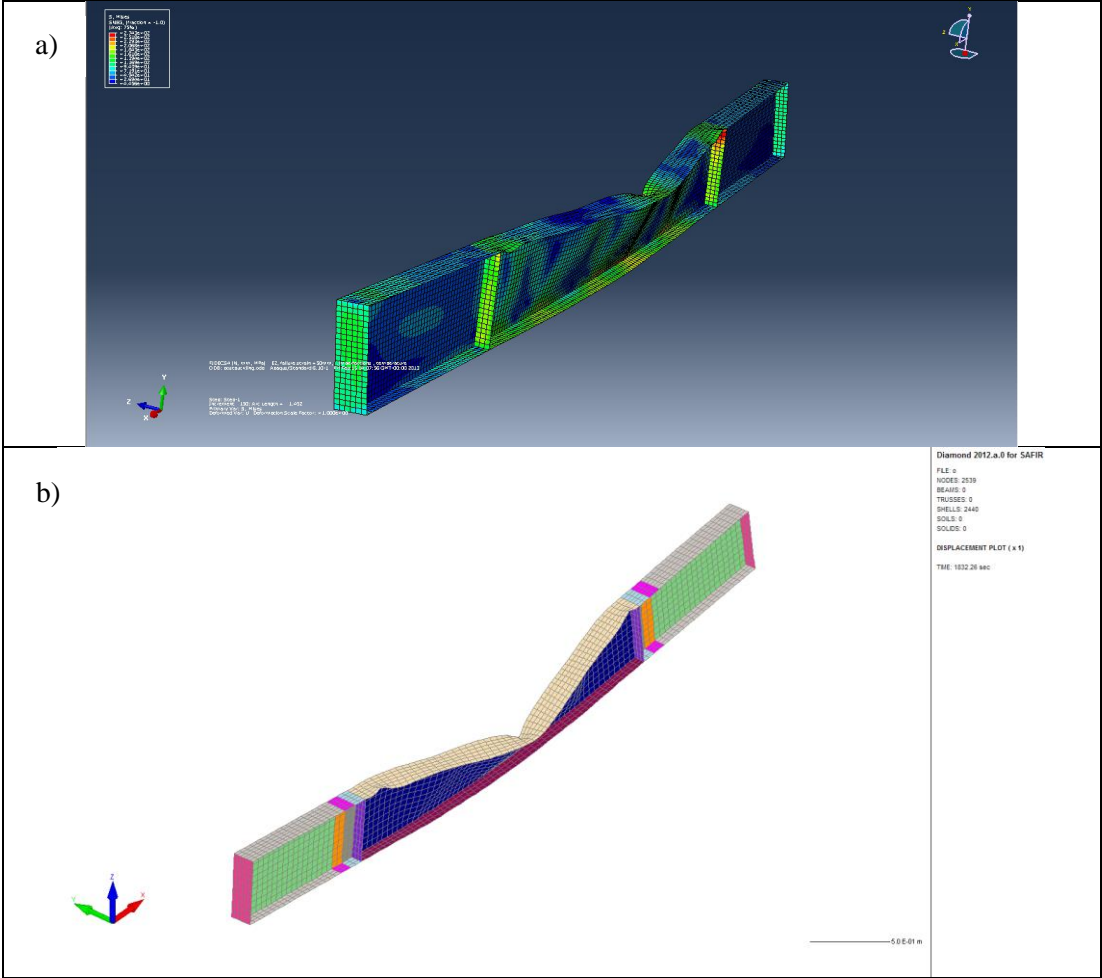


Figure 55: Failure mode obtained numerically with: a) ABAQUS; b) SAFIR

* Due to some problems which occurred on the lateral restraints, this test was not successful and the experimental results are not available. The following pictures illustrate this issue:



Figure 56: Problem with lateral restraints during the second fire test

1.2.2.3 Test 3

The real material properties of steel which are obtained with the sample tests are given for the third tested beam in the following table:

Part of beam	Maximum Yield stress (MPa)	Young Modulus (MPa)
Web (middle span)	393	176897
Web (side span)	374	199200
Flanges	412	208889
stiffeners	355	210000

Table 15: Material properties used for numerical model of test 3

The applied temperatures on beam of test 3 are listed in the following table:

Part of beam	Temperature (°C)
Web	443.2
Bottom flange	368.8
Upper flange	481.4

Table 16: Temperatures applied on numerical model of test 3

The amplitude of the imperfections taken into account are listed in the next table and the shape of buckling modes used are illustrated in Figure 63:

Global imperfection (mm)	Local imperfection of upper flange (mm)	Global imperfection of flange (mm)
1.50	0.69	2.65

Table 17: Amplitude of imperfections

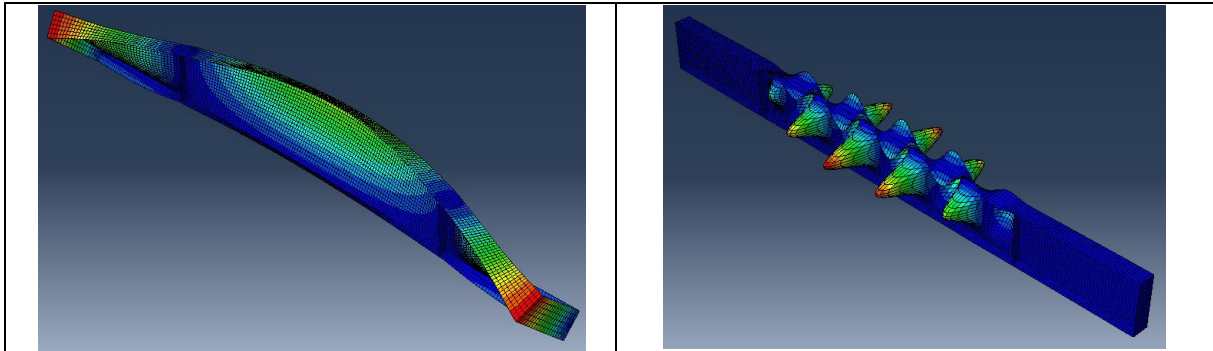


Figure 57: Mode shape from linear buckling analysis: left) lateral torsional buckling failure mode, right) local buckling failure mode

The next diagram shows the comparison in terms of total applied force in function of deflection for both fire test and numerical analysis:

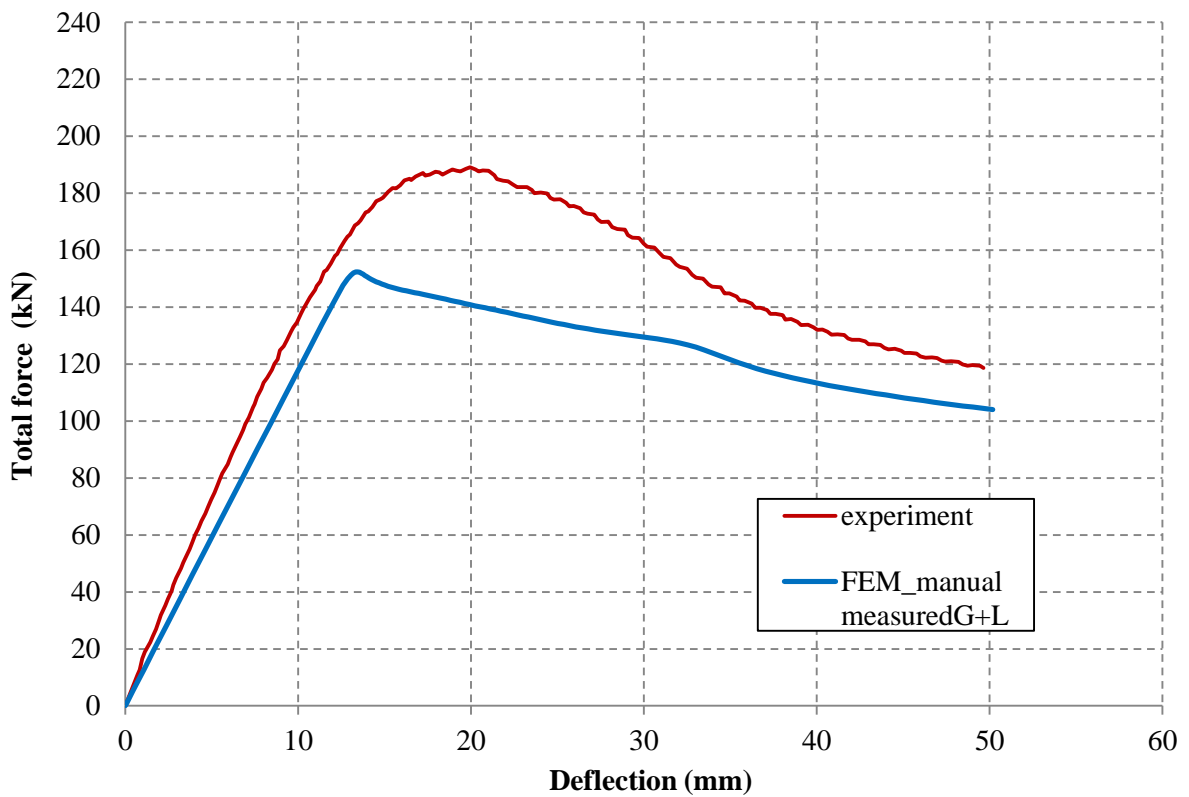


Figure 58: Numerical simulations against experimental fire test

The next table illustrates the comparison between the numerical simulation and experimental test in terms of ultimate load:

	Total force (kN)	Half-force (kN)	Ultimate bending moment (kN.m)
ABAQUS	151.80	75.90	83.48
SAFIR	168.50	84.25	92.66
Experiment	189.05	94.23	103.98

Table 18: Numerical simulation against experimental fire test

The next figure illustrates the failure mode for both numerical simulation and experimental test:

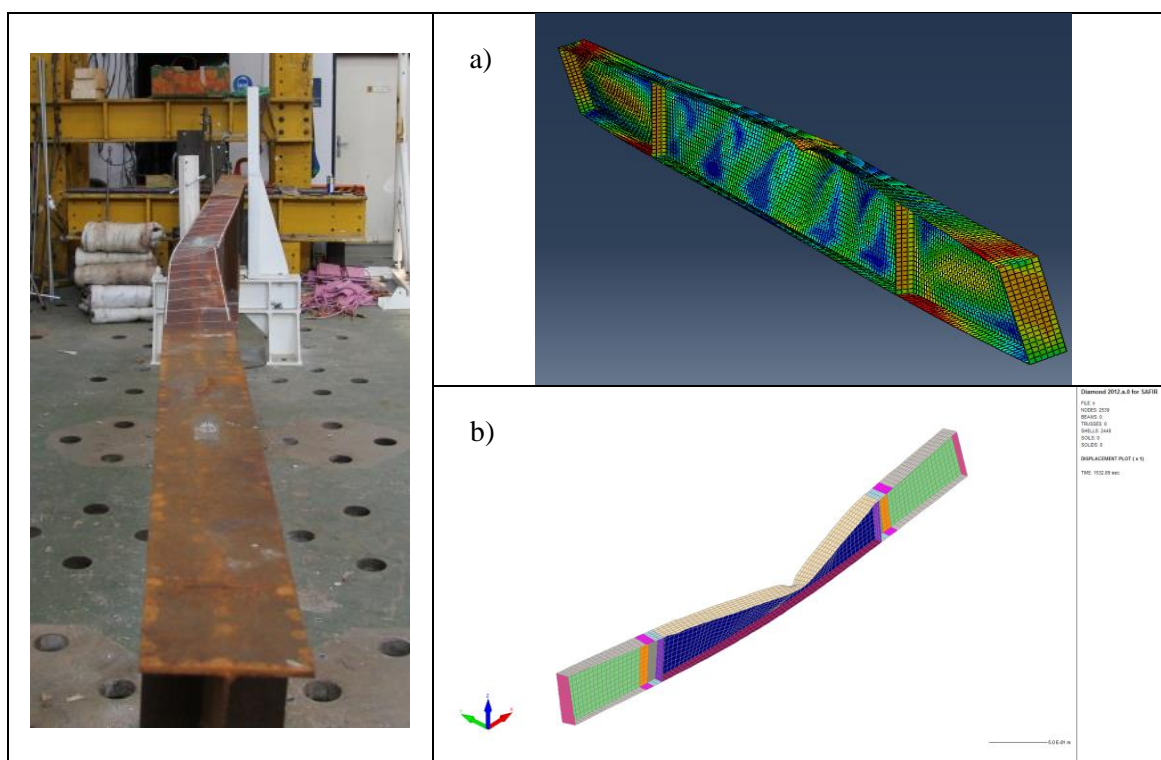


Figure 59: Failure mode shape for fire test and numerical simulation with: a) ABAQUS, b) SAFIR

1.2.2.4 Test 4

The real material properties of steel which are obtained with the sample tests are given for the fourth tested beam in the following table:

Part of beam	Maximum Yield stress (MPa)	Young Modulus (MPa)
Web	393	176897
Flanges	382	209988
stiffeners	355	210000

Table 19: Material properties used for numerical model of test 4

The applied temperatures on beam of test 4 are listed in the following table:

Part of beam	Temperature (°C)
Web	567.0
Bottom flange	415.6
Upper flange	623.7

Table 20: Temperatures applied on numerical model of test 4

The amplitude of the imperfections taken into account are listed in the next table and the shape of buckling modes used are illustrated in Figure 60:

Global imperfection (mm)	Local imperfection of upper flange (mm)	Global imperfection of flange (mm)
1.50	2.13	*

Table 21: Amplitude of imperfections

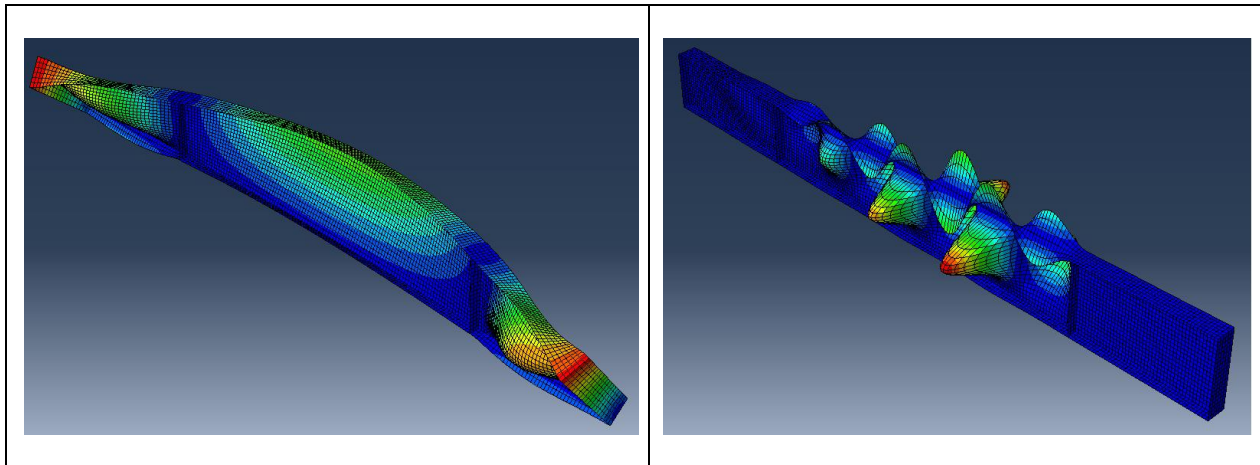


Figure 60: Mode shape from linear buckling analysis: *left) lateral torsional buckling failure mode, right) local buckling failure mode*

The next diagram shows the comparison in terms of total applied force in function of deflection for both fire test and numerical analysis:

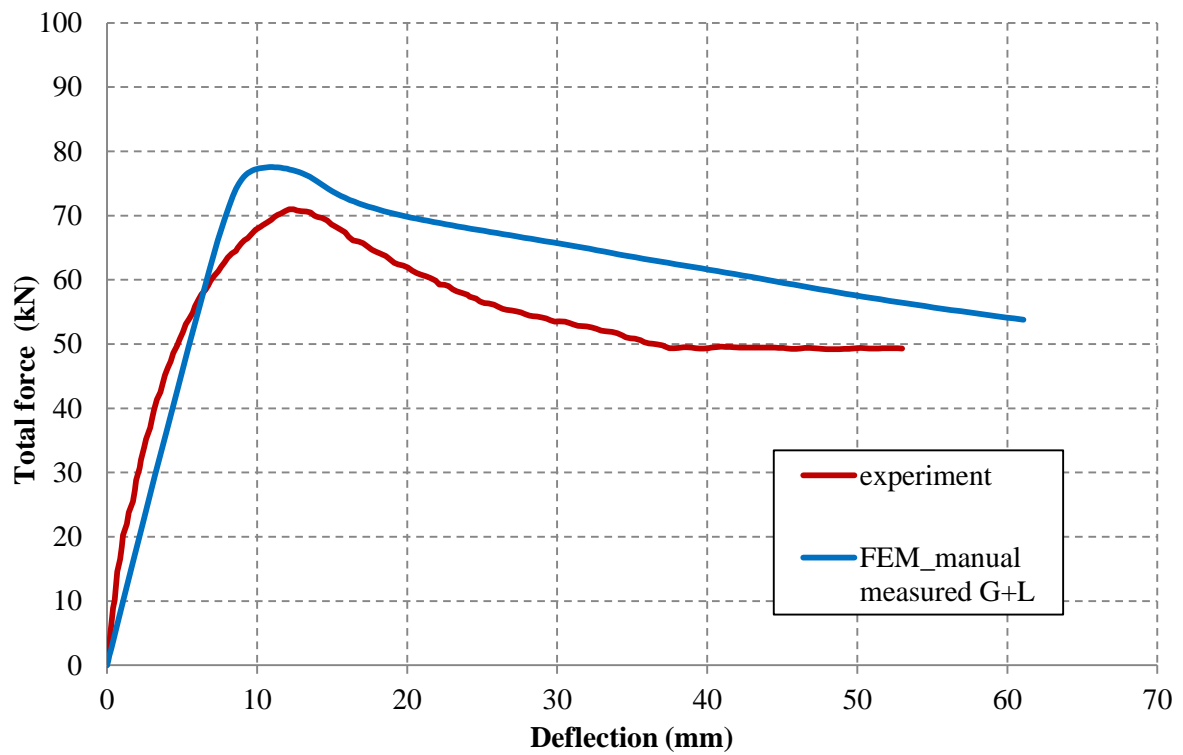


Figure 61: Numerical simulations against experimental fire test

The next table illustrates the comparison between the numerical simulation and experimental test in terms of ultimate load:

	Total force (kN)	Half-force (kN)	Ultimate bending moment (kN.m)
ABAQUS	74.10	37.05	40.76
SAFIR	68.20	34.10	37.51
Experiment	70.96	35.48	39.03

Table 22: Numerical simulation against experimental fire test

The next figure illustrates the failure mode for both numerical simulation and experimental test:

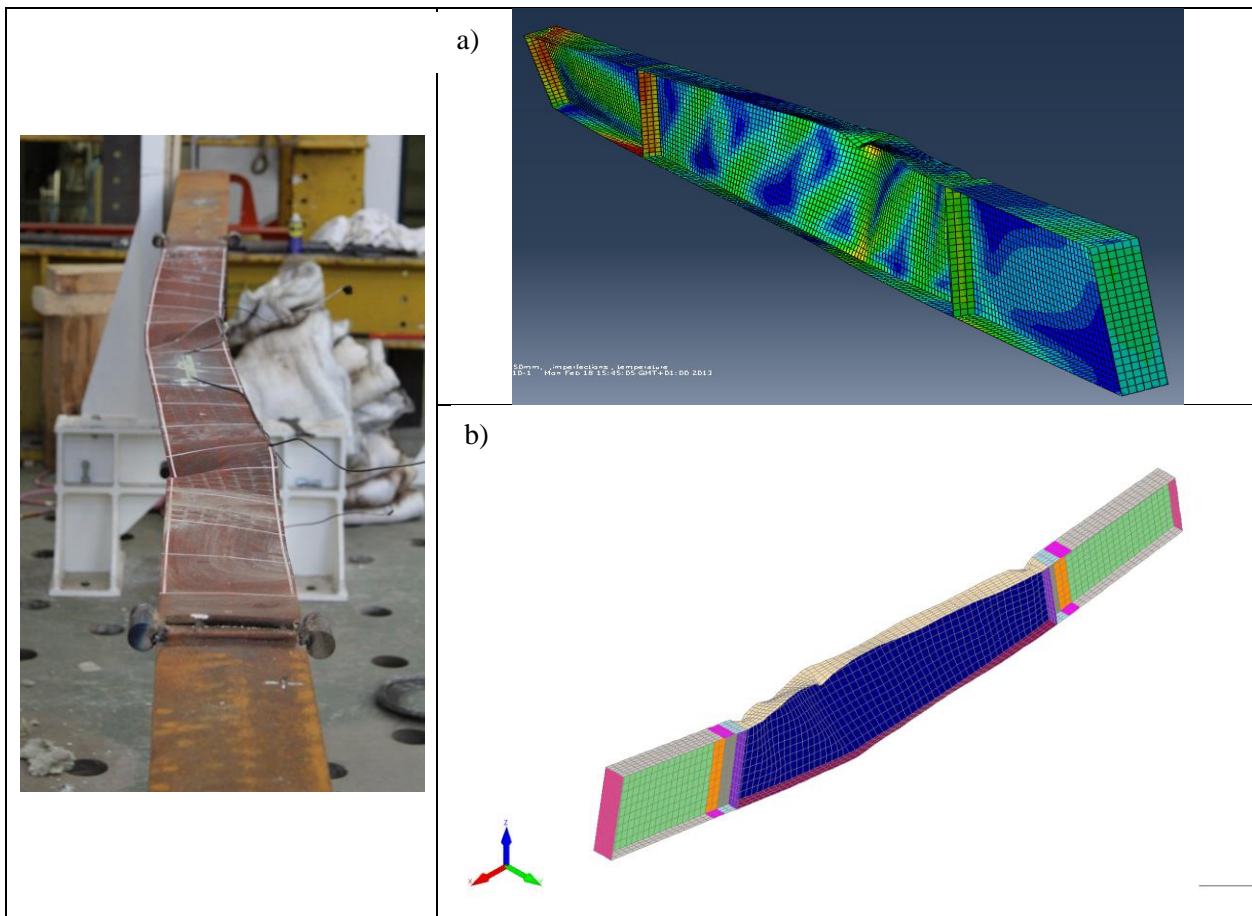


Figure 62: Failure mode shape for fire test and numerical simulation with: a) ABAQUS, b) SAFIR

The obtained results demonstrate the difficulties of lateral torsional buckling tests, moreover, when high temperature effects are taken into account. The problem of friction at the lateral restraints significantly affects the second test. For the third test, the experimental curve of load displacement relationship is not smooth and the force is suddenly increased at some locations. The obtained experimental initial stiffness is different from the numerical curves mainly in the third test and in the fourth test. The temperatures slightly vary during the tests and are not uniform for the whole section. The temperatures that are employed in the numerical models are considered as the average temperature for each part of the beam (web, upper flange, bottom flange). The maximum loads in the first test and in the third test are higher than the corresponded numerical tests values. Overall, the approximations are reasonable considering the nature of the different parameters involved in the presented tests, as for instance the heating process. The numerical model is able to predict the behaviour of beams observed in the tests, however mostly just for the mode of failure. The model is subsequently simplified and used for the numerical parametric study.

2 Description of the parametric studies and comparisons with simple design rules

2.1 Numerical parametric study for class 4 cross-sections subjected to simple bending

This parametric study is set up to have a consequent set of results regarding the cross-sectional resistance of welded cross-sections under simple bending. Within the context of this project it is necessary to study the influence of the slenderness of both internal and external parts of the beam on the cross-sectional resistance. The chosen strategy is illustrated in the following diagram (Figure 63):

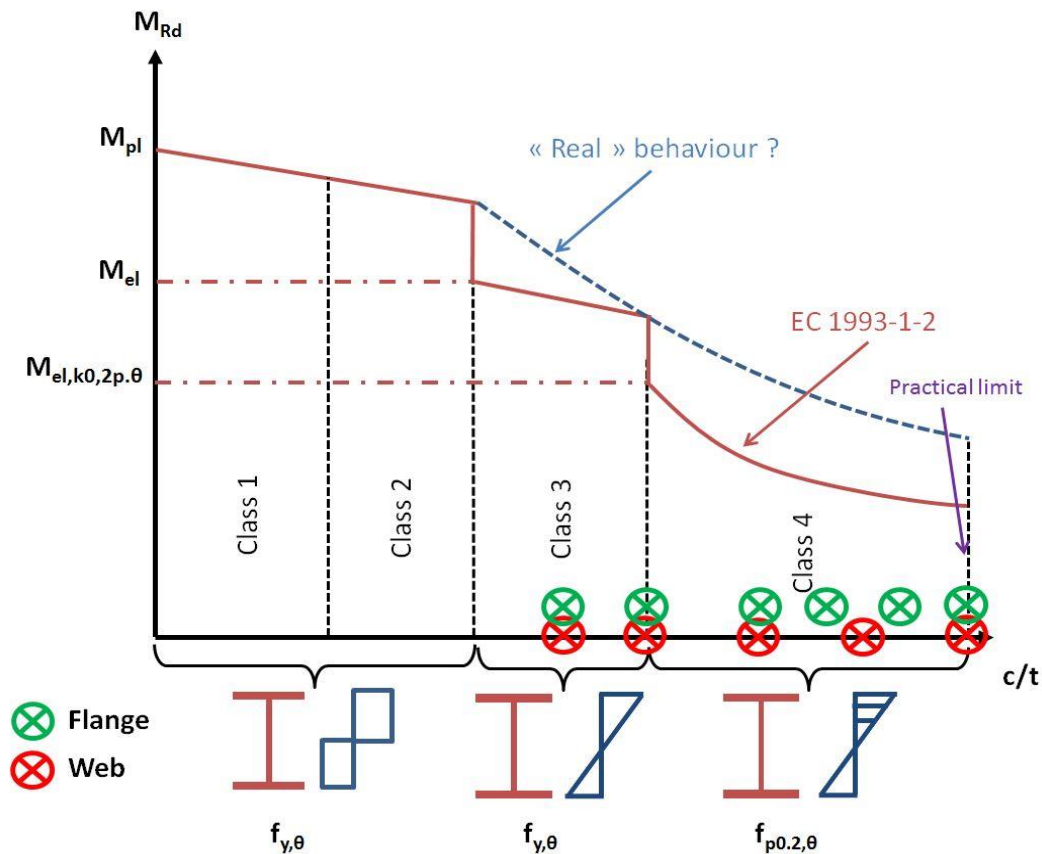


Figure 63: Illustration of range of investigation for WP2 numerical parametric study

2.1.1 Presentation of chosen parameters

With the numerical models validated against the tests at elevated temperatures, it is possible to conduct the numerical parametric studies to cover the full application domain of investigated steel members. With respect to I or H shape class 4 cross-section steel beams under simple bending, the following parameters are taken into account:

- global sizes of cross-sections
- wall slenderness of cross-sections
- steel grade
- residual stresses
- temperature levels

The values adopted for above parameters in the parametric studies are more precisely described hereafter.

A total of three sets of welded cross-sections have been used to conduct the parametric study. Each set has fixed web depth and flange width, which means a fixed global size of all cross-sections in this set. The accurate values relative to the global sizes of these cross-sections are listed in following table:

	Web depth h_w (mm)	Flange width b (mm)
Cross-section 1	450	150
Cross-section 2	1000	300
Cross-section 3	2000	420

Table 23 : Global sizes of the studied cross-sections

It needs to be pointed out here that the sizes provided in Table 23 are derived from the catalogue of a steel construction company specialized in steel frames composed of class 4 cross-section members and respect the fabrication rules in order to be as realistic as possible and meanwhile cover the common application range with this type of steel members.

For each cross-section, the web and flanges thicknesses vary in a predefined area in order to cover the slenderness from class 3 to class 4 for web and from class 2 to class 4 for flanges. The accurate values as well as the classification of these walls according to the design rule at elevated temperatures are given respectively in Table 24, Table 25 and Table 26 for the three sets of cross-sections.

Cross-section type 1: $H_w \times B = 450 \times 150$								
Web								
Thickness t_w (mm)	6	5	4.5	4				
Slenderness c_w/t_w	75.0	90.0	100.0	112.5				
Slenderness limit		Limit of class 3: $124 \times \epsilon \approx 85.8$						
Class	3	3	4	4				
Flange								
Thickness t_f (mm)	11	9	8	7	6.5	6	5.5	5
Slenderness c_f/t_f	6.6	8.1	9.1	10.4	11.2	12.1	13.2	14.5
Slenderness limit	Limit of class 2: $10 \times \epsilon \approx 6.9$		Limit of class 3: $14 \times \epsilon \approx 9.7$					
Class	2	3	3	4	4	4	4	4

Table 24 : Studied wall thicknesses for cross-section type 1

Cross-section type 1: $H_w \times B = 1000 \times 300$						
Web						
Thickness t_w (mm)	14	12	10	8	6	5
Slenderness c_w/t_w	71.4	83.3	100.0	125.0	166.7	200.0
Slenderness limit		Limit of class 3: $124 \times \epsilon \approx 85.8$				
Class	3	3-4	4	4	4	4

Flange								
Thickness t_f (mm)	22	18	16	14	13	12	11	10
Slenderness c_f/t_f	6.6	8.1	9.1	10.4	11.2	12.1	13.2	14.6
Slenderness limit	Limit of class 2: $10 \times \epsilon \approx 6.9$		Limit of class 3: $14 \times \epsilon \approx 9.7$					
Class	2-3	3	3-4	4	4	4	4	4

Table 25 : Studied wall thicknesses for cross-section type 2

Cross-section type 1: $H_w \times B = 2000 \times 420$							
Web							
Thickness t_w (mm)	28	24	20	16	12	10	
Slenderness c_w/t_w	71.4	83.3	100.0	125.0	166.7	200.0	
Slenderness limit		Limit of class 3: $124 \times \epsilon \approx 85.8$					
Class	3	3	4	4			
Flange							
Thickness t_f (mm)	30	24	20	18	16	15	14
Slenderness c_f/t_f	6.7	8.4	10.1	11.2	12.6	13.5	14.4
Slenderness limit	Limit of class 2: $10 \times \epsilon \approx 6.9$		Limit of class 3: $14 \times \epsilon \approx 9.7$				
Class	2-3	3	3	4	4	4	4

Table 26 : Studied wall thicknesses for cross-section type 3

Two steel grades have been investigated in this parametric study: S355 and S460 which are the mostly used ones for this type of steel members.

The initial residual stresses are in general quite important in welded cross-sections. In the numerical models, they are incorporated with the help of initial state data before applying thermal and mechanical loadings. The following scheme (see Figure 64) represents the residual stress pattern adopted in case of welded cross-sections:

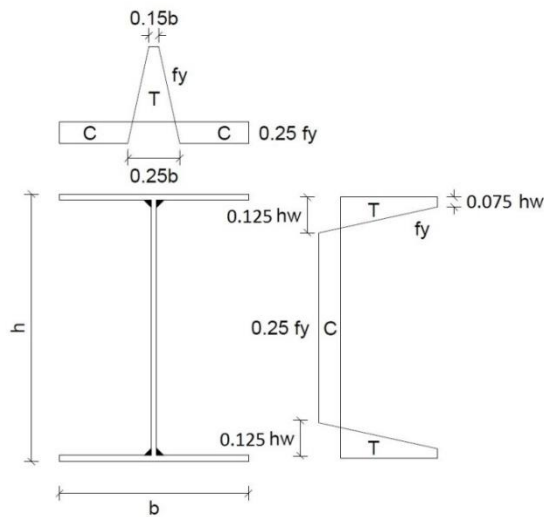


Figure 64 : Residual stress pattern for welded cross-sections (T represents tensile stress whereas C represents compressive stress)

Five heating levels have been selected to conduct the parametric study: 20 °C, 350 °C, 450 °C, 550 °C and 700 °C. The room temperature (20 °C) is selected mainly to get the reference load-bearing capacity of investigated member.

In addition to various parameters taken into account in the parametric studies, following general assumptions are adopted for all numerical analyses:

- To avoid any edge effects, the length of each beam has been taken as ten times of the height of the web. The beam is considered to be subjected uniformly to a constant bending moment about its strong axis;
- The mesh size of shell element is proportional to global size of cross-section and the mesh refinement is similar to that used in the numerical models to simulate the tests at elevated temperatures;
- In order to account for second order effects, local imperfections based on the buckling shape of the lowest Eigenvalue have been implemented. These imperfections have been applied to different walls (web and flange in compression) in accordance with the recommendation of EN 1993-1-5. The amplitude of these imperfections is 0.8 times of the class 1 fabrication tolerance given in the execution standard EN 1090-2:2008 and more accurately in tables D.2.3 and D.2.5;
- The beam is considered firstly to be heated uniformly to target temperature level before the application of the mechanical loading;
- The loading of the beam is realized through a moment couple applied at the ends of the beam with the help of a rigid body element at each end to prevent any irrelevant local behaviour;
- One end of the beam is free to expand axially and thermal expansion of steel is taken into account according to section 3.4 of EN 1993-1-2;
- Whatever the steel grade is, the modulus of elasticity is taken as 210 000 MPa whereas the Poisson's ratio is taken as 0.3;
- The mechanical properties of the steel at elevated temperatures comply fully with section 3.2 of EN 1993-1-2.

2200 numerical simulations were conducted for this numerical parametric study.

An example of a numerical model developed according to above assumptions is shown in Figure 65:

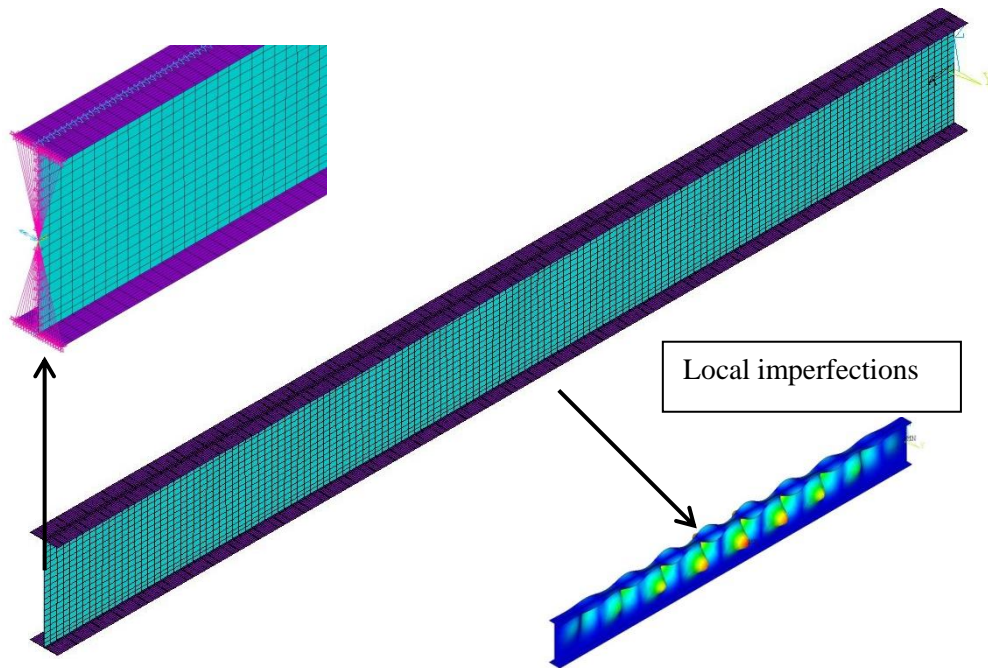


Figure 65 : Meshing of the beams, shape of imperfection and applied boundary conditions

For each parametric case, the following simulation procedure is applied:

1. Creation of model geometry and attribution of boundary conditions
2. Implementation of internal residual stresses
3. Introduction of initial imperfections
4. Progressive heating of the model up to target temperature level
5. Application of loading in incremental manner until the collapse

2.1.2 Detailed list of results of the parametric study and comparisons with simple design rules

Some of the defined cases are chosen to check the consistency between softwares ABAQUS and ANSYS and modelling assumptions. Two steel grades and two temperatures are taken into account: S355 and S460, 550 °C and 700 °C. The contribution of the residual stress in cross-sectional resistance is also investigated. These parameters are chosen because they can be considered as the most critical ones in terms of numerical resolution. A good consistency between these cases ensures good agreement for more conventional cases (no residual stress, room temperature). The forty-two concerned cases are represented in the following diagram (Figure 66):

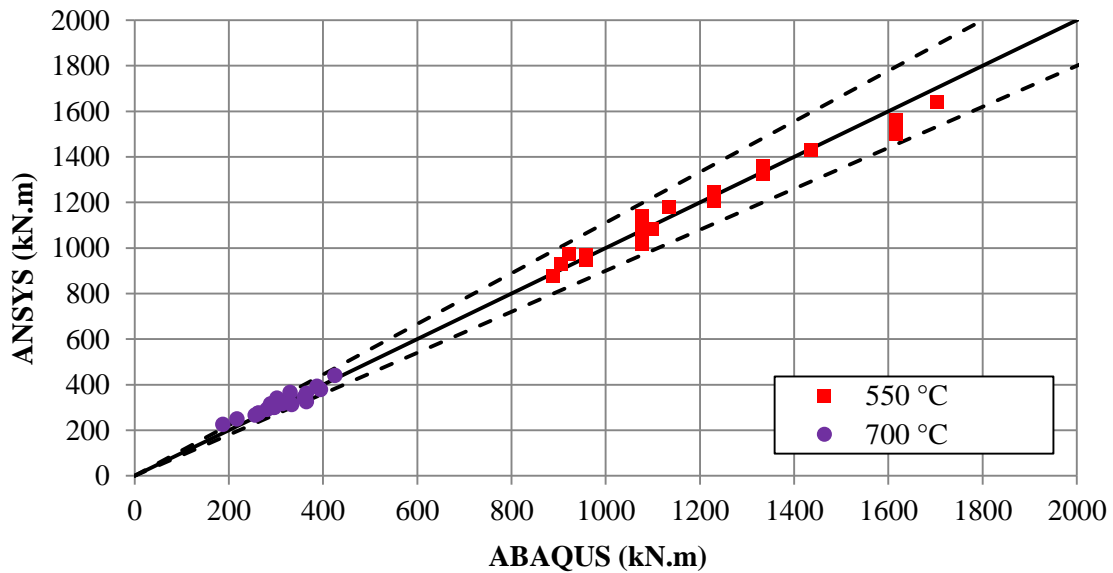


Figure 66 : Distribution of the results between ABAQUS and ANSYS

At 550 °C the differences between the concerned softwares always remain fewer than 10%. At 700 °C, most of the cases remain in the 10% tolerance range. However some cases are slightly out of it but it can be due to some problems encountered in ANSYS when taking account of residual stress at very high temperatures. Partner 4 (UniAv) provided additional results for the first studied section type. This enhanced the consistency study and proved that SAFIR and ANSYS also had good agreement for this study, see following diagram (Figure 67):

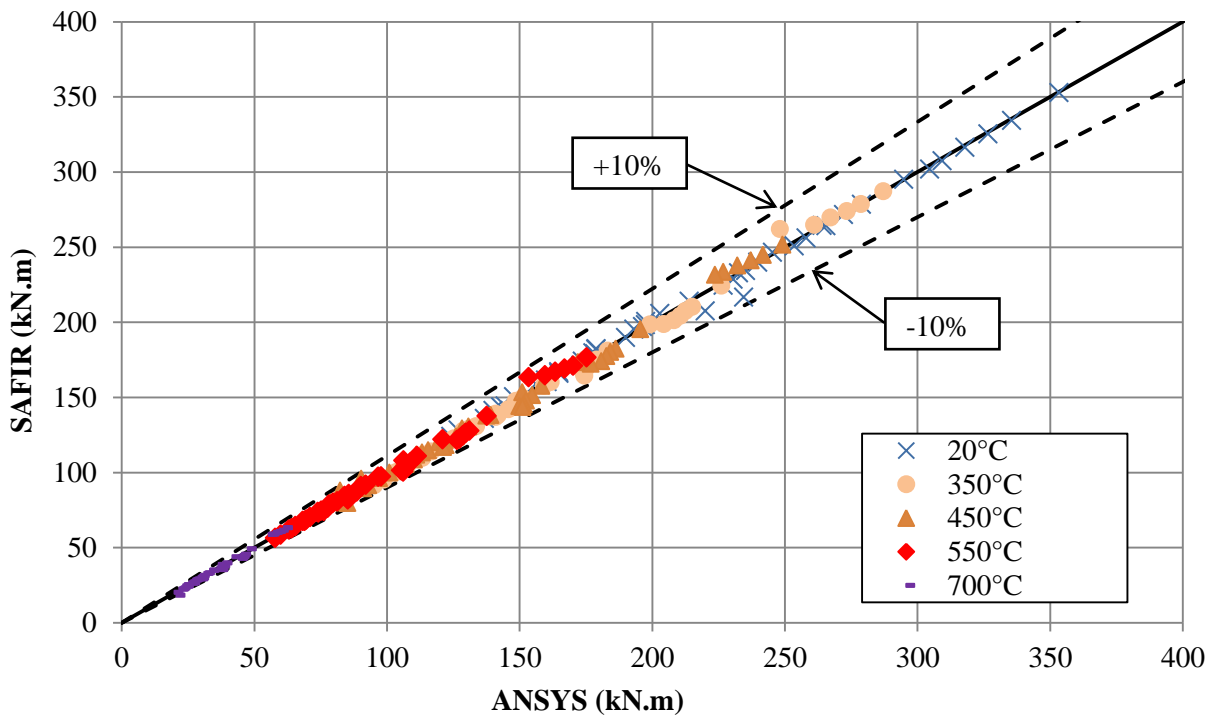


Figure 67 : Distribution of the results between SAFIR and ANSYS

Those additional results reinforce the agreement between used softwares and let the partners conduct the main part of the parametric study. The results are listed and described below as comparisons with current Eurocode design rules.

As all the cases of the numerical parametric study are conducted with and without the application of the residual stress, it is necessary to know the effect of residual stress on the cross-sectional resistance of the beam. The following diagrams show the dispersion of the results according to the use or not of residual stress, see Figure 68 to Figure 71:

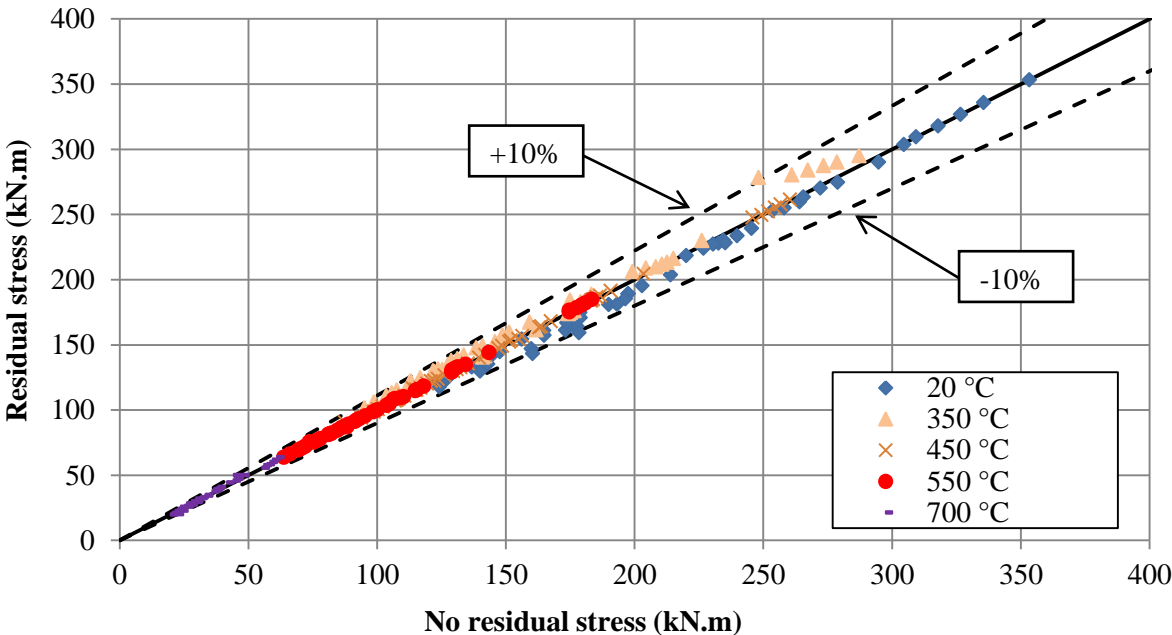


Figure 68 : Section 1 - S355 - Influence of the residual stress on the cross-sectional resistance

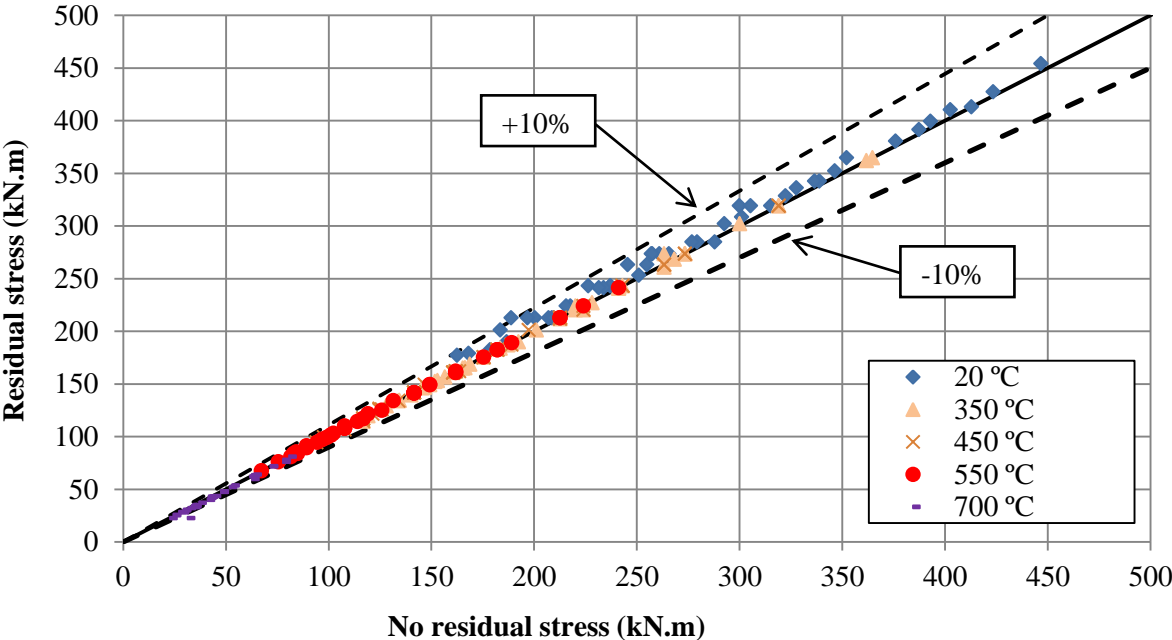


Figure 69 : Section 1 - S460 - Influence of the residual stress on the cross-sectional resistance

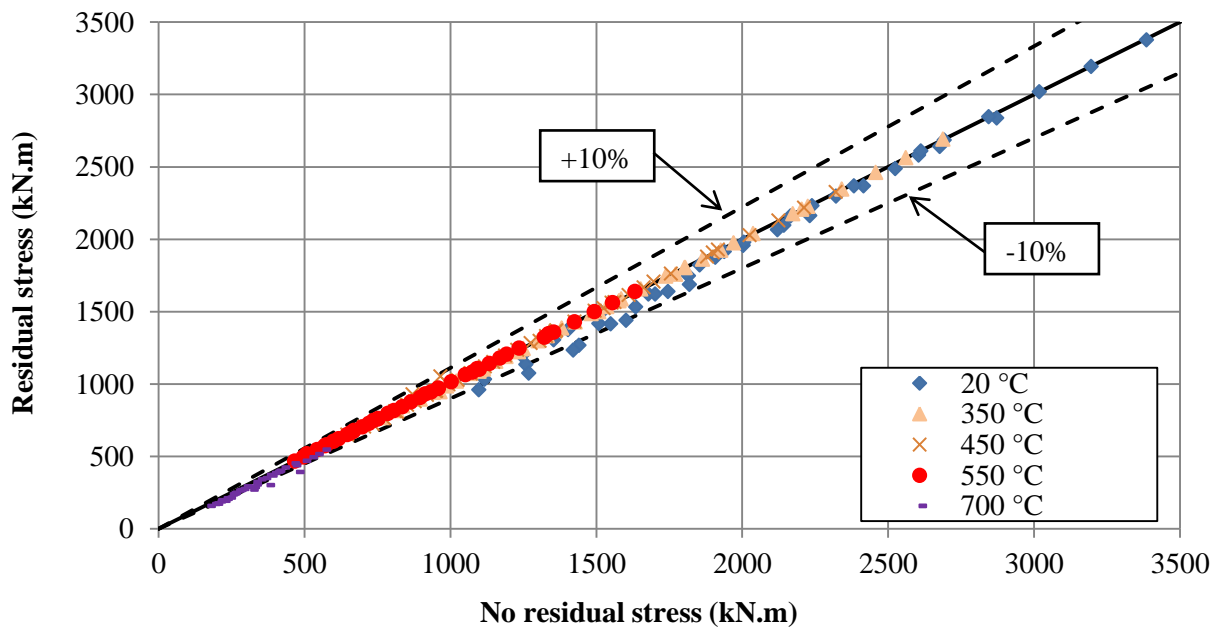


Figure 70 : Section 2 – S355 - Influence of the residual stress on the cross-sectional resistance

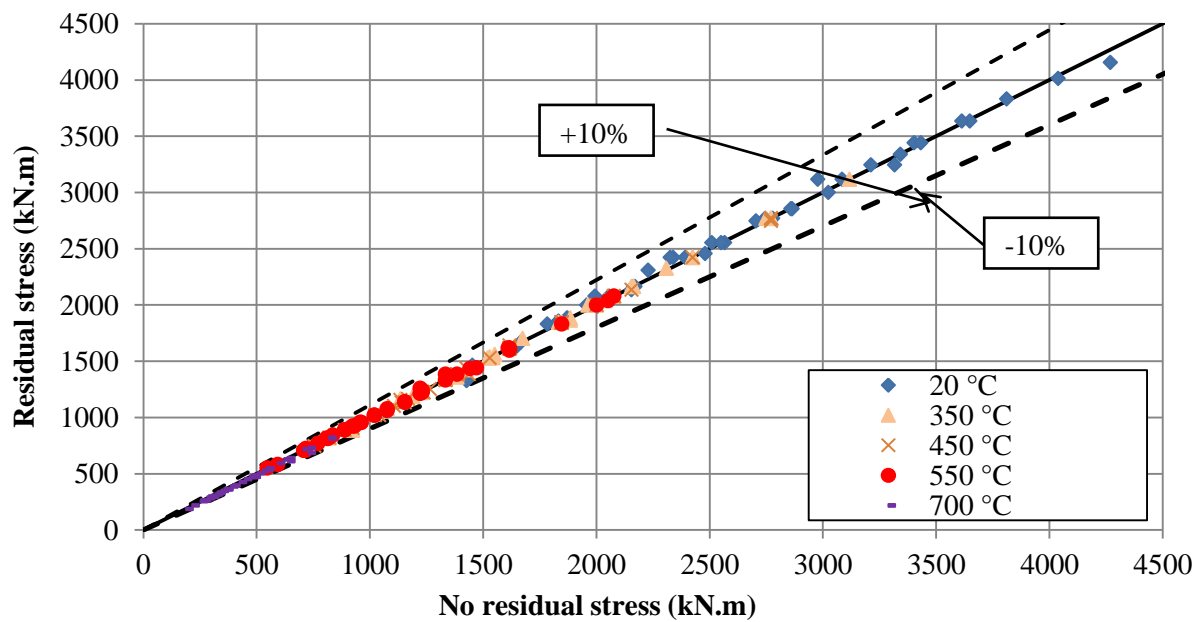


Figure 71 : Section 2 – S460 - Influence of the residual stress on the cross-sectional resistance

As a conclusion of these calculations it appears that at high temperatures residual stress does not influence the cross-sectional resistance of the beams submitted to simple bending. At room temperature the residual stress slightly modifies the cross-sectional resistance of the element.

According to EN 1993-1-2, the pure bending moment resistance, $M_{fi,\theta,Rd}$ of a steel member with its cross-section in class 1,2 or 3 at a uniform temperature θ can be determined on the basis of the following expression:

$$M_{fi,\theta,Rd} = k_{y,\theta} \left[\frac{\gamma_{M,0}}{\gamma_{M,fi}} \right] M_{Rd} \quad (1)$$

Where $k_{y,\theta}$ is the reduction factor of the yield strength of a steel at temperature θ , $\gamma_{M,fi}$ is the partial factor of steel for the fire situation.

In the case of class 4 cross-section steel members, the previous formula becomes:

$$M_{fi,\theta,Rd} = k_{0.2p,\theta} \left[\frac{\gamma_{M,0}}{\gamma_{M,fi}} \right] M_{Rd} \quad (2)$$

The previously cited different reduction factors are illustrated in Figure 72 and are available in EN 1993-1-2:

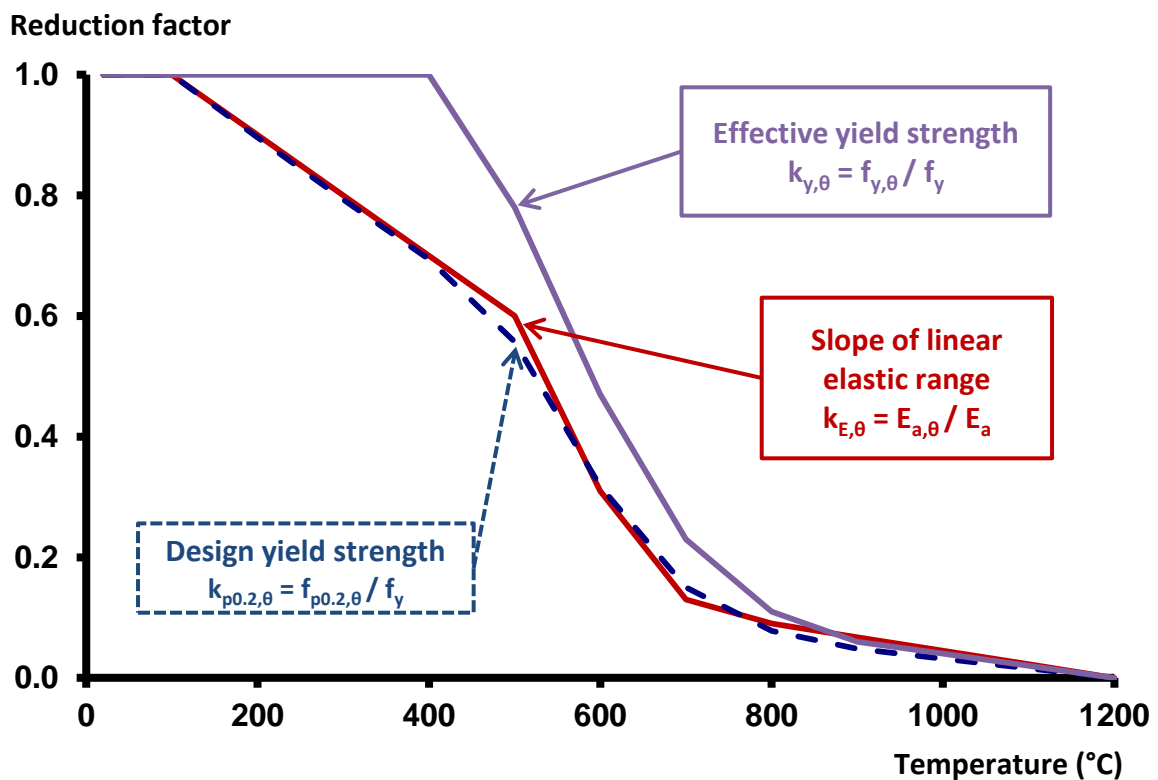


Figure 72: Reduction factors for the stress-strain relationship of hot-rolled class 4 steel sections at elevated temperatures

The bending resistance moment in fire conditions $M_{fi,Rd}$ of a cross-section is determined with the following expressions in function of its class:

$M_{fi,\theta,Rd} = M_{fi,pl,Rd} = \frac{k_y W_{pl} f_y}{\gamma_{M,0}}$	for class 1 or class 2 cross-sections	(3)
$M_{fi,\theta,Rd} = M_{fi,el,Rd} = \frac{k_y W_{el} f_y}{\gamma_{M,0}}$	for class 3 cross-sections	(4)
$M_{fi,\theta,Rd} = M_{fi,eff,Rd} = \frac{k_{0,2p,\theta} W_{eff} f_y}{\gamma_{M,0}}$	for class 4 cross-sections	(5)

With a small simplification and as $\gamma_{M,fi}$ is usually equal to 1, we get for class 4 cross-sections in fire conditions the following equation:

$$M_{fi,\theta,Rd} = k_{0,2p,\theta} W_{eff} f_y \tag{6}$$

Where W_{eff} is the effective section modulus of the section.

It can be found easily that the design moment resistance in fire conditions for steel members with class 4 cross-sections is determined in a different way than other classes with the use of the reduction factor $k_{0,2p,\theta}$ and the effective section modulus W_{eff} . The cross-sectional resistances of proposed beams are calculated following the rules of the EN 1993-1-2. The following diagrams show the comparison between the results obtained with the simplified method of EN 1993-1-2 and the results of the numerical parametric study for the two studied steel grades and the three chosen section dimensions (from Figure 73 to Figure 78):

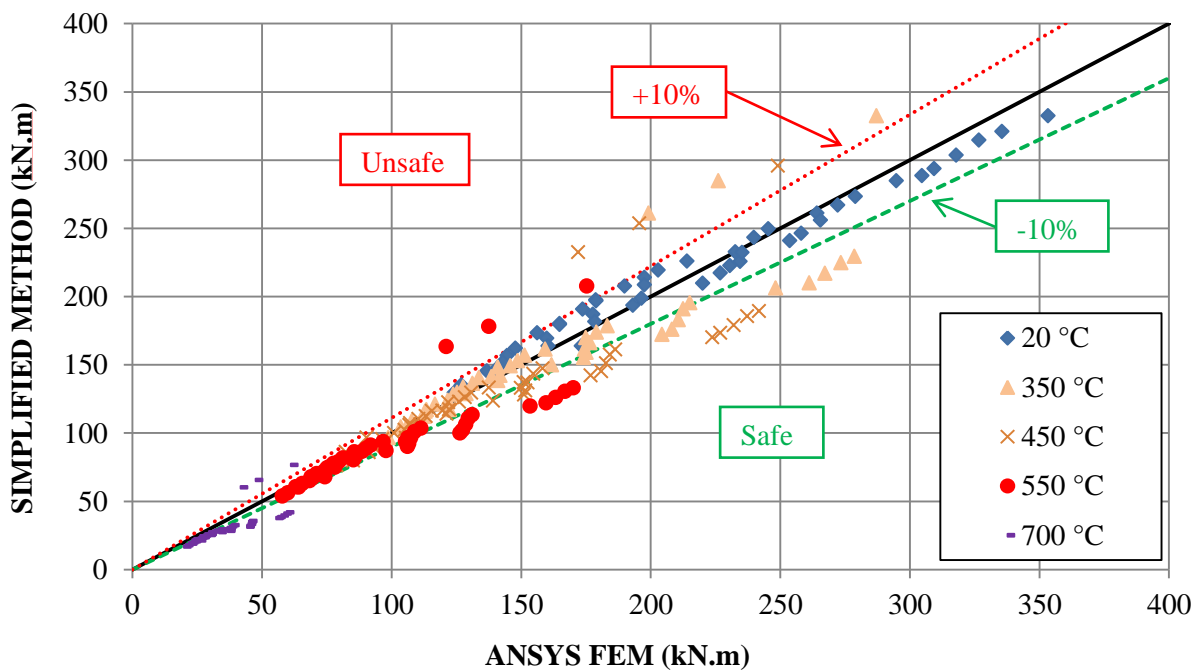


Figure 73 : Section 1 - S355 - Distribution of the results between Eurocode and ANSYS

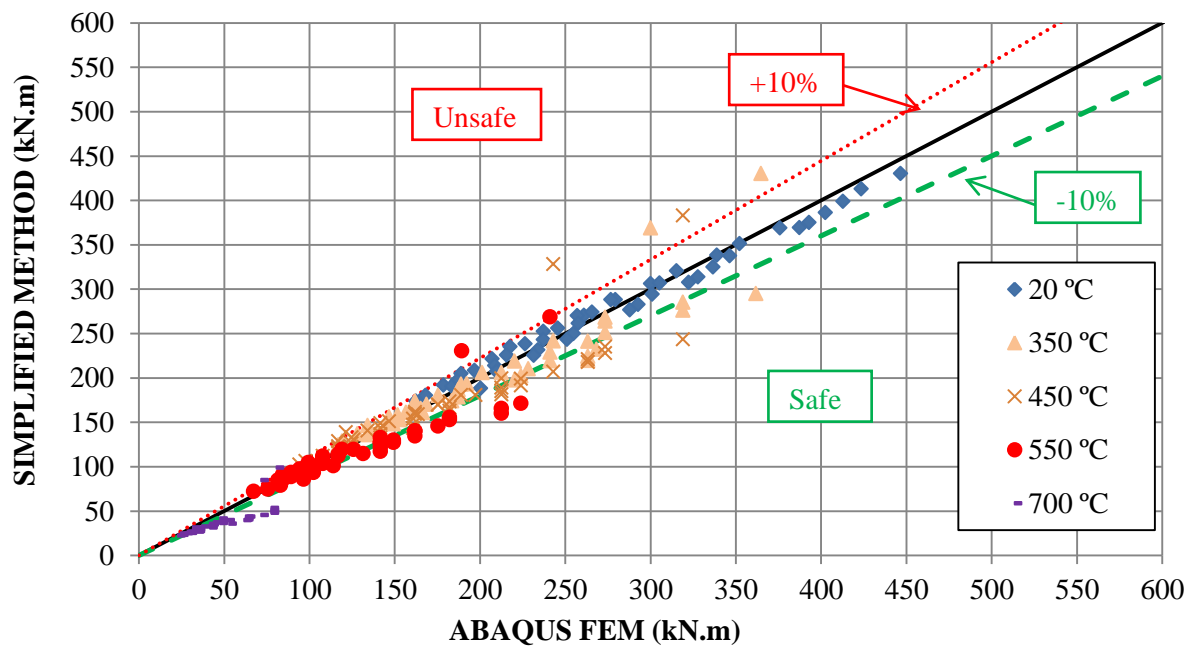


Figure 74 : Section 1 - S460 - Distribution of the results between Eurocode and ABAQUS

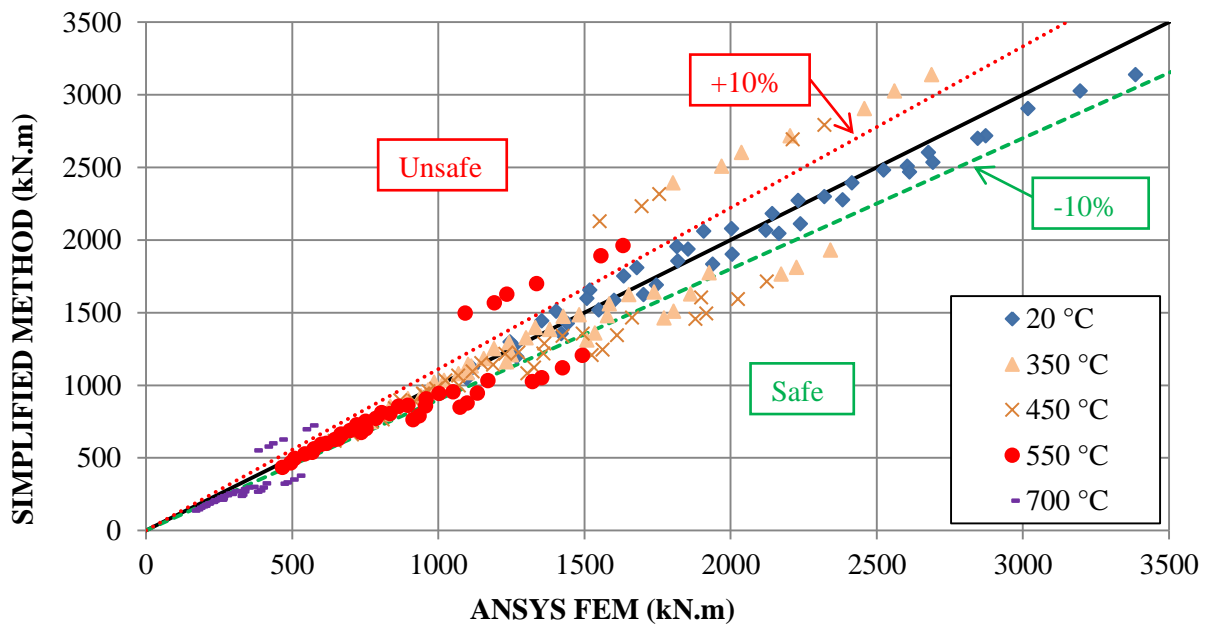


Figure 75 : Section 2 - S355 - Distribution of the results between Eurocode and ANSYS

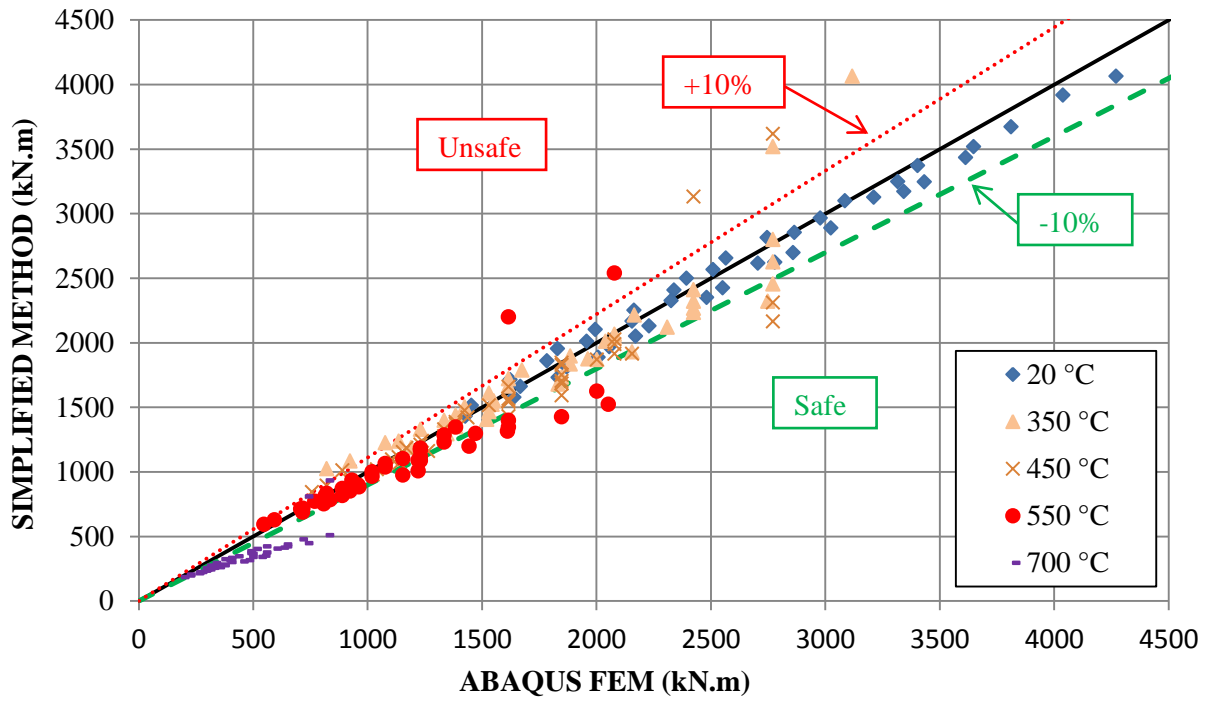


Figure 76 : Section 2 - S460 - Distribution of the results between Eurocode and ABAQUS

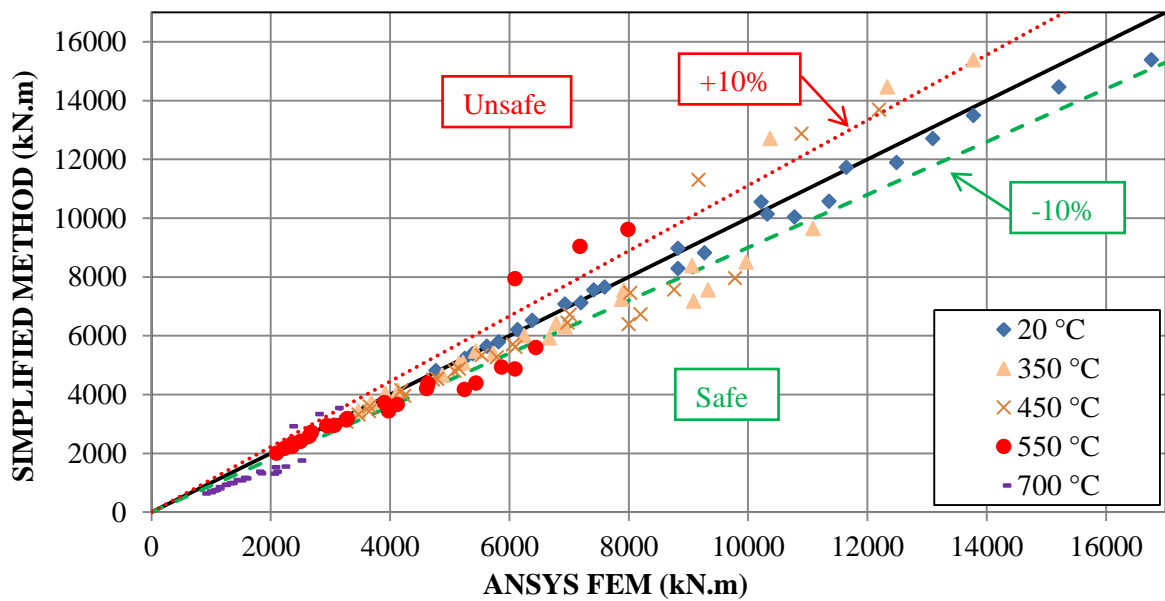


Figure 77 : Section 3 - S355 - Distribution of the results between Eurocode and ANSYS

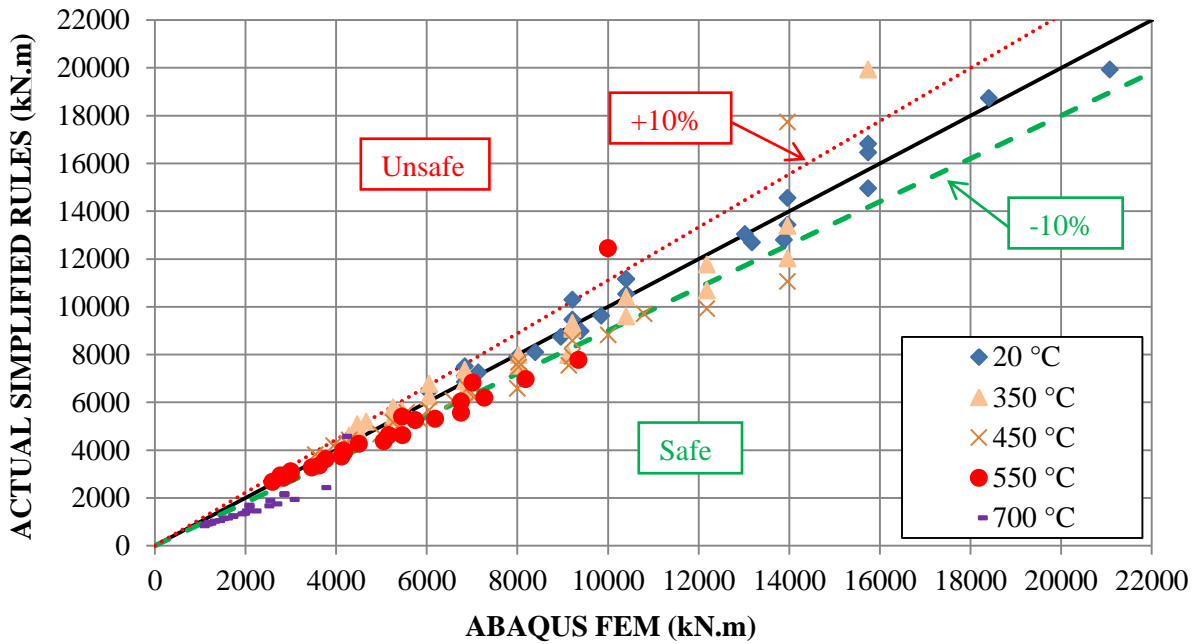


Figure 78 : Section 3 - S460 - Distribution of the results between Eurocode and ABAQUS

An important discrepancy is observed between the current simple calculation rules and the numerical models. This is the case for the three studied cross-sections and regardless the steel grade. It appears that some points are situated on the safe side but some others are situated on the unsafe side. A small investigation on these results helped to identify two different behaviours.

In fact, the cross-sections considered as class 3 cross-sections but “located” close to the boundary between class 3 and class 4 have their cross-sectional resistance over-estimated when calculated by current Eurocode design rules (see Figure 79 to Figure 82):

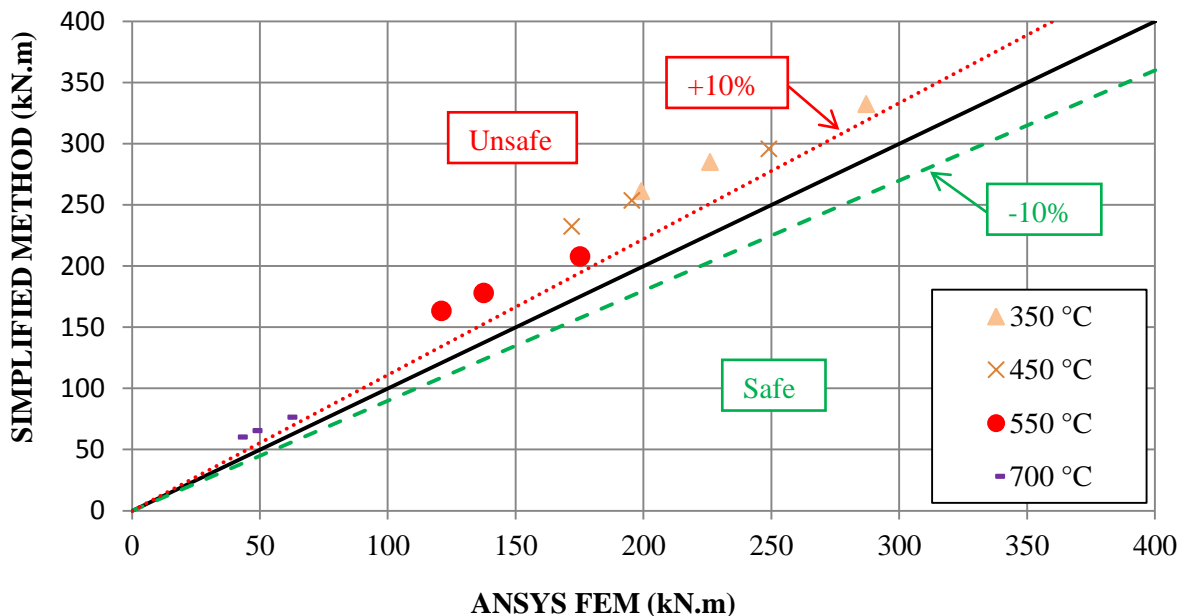


Figure 79 : Section 1 - S355 - Overestimated resistance in current simplified method

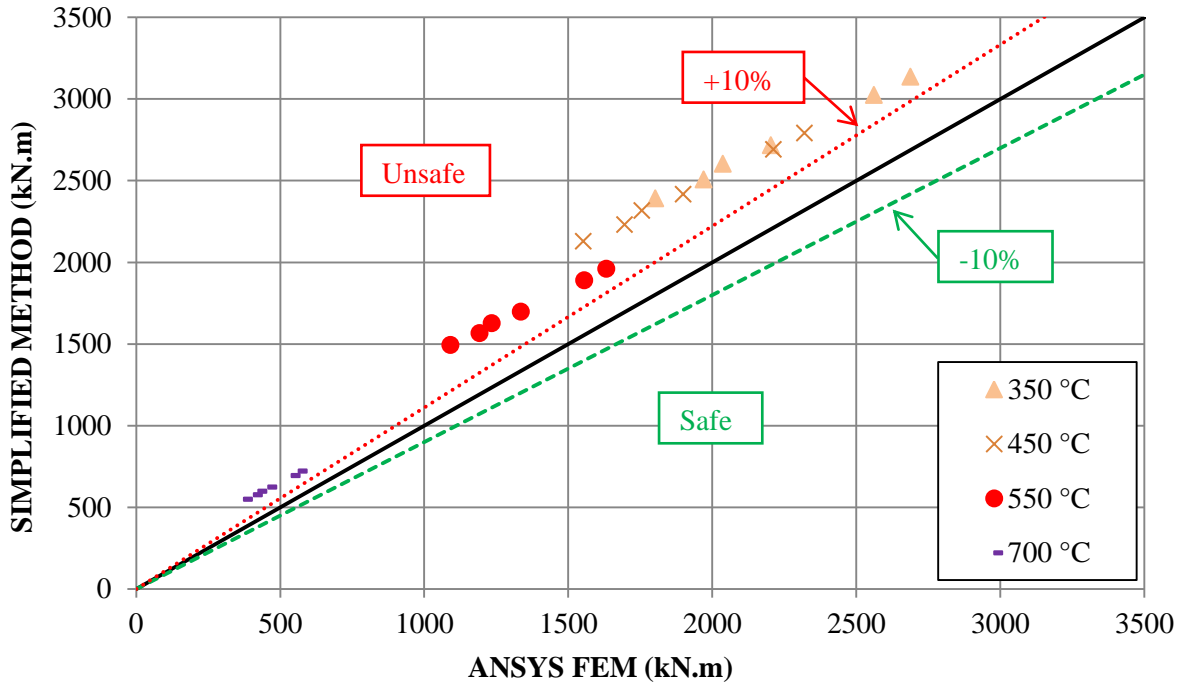


Figure 80 : Section 2 - S355 - Overestimated resistance in current simplified method

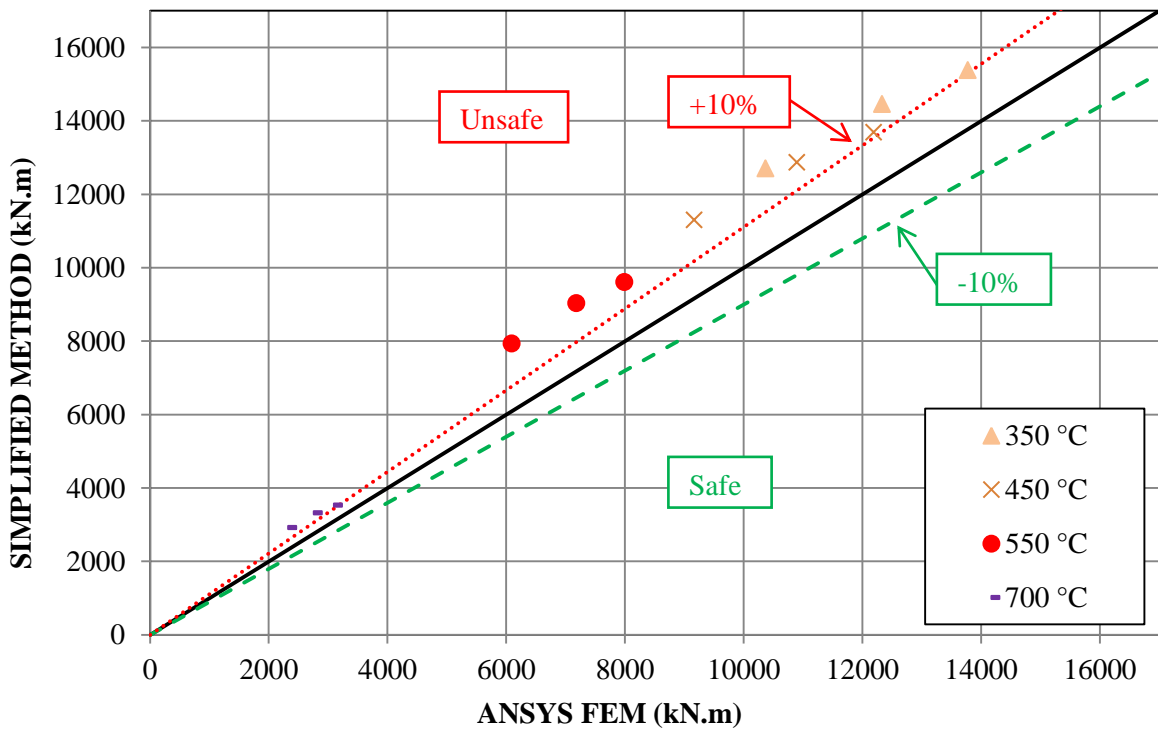


Figure 81 : Section 3 - S355 - Overestimated resistance in current simplified method

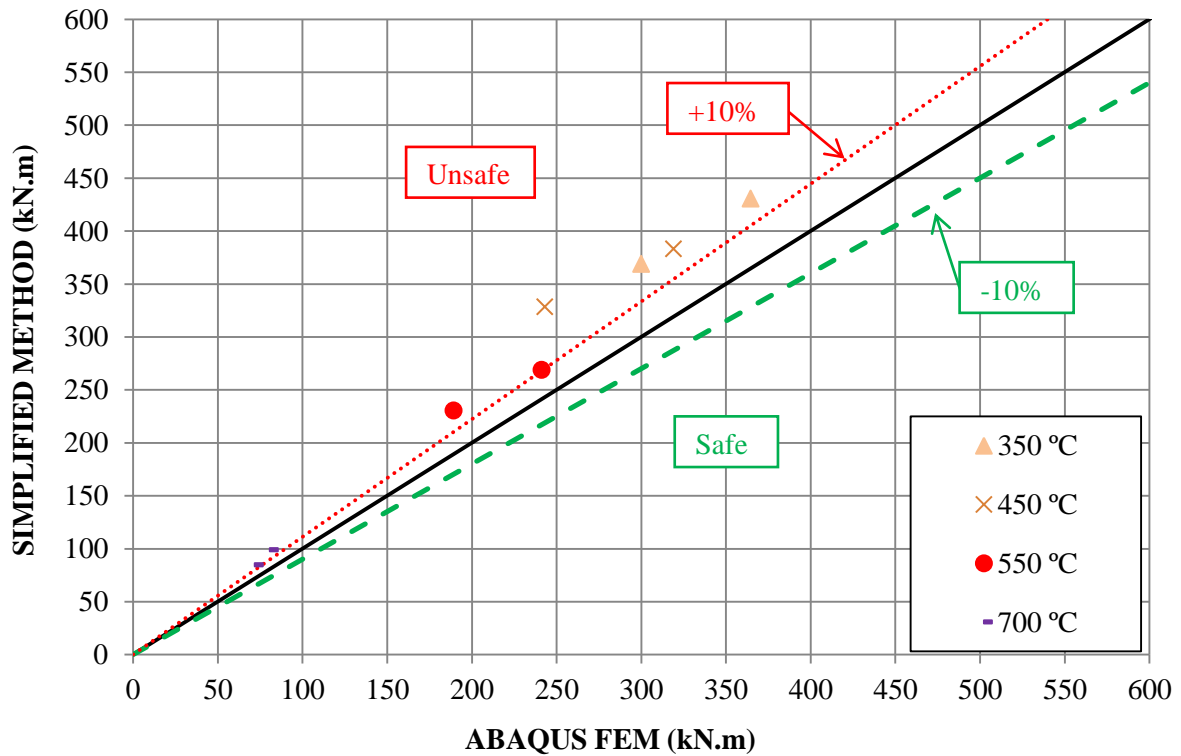


Figure 82 : Section 1 - S460 - Overestimated resistance in current simplified method

This behaviour is noticeable regardless of the cross-section size and the steel grade. However, by changing the steel grade the class boundaries have also been modified, that is the reason why some “boundary” cases for S355 were real class 4 cases for steel grade S460 and are not considered in the last diagram.

On the other side cross-sectional resistance of class 4 cross-sections whose flanges are class 2 or class 3 is underestimated when calculating with the help of the current EN simple design rule. Currently, for these cases the design rule is too much conservative (see Figure 83 to Figure 86):

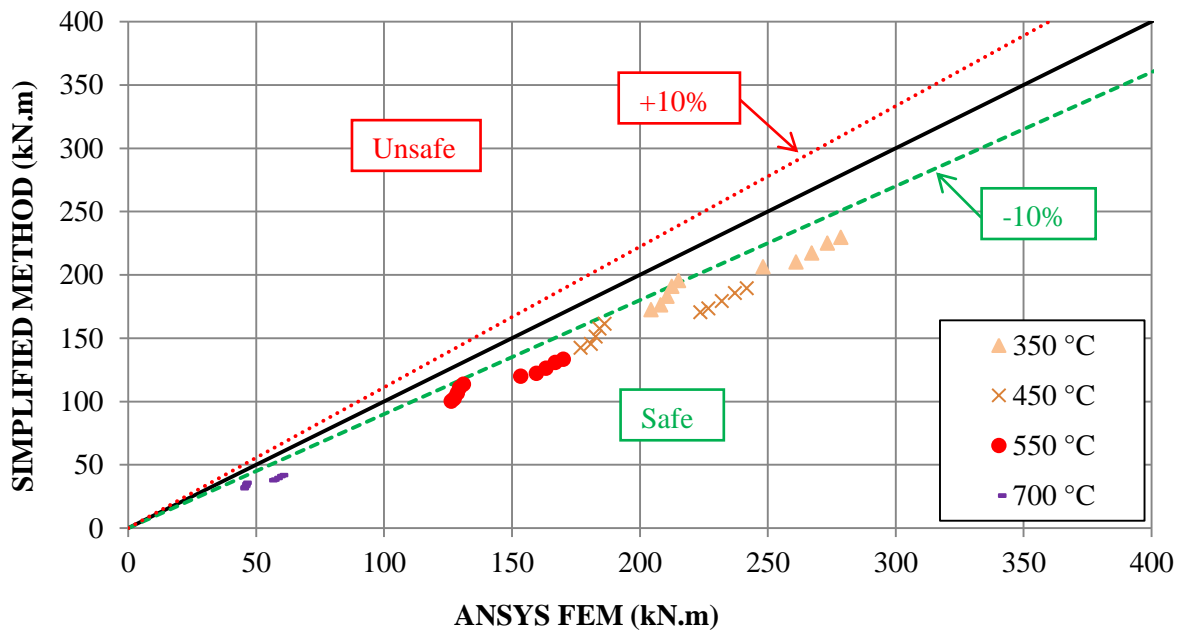


Figure 83 : Section 1 - S355 - Underestimated resistance in current simplified method

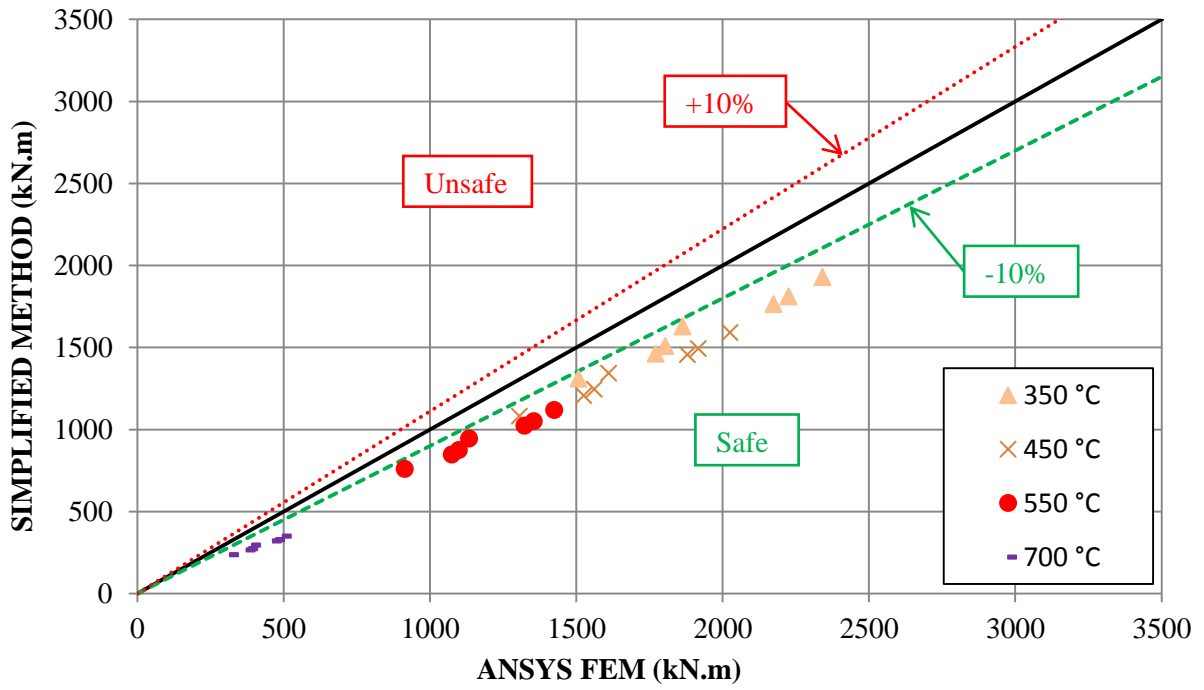


Figure 84 : Section 2 - S355 - Underestimated resistance in current simplified method

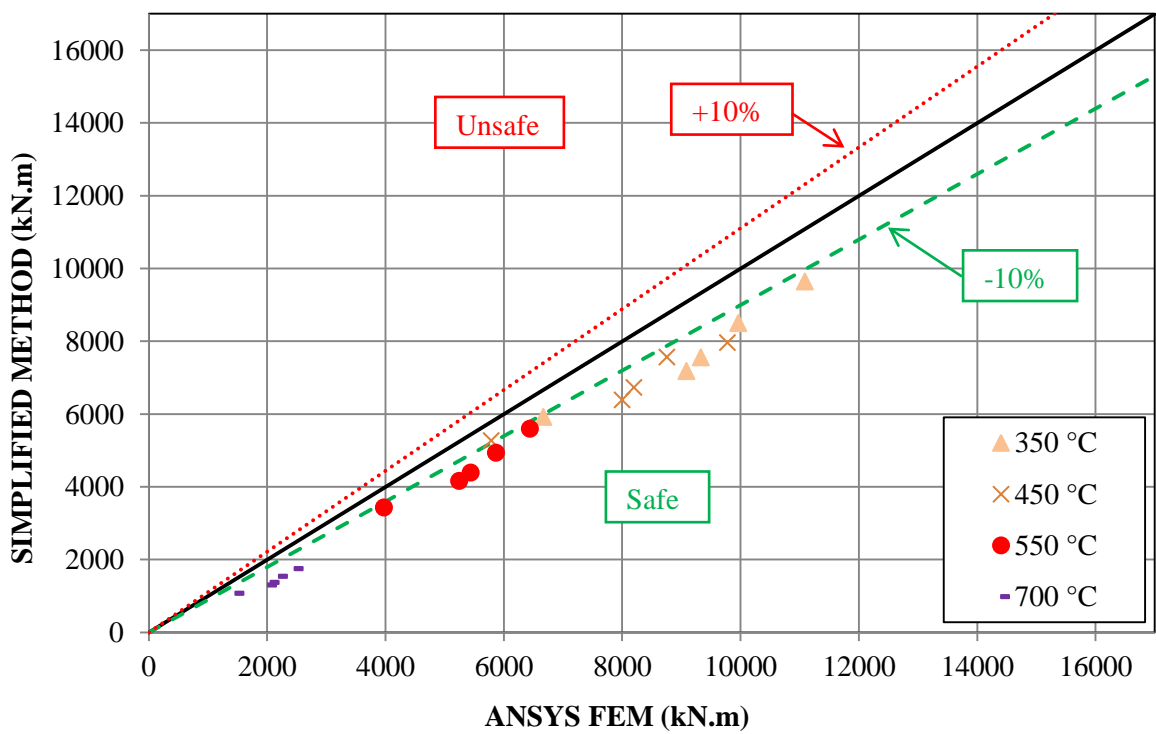


Figure 85 : Section 3 - S355 - Underestimated resistance in current simplified method

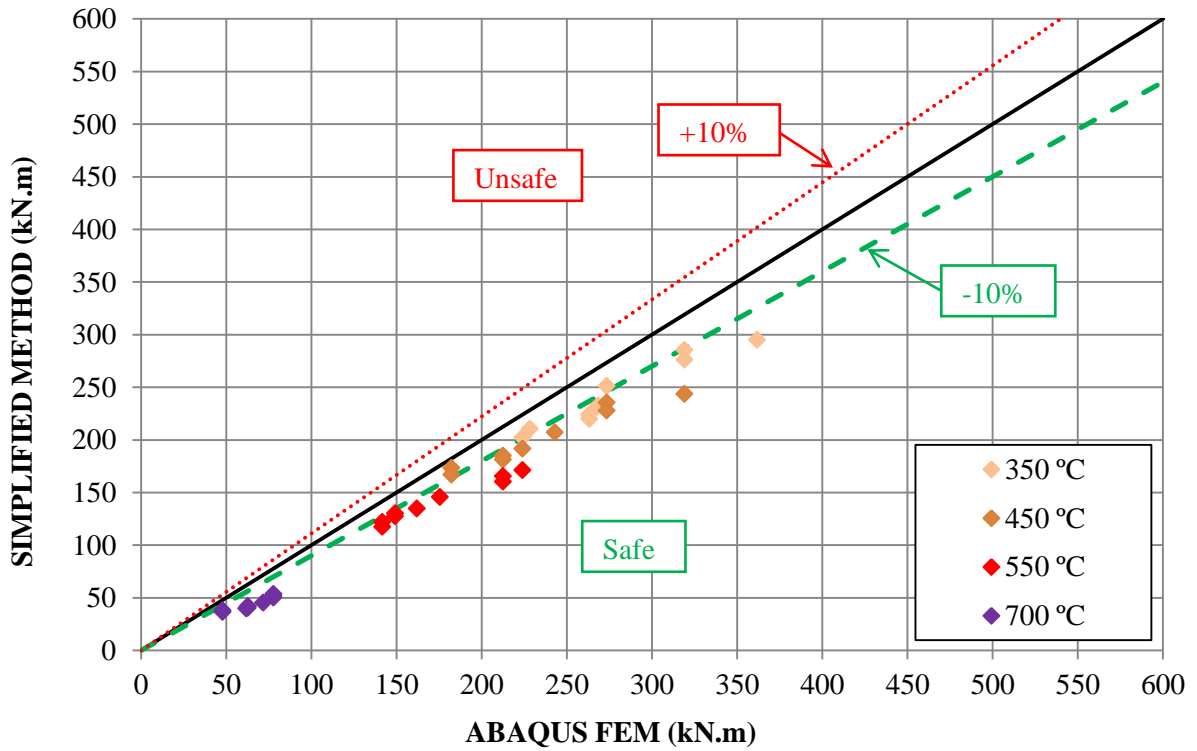


Figure 86 : Section 1 - S460 - Underestimated resistance in current simplified method

This behaviour is noticeable regardless of the cross-section size and the steel grade.

Additional cases were conducted by UniAv with software SAFIR and confirm the previous behaviours obtained with ABAQUS and ANSYS:

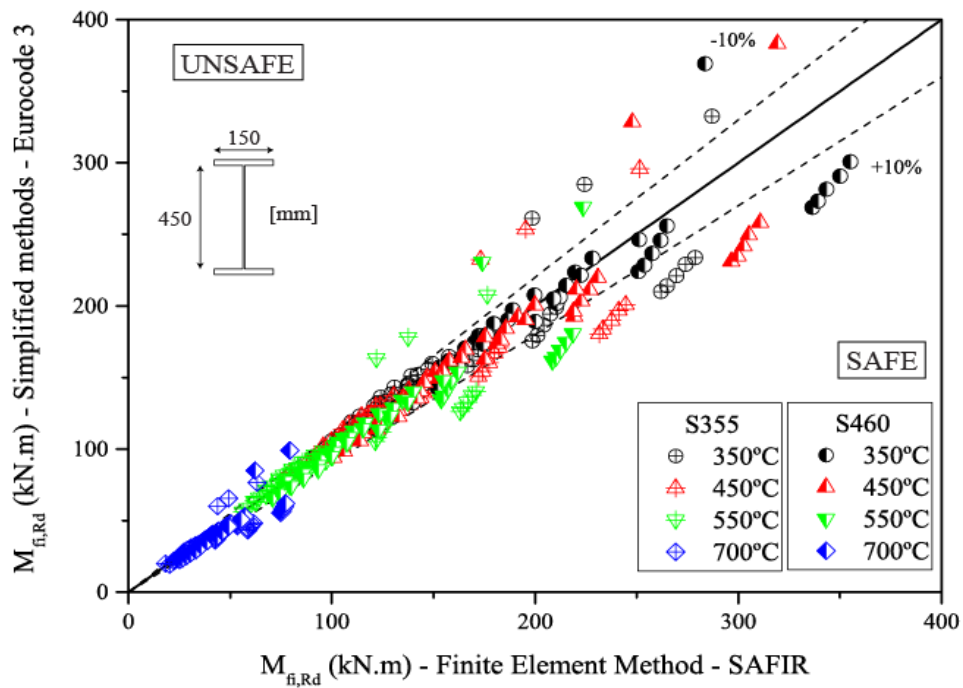


Figure 87 : Section 1 - S355 - S460 - Distribution of the results between Eurocode and SAFIR

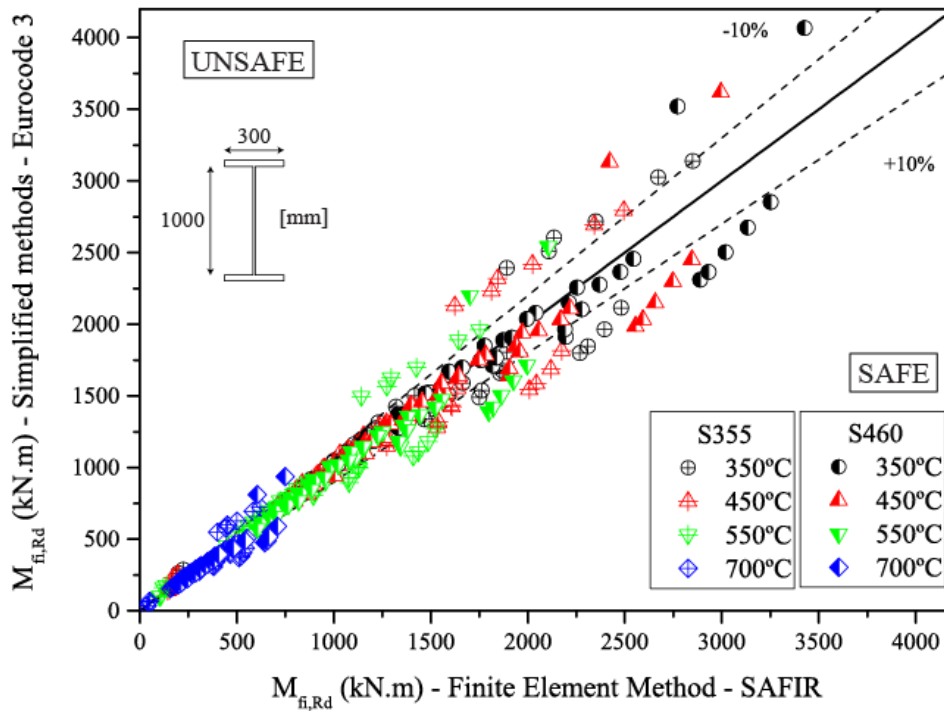


Figure 88 : Section 2 - S355 - S460 - Distribution of the results between Eurocode and SAFIR

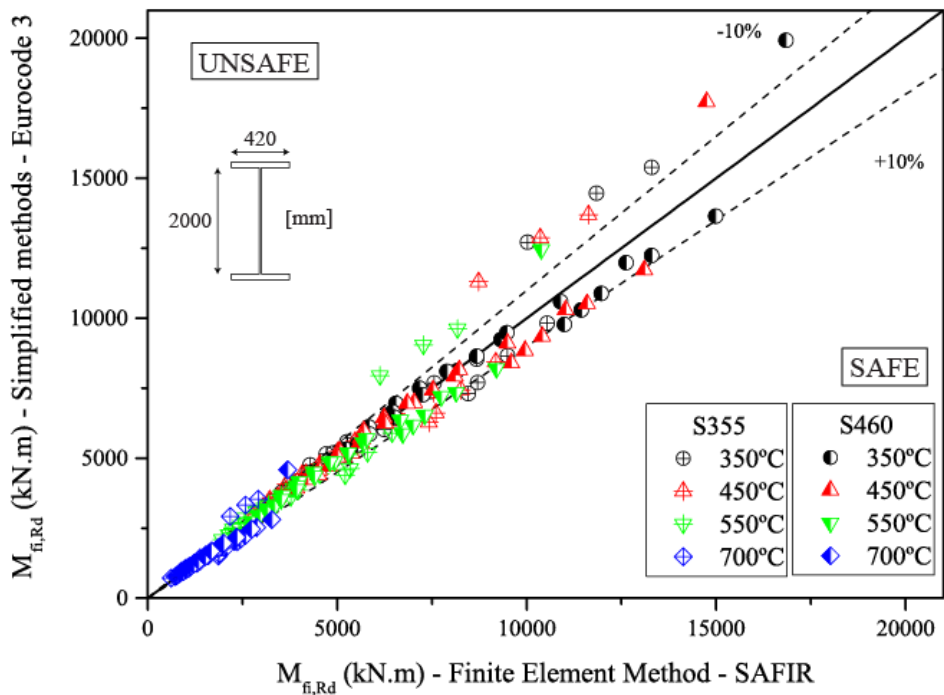


Figure 89 : Section 3 - S355 - S460 - Distribution of the results between Eurocode and SAFIR

The following general conclusions can be derived from the correlation analysis of current simple design rules of Eurocode 3 with respect to the bending moment resistance of class 4 steel members in fire situation:

- the discrepancy between the simple design rules and the numerical analysis is quite important, regardless of the cross-section size and temperature levels

- the simple design rules underestimate the bending moment resistance of class 4 steel members with the flanges in class 2 or class 3, they are too conservative
- for steel members at the border between class 3 and class 4, the jump in terms of bending moment resistance according to simple design rules is not physical at all
- in case of class 4 steel members with both flanges and web in class 4, the results given by the simple design rules and those given by the numerical analysis are close to each other

As a result of above observations, an alternative solution to the current simple design rules of the EN 1993-1-2 for the bending moment resistance of class 4 and also class 3 steel members is proposed in order to improve the accuracy of current simple design rules. This new solution for simple design method of class 4 steel members under simple bending in fire condition is developed on the basis of the Winter's formulation for the calculation of the ultimate strength of steel plates under compression. This method was firstly proposed by the University of Aveiro by P. VILA REAL, N. LOPES and C. COUTO in *Effective width method to account for the local buckling of steel thin plates at elevated temperatures* [3].

The key points of this new method are:

- the design strength of steel at elevated temperatures is $f_{y,0}$ whatever the class of the steel member is
- the effective cross-section of thin wall steel members is determined on the basis of the wall slenderness instead of using the class of cross-sections

The first point permits to keep the same design strength for steel at elevated temperatures which simplify the design rules and the second one allows a continuous resistance evolution with respect to slenderness of cross-section walls.

The final retained method is described in the following expressions. The following relations are proposed for effective length of walls in compression:

- In the case of internal components (web in bending):

$$\rho = \frac{\left(\bar{\lambda}_p + 0.9 - \frac{0.26}{\varepsilon}\right)^{1.5} - 0.055(3 + \psi)}{\left(\bar{\lambda}_p + 0.9 - \frac{0.26}{\varepsilon}\right)^3} \leq 1.0 \quad (7)$$

- And in the case of outstand elements (flange under compression):

$$\rho = \frac{\left(\bar{\lambda}_p + 1.1 - \frac{0.52}{\varepsilon}\right)^{1.2} - 0.188}{\left(\bar{\lambda}_p + 1.1 - \frac{0.52}{\varepsilon}\right)^{2.4}} \leq 1.0 \quad (8)$$

Where $\bar{\lambda}_p$ represents the normalised slenderness at room temperature and is given by the following equation:

$$\bar{\lambda}_p = \sqrt{\frac{f_y}{\sigma_{cr}}} = \frac{b}{28.4\varepsilon\sqrt{k_\sigma}} \quad (9)$$

Where f_y is the yield strength and σ_{cr} is the Euler's critical stress and b is the width of the plate, t its thickness, ε is the factor depending on f_y and k_σ the buckling factor corresponding to the stress ratio and to the boundary conditions.

$$\varepsilon = \sqrt{\frac{235}{f_y}} \quad (10)$$

Once the effective cross-section is determined with above relations, the bending moment resistance of the concerned steel member can be determined as follows:

$$M_{fi,\theta,Rd} = k_{y,\theta} W_{eff} f_y \quad (11)$$

According to this new design rule, only the relative slenderness $\bar{\lambda}_p$, the coefficient relative to stress distribution state over the length of the wall ψ and ε are necessary to determine the effective width of the wall.

Once again, the results in terms of bending moment resistance obtained with these new relations for effective width of thin walls are systematically compared with the results of numerical analysis in order to show the accuracy of these modified simple design rules:

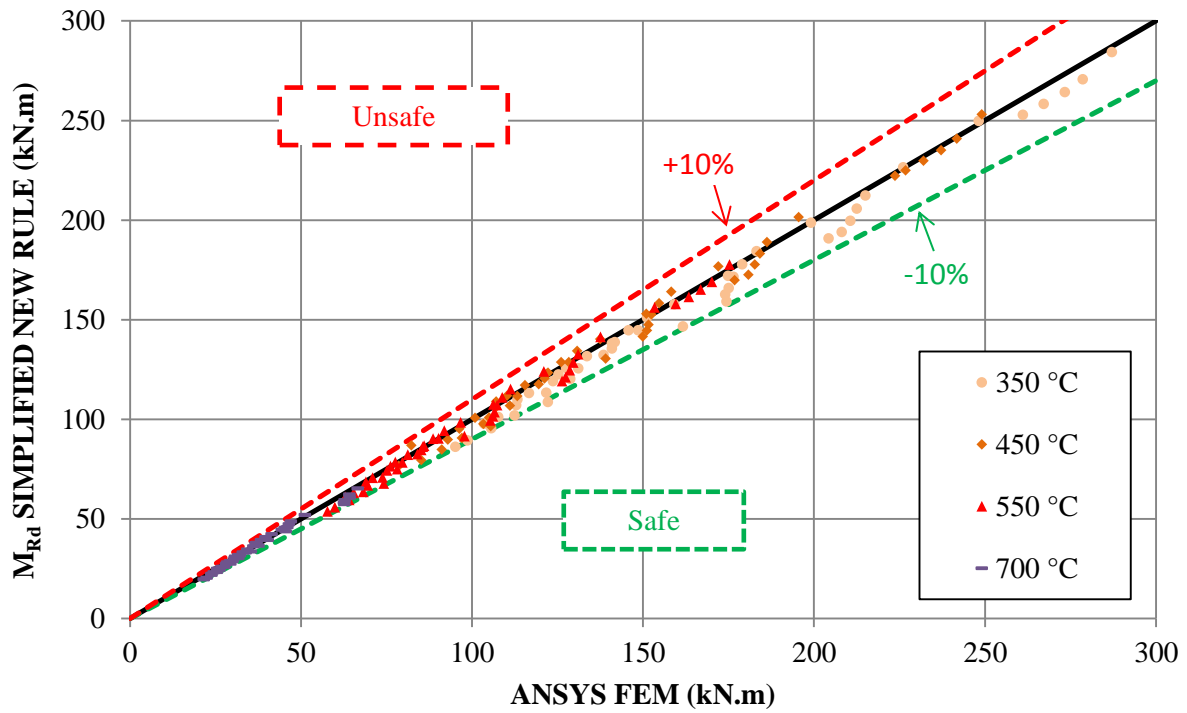


Figure 90 : Comparison between numerical analysis and modified new simple design rule for bending moment resistance of section type 1 with steel grade S355

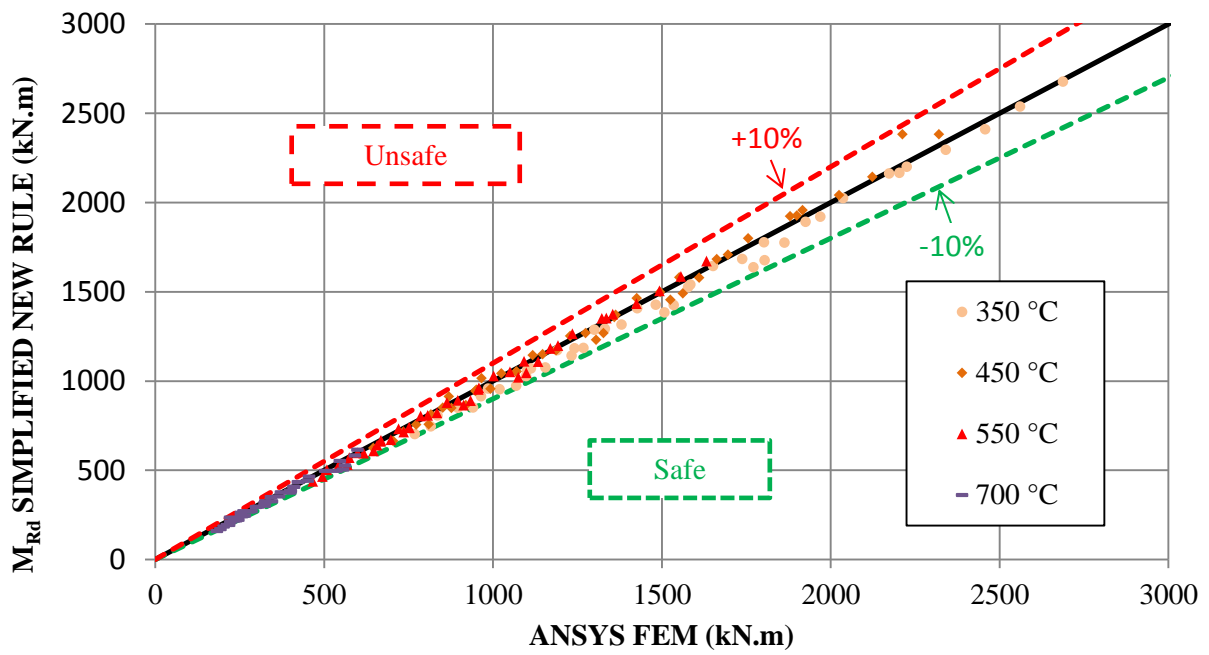


Figure 91 : Comparison between numerical analysis and modified new simple design rule for bending moment resistance of section type 2 with steel grade S355

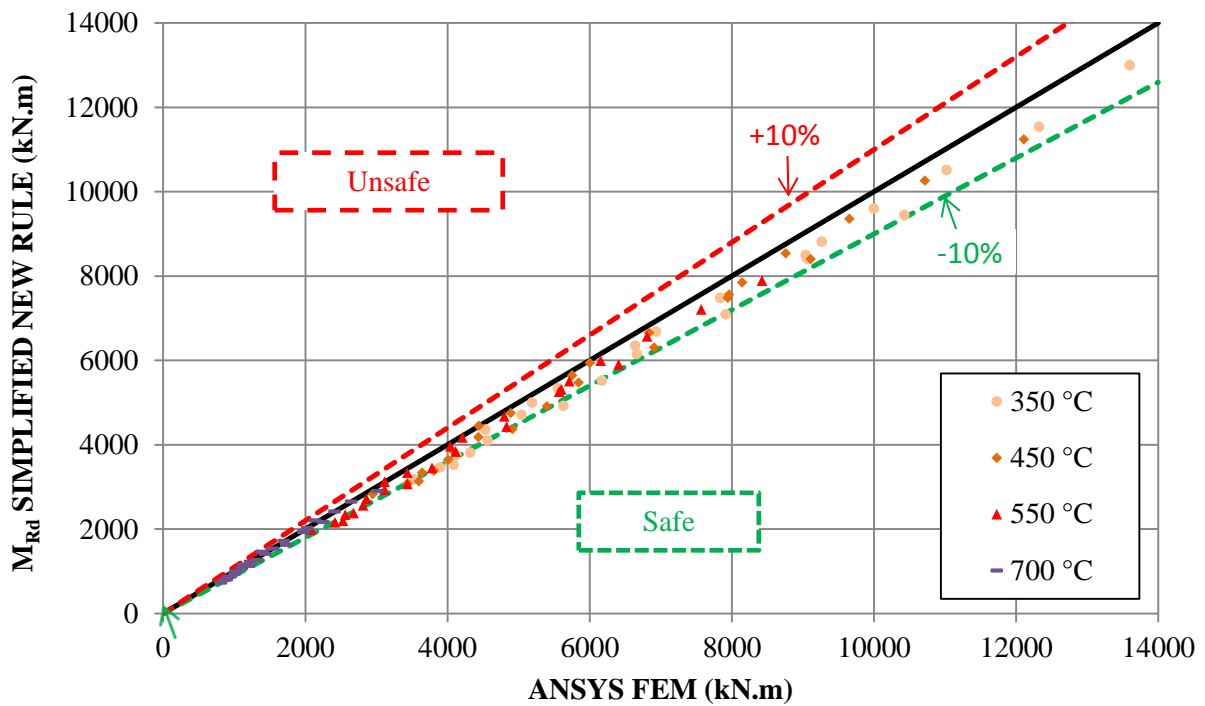


Figure 92 : Comparison between numerical analysis and modified new simple design rule for bending moment resistance of section type 3 with steel grade S355

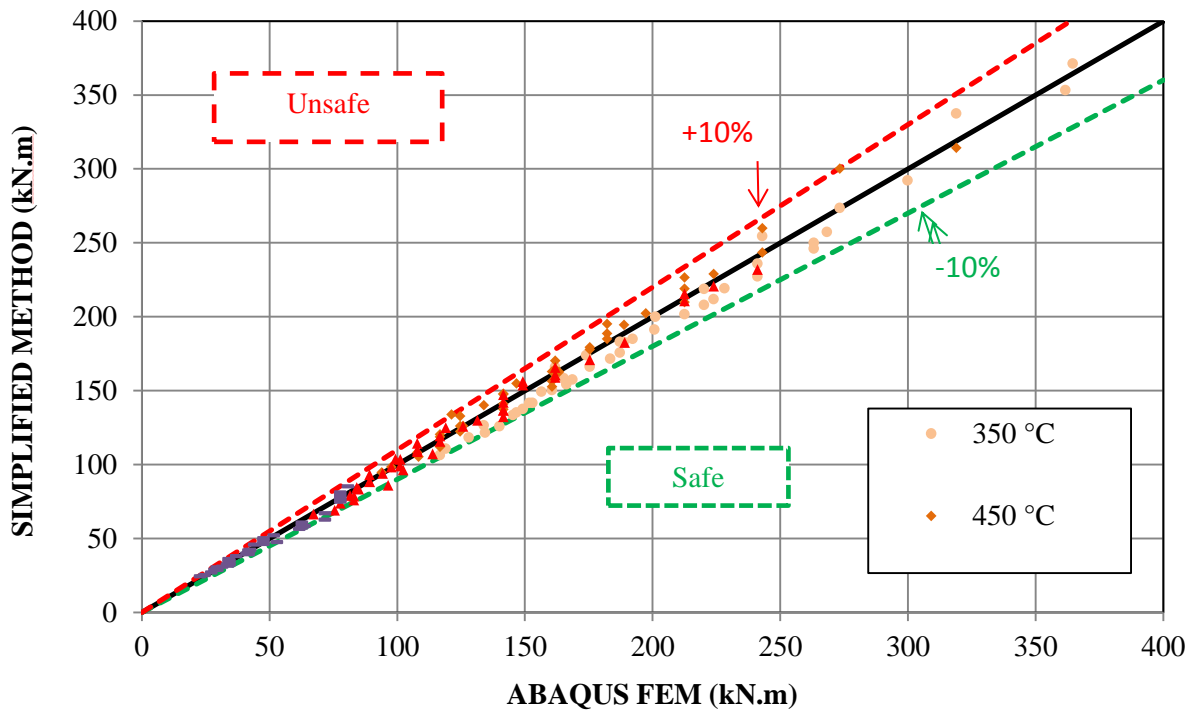


Figure 93: Comparison between numerical analysis and new simple design rule for bending moment resistance of section type 1 with steel grade S460

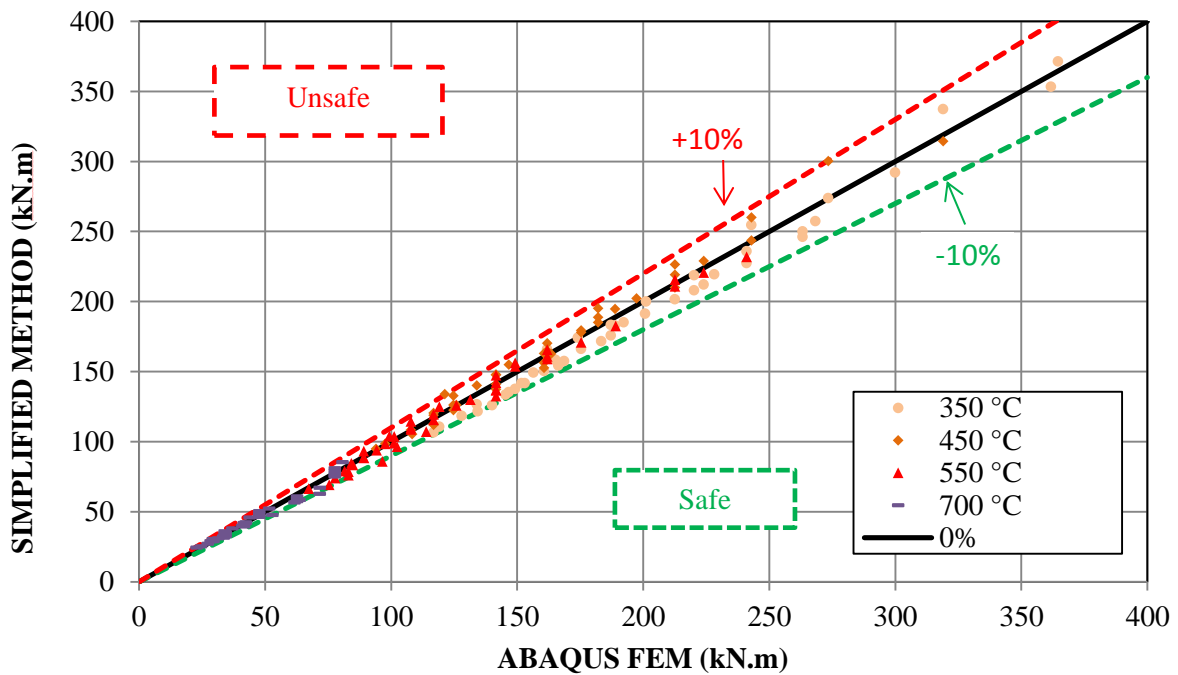


Figure 94: Comparison between numerical analysis and new simple design rule for bending moment resistance of section type 2 with steel grade S460

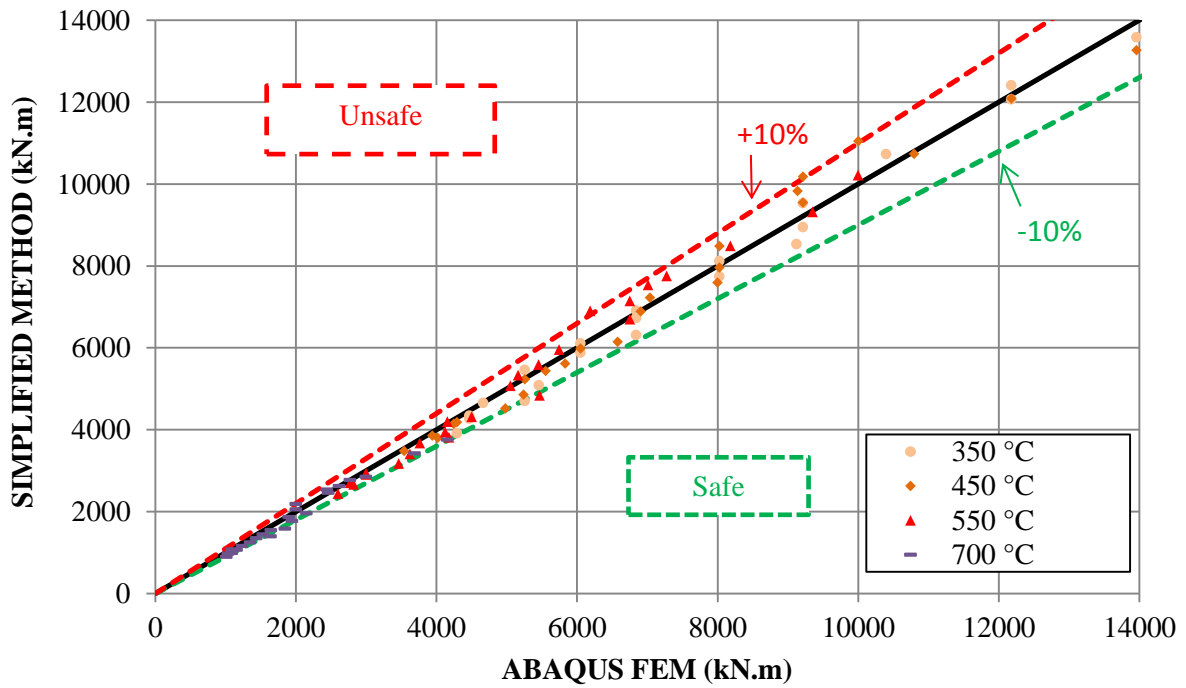


Figure 95: Comparison between numerical analysis and new simple design rule for bending moment resistance of section type 3 with steel grade S460

This parametric study allows getting a number of numerical results to check the accuracy of current simple design rules of the fire part of Eurocode 3. The comparison between the numerical analysis and above simple design rules has clearly highlighted the weakness of the latter. That is the reason why a new simple design rule for class 3 and class 4 steel members with I or H shape cross-sections is proposed. The correlation investigation has revealed that the improved new simple design rules predicts with a great accuracy the bending moment resistances of class 3 and class 4 steel members with I or H shape cross-sections.

2.2 Numerical parametric study for class 4 beams subjected to lateral torsional buckling

This parametric study is set up to have an important set of results regarding the lateral torsional buckling resistance of welded or hot-rolled cross-sections subjected to bending. It is necessary to study the influence of various parameters as the moment distribution and the slenderness of beams.

2.2.1 Presentation of chosen parameters

As for the numerical parametric study on cross-sectional resistance (see 2.1.1), two steel grades (S355 and S460) and five steel temperatures (20, 350, 450, 550 and 700 °C) are investigated. Moreover, nine different values of slenderness are chosen to have a large set of data concerning the consequences of the length of the beam on its bending resistance when lateral torsional buckling occurs. The non-dimensional slenderness values are described hereafter:

$\bar{\lambda}_{LT} =$	0.2	0.4	0.6	0.8	1.0	1.2	1.5	1.8	2.5
------------------------	-----	-----	-----	-----	-----	-----	-----	-----	-----

Table 27: Investigated non-dimensional slenderness

Two types of boundary conditions are defined at both ends of the studied beams:

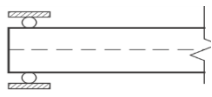
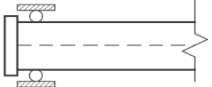
Simply supported – both ends of the beam ($k_z = 1, k_w = 1$)	
Warping prevented – both ends of the beam ($k_z = 1, k_w = 0.5$)	

Table 28: Type of boundary conditions at beam ends

As mentioned above, four moment distributions have been taken into account in the scope of this parametric study:

Uniform bending diagram ($\psi = 1$)	
Triangular bending diagram ($\psi = 0$)	
Bi-triangular bending diagram ($\psi = -1$)	
Parabolic bending diagram	

Table 29: Possible distribution moments

Two different locations for the load are also defined:

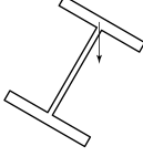
Load applied on the tension flange		Load applied on the compression flange	
---	---	---	---

Table 30: Load location on beams

The list of the simulated constant I sections is given below (Table 31):

Section 1: 450 x t_w + 150 x t_f			
450 x 5 + 150 x 10	Welded and hot-rolled sections	Class 4 web	Class 3 flange
450 x 4 + 150 x 5	Welded and hot-rolled sections	Class 4 web	Class 4 flange
Section 2: 450 x t_w + 250 x t_f			
450 x 5 + 250 x 16	Welded and hot-rolled sections	Class 4 web	Class 3 flange
450 x 4 + 250 x 10	Welded section	Class 4 web	Class 4 flange
450 x 4 + 250 x 5	Welded section	Class 4 web	Class 4 flange
Section 3: 1000 x t_w + 300 x t_f			
1000 x 8 + 300 x 20	Welded and hot-rolled sections	Class 4 web	Class 3 flange
1000 x 7 + 300 x 12	Welded section	Class 4 web	Class 4 flange
1000 x 5 + 300 x 10	Welded section	Class 4 web	Class 4 flange

Table 31 : Used dimensions for constant I sections

The list of the simulated tapered I sections is given in the table below (Table 32):

Section 1: 450 x t_w + 250 x t_f		
h₁ = 450 x 5 + 250 x 16	$h_2 = 0.6 \times h_1$	$h_2 = 250 \times 5 + 250 \times 16$
Section 2: 1000 x t_w + 300 x t_f		
h₁ = 1000 x 8 + 300 x 20	$h_2 = 0.5 \times h_1$	$h_2 = 500 \times 8 + 300 \times 20$
	$h_2 = 0.75 \times h_1$	$h_2 = 750 \times 8 + 300 \times 20$
h₁ = 1000 x 5 + 300 x 10	$h_2 = 0.5 \times h_1$	$h_2 = 500 \times 5 + 300 \times 10$
	$h_2 = 0.75 \times h_1$	$h_2 = 750 \times 5 + 300 \times 10$

Table 32 : Used dimensions for tapered I sections

The beam is meshed with quadrilateral conventional shell elements (namely type S4). Conventional shell elements discretize a body by defining the geometry at a reference surface. In this case the thickness is defined through the section property definition. Conventional shell elements have displacement and rotational degrees of freedom. Only static simulation is used for this numerical parametric study.

Element type S4 is a fully integrated, general-purpose, finite-membrane-strain shell element. The element has four integration points per element.

Concerning the boundary conditions, all the beams are laterally restrained at both ends over the whole height of the web. The node at mid-height of the web is also supported vertically and on one end also horizontally in the direction of the beam axis.

In the model, equation functions are used. This function defines linear multi-point constraints to transmit boundary condition and loads to the beam (this means linear deformation for each part of the cross section). The following figure shows a case which allows free warping and case which prevents warping for occurring:

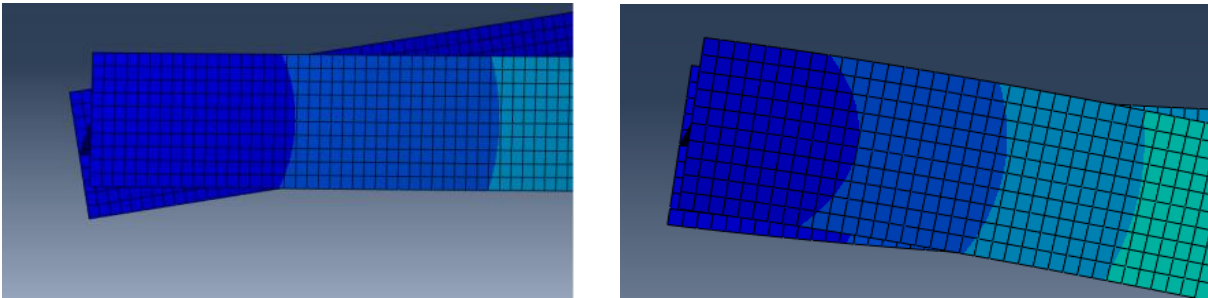


Figure 96 : *left*) free warping; *right*) prevention of warping

The bending moment is applied by a couple of forces. Forces are applied on the middle of upper and bottom flanges, see Figure 97, with an increasing magnitude depending on time increments. There are other loading schemes for cases where load is applied to each node of the upper or bottom flange centre along the beam length, see Figure 98, (for cross-section 1000x7+300x12 only):

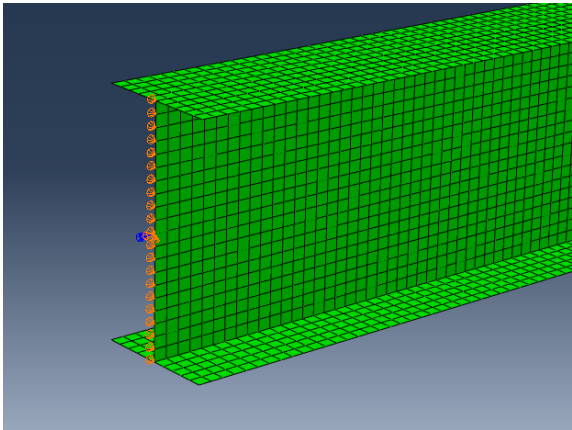


Figure 97 : Load application (for cases loaded by end bending moment)

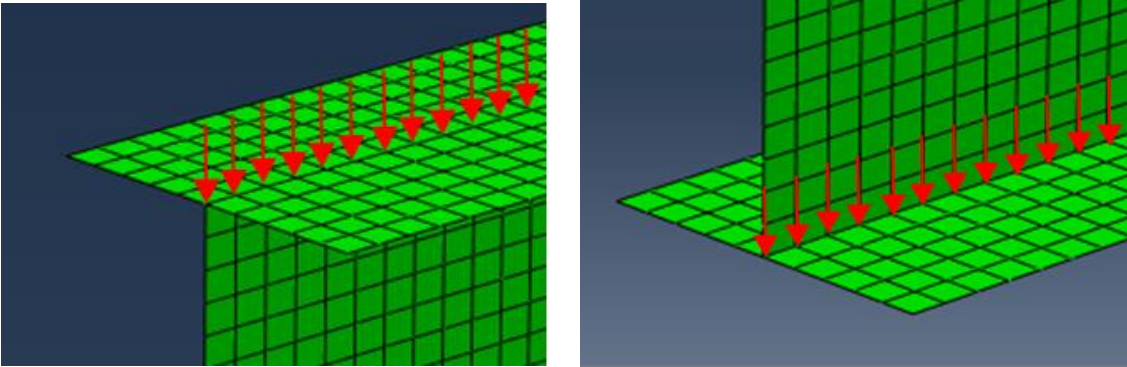


Figure 98 : *left*) load applied at the compression flange; *right*) load applied at the tension flange - to each node along the longitudinal axis of the flange centroid

In ABAQUS model, ten elements for flange width and twenty elements for web height are used. Along the beam, 25 mm element length are used, see Figure 99:

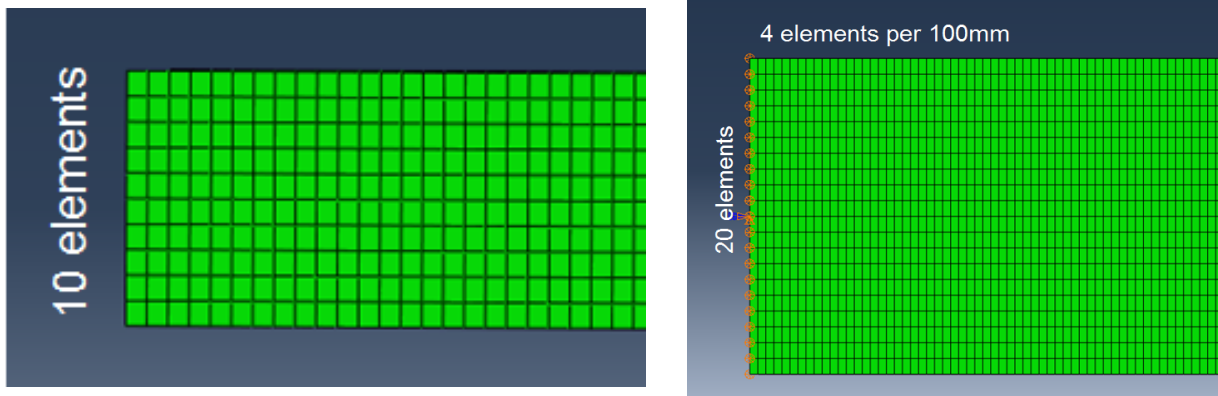


Figure 99 : Number of elements on beam

For the case of welded cross-sections sections, the residual stresses are modelled without the gradient unlike the original stresses distribution as shown in Figure 64. This is due to the mesh coarseness compared to the real residual stress pattern. The current residual stress distribution is illustrated in Figure 100:

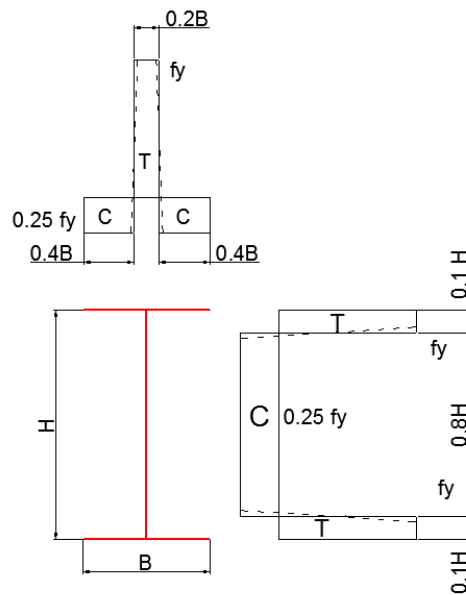


Figure 100 : Current residual stress distribution

2.2.2 Detailed results of the parametric study and comparisons with current EC3 design rules

The results of the numerical parametric study were compared with current design rules of EN 1993-1-2. The formulae are presented here after. For the correctness of the comparison it was aimed to eliminate all possible unknown variables in the calculation, except the lateral torsional buckling behaviour. Therefore, the resistance of the cross-section for each temperature is determined in ABAQUS and in SAFIR. Non-dimensional slenderness for lateral torsional buckling is given:

$$\lambda_{LT,\theta} = \sqrt{\frac{M_{fi,\theta,Rd}}{M_{Cr}}} \times \sqrt{\frac{1}{k_{E,\theta}}} \quad (12)$$

With:

$M_{Rd,\theta}$ is the resistance of cross-section at temperature θ determined in ABAQUS and in SAFIR, M_{cr} is the elastic critical moment at room temperature obtained from the finite element method with ABAQUS and CASTEM and $k_{E,\theta}$ is the reduction factor (relative to E) for the slope of the linear elastic range.

The value of $\chi_{LT,\theta}$ is determined according to the following equations:

$$\chi_{LT,\theta} = \frac{1}{\phi_{LT,\theta} + \sqrt{[\phi_{LT,\theta}]^2 - [\lambda_{LT,\theta}]^2}} \quad (13)$$

With:

$$\phi_{LT,\theta} = 0.5[1 + \alpha \times \bar{\lambda}_{LT,\theta} + (\bar{\lambda}_{LT,\theta})^2] \quad (14)$$

And

$$\alpha = 0,65 \times \sqrt{235/f_y} \quad (15)$$

The lateral torsional buckling resistance moment in the fire design situation is finally obtained with the following formula:

$$M_{b,Rd,\theta} = \chi_{LT,\theta} \times M_{fi,\theta,Rd} \quad (16)$$

2.2.2.1 Comparisons of the numerical results with the current design rules of EN 1993-1-2

The comparisons between numerical results and current EN 1993-1-2 design rule for all the conducted numerical simulations with SAFIR and ABAQUS are shown in the following diagrams, Figure 101 and Figure 102. The numerical parametric study represents a total of about 3700 finite element calculations. In these simulations, the beams are loaded with uniform bending diagram, triangular bending diagram, and bi-triangular bending diagram or with uniform distributed load and both ends of the beams are simply supported. The following diagram illustrates the results for S355 steel grade:

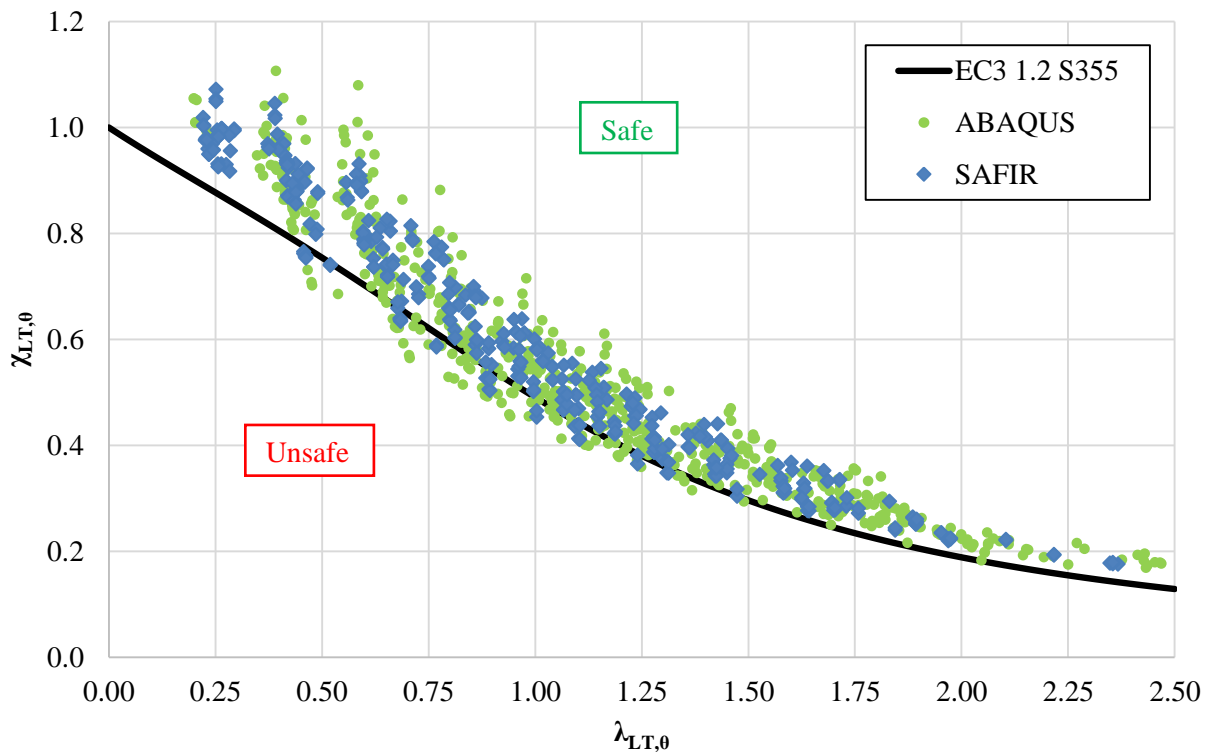


Figure 101: Comparison between FEM LTB curve and LTB curve from EN 1993-1-2 for S355 steel grade

The following diagram illustrates the results for S460 steel grade:

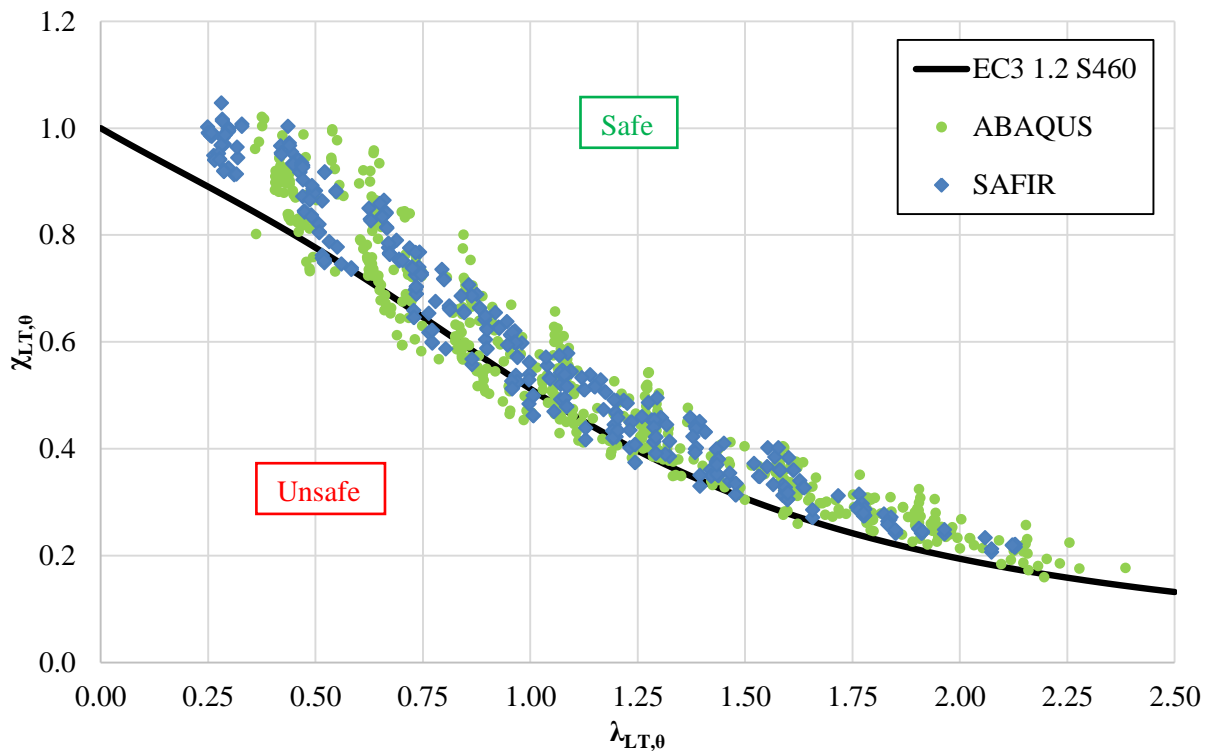


Figure 102: Comparison between FEM LTB curve and LTB curve from EN 1993-1-2 for S460 steel grade

Previous results for both S355 and S460 steel grades are summarized in the following chart. The ratio of the lateral torsional buckling moment resistance, which is obtained from ABAQUS and SAFIR ($M_{b,FEM}$) and lateral torsional buckling moment resistance calculated according to EN 1993-1-2 as described above, is illustrated. It appears that the current EN 1993-1-2 design rules for lateral torsional buckling is really safe. But it also shows that it can lead to an un-economical design of beams subjected to this type of loading, regardless of the slenderness:

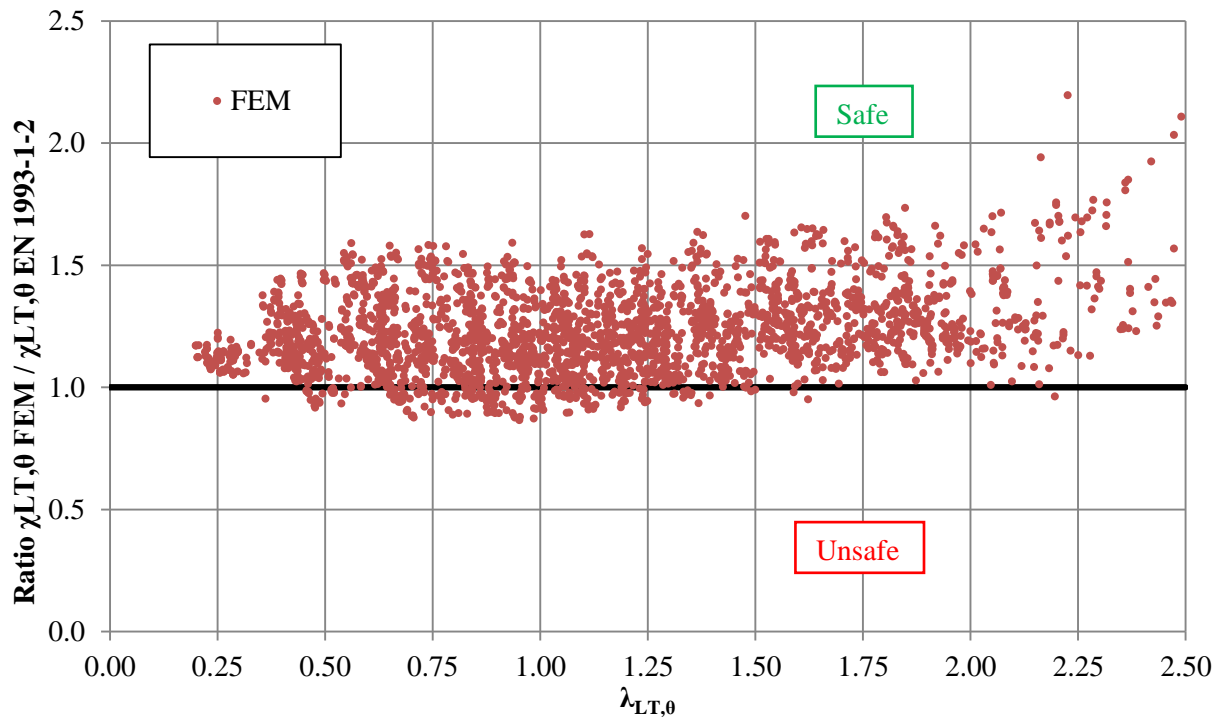


Figure 103: Comparison between results of the parametric study and the current design rules (EN 1993-1-2) for both S355 and S460

About 47% of the 3700 simulations are situated on the safe side by more than 15%. This really shows the non-economical design which can be undertaken by using current EN 1993-1-2 to deal with lateral torsional buckling. That is why it was proposed to improve the design rule mainly in term of accuracy.

The influence of several parameters was checked in the comparisons. The residual stress pattern, the applied temperature and the width to depth ratio (h/b) almost does not influence the lateral torsional buckling response of the beams. However, the cross-section slenderness clearly influences this response. The ratio between the effective section modulus on the elastic section modulus was precisely investigated. It showed a distribution of the results according to the cross-section slenderness. The proposed limits are listed in the following table:

Curve	Limits (ratio $s=$)
L1	$W_{eff,y}/W_{el,y} > 0.9$
L2	$0.8 < W_{eff,y}/W_{el,y} \leq 0.9$
L3	$W_{eff,y}/W_{el,y} \leq 0.8$

Table 33: Slenderness limits

The following chart illustrates for the uniform bending moment distribution load and for S355 steel grade the evolution of $\chi_{LT,0}$ in function of the slenderness according to the three defined ranges:

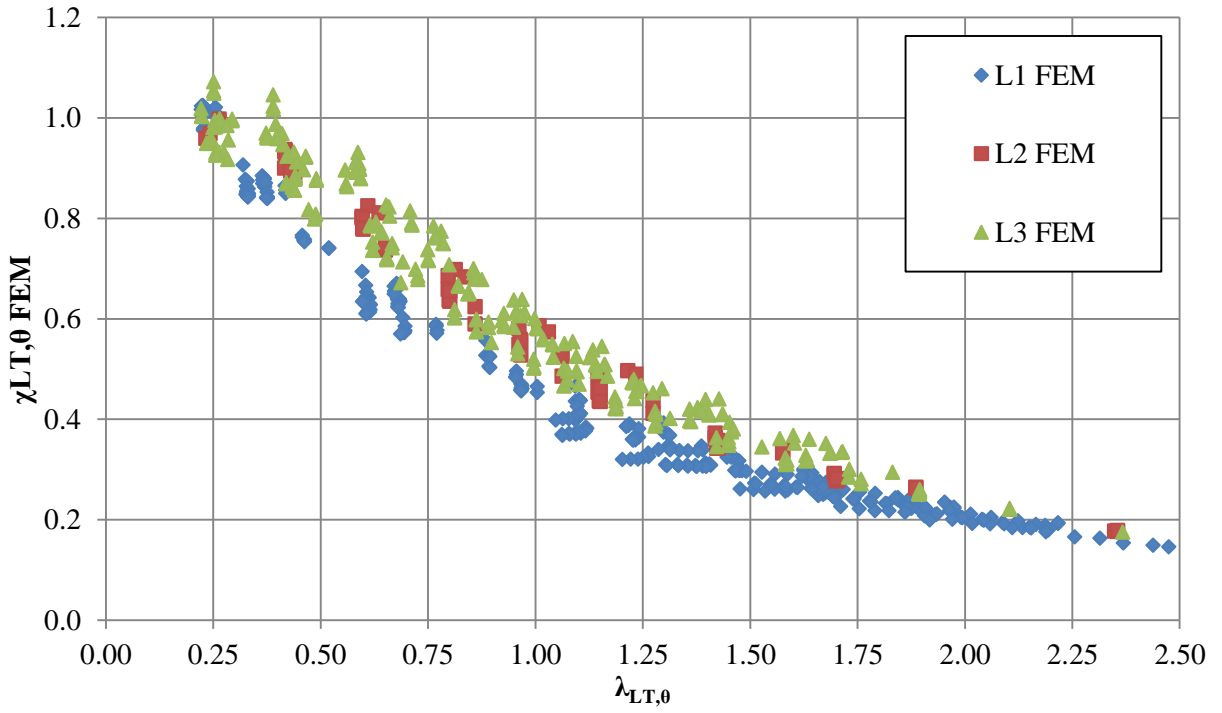


Figure 104: Distribution of χ_{LT} with the separation according to the defined cross-section slenderness ranges

2.2.2.2 New proposal for lateral torsional buckling of class 4 beam

As shown in Table 33 and in Figure 104, a new imperfection factor, which takes into account the influence of cross-section slenderness by means of factor $s = W_{eff,y}/W_{el,y}$ (effective section factor), is proposed. The lateral-torsional buckling resistance moment in the fire design situation is to be determined as proposed in the following equations:

$$M_{b,Rd,\theta,NEW} = \chi_{LT,\theta,NEW} \times W_{eff,y, \min} \times f_y \times k_{y,\theta} / \gamma_{M,\theta} \quad (17)$$

Non-dimensional slenderness for lateral torsional buckling is given by:

$$\bar{\lambda}_{LT,\theta} = \bar{\lambda}_{LT} \times \sqrt{k_{y,\theta}/k_{E,\theta}} \quad (18)$$

With

$$\bar{\lambda}_{LT} = \sqrt{W_{eff,y, \min} \times f_y / M_{cr}} \quad (19)$$

The value of $\chi_{LT,\theta,NEW}$ is determined according to the following equation:

$$\chi_{LT,\theta,NEW} = \frac{1/f}{\phi_{LT,\theta} + \sqrt{\phi_{LT,\theta}^2 - \bar{\lambda}_{LT,\theta}^2}} \quad (20)$$

With

$$\phi_{LT,\theta} = 0.5 \times (1 + \alpha_{LT} \times [\bar{\lambda}_{LT,\theta} - 0.2] + \bar{\lambda}_{LT,\theta}^2) \quad (21)$$

The value of the imperfection factor α_{LT} now depends on the limit of cross-sectional slenderness and is taken from the following table:

Curve	Limits (ratio $s=$)	α_{LT}
L1	$W_{eff,y}/W_{el,y} > 0.9$	1.25ε
L2	$0.8 < W_{eff,y}/W_{el,y} \leq 0.9$	1.00ε
L3	$W_{eff,y}/W_{el,y} \leq 0.8$	0.75ε

Table 34: Imperfection factor α_{LT}

Factor f should be used in accordance with the approval of the Evolution Group. Therefore, factor f depends on the loading type and is defined for class 4 cross-sections in the following equation:

$$f = 1 - 0.5 \times (1 - k_c) \geq 0.8 \quad (22)$$

With k_c defined as a correction factor defined in the following table:

Moment distribution	k_c
<div style="display: flex; justify-content: space-between;"> M ψM </div>  <p style="text-align: center;">$-1 \leq \psi \leq 1$</p>	$0.6 + 0.3 \times \psi + 0.15 \times \psi^2$ but $k_c \leq 1$
	0.91
	0.90
	0.91
	0.79
	0.73
	0.75

Table 35: Correction factors k_c to be used for factor f

In the following comparisons between finite element results and new proposed simple design rule, the expression $W_{eff,y, \min} f_y k_{y,\theta}$ was replaced by $M_{Rd,\theta}$ (resistance of the cross-section determined in ABAQUS and in SAFIR, for each temperature) and to remain consistent the $W_{el,y}$ was replaced M_{el} .

The following diagrams show the comparisons between the modified approach and all constant cross-section beam simulations, for all investigated temperatures and for both S355 and S460 steel grades. In these simulations, the beams are loaded with uniform bending diagram and both ends of the beams are simply supported. The choice of only using uniform bending diagram moment allowed the comparison of the new design curve with the numerical simulations. The following diagram illustrates the results for S355 steel grade:

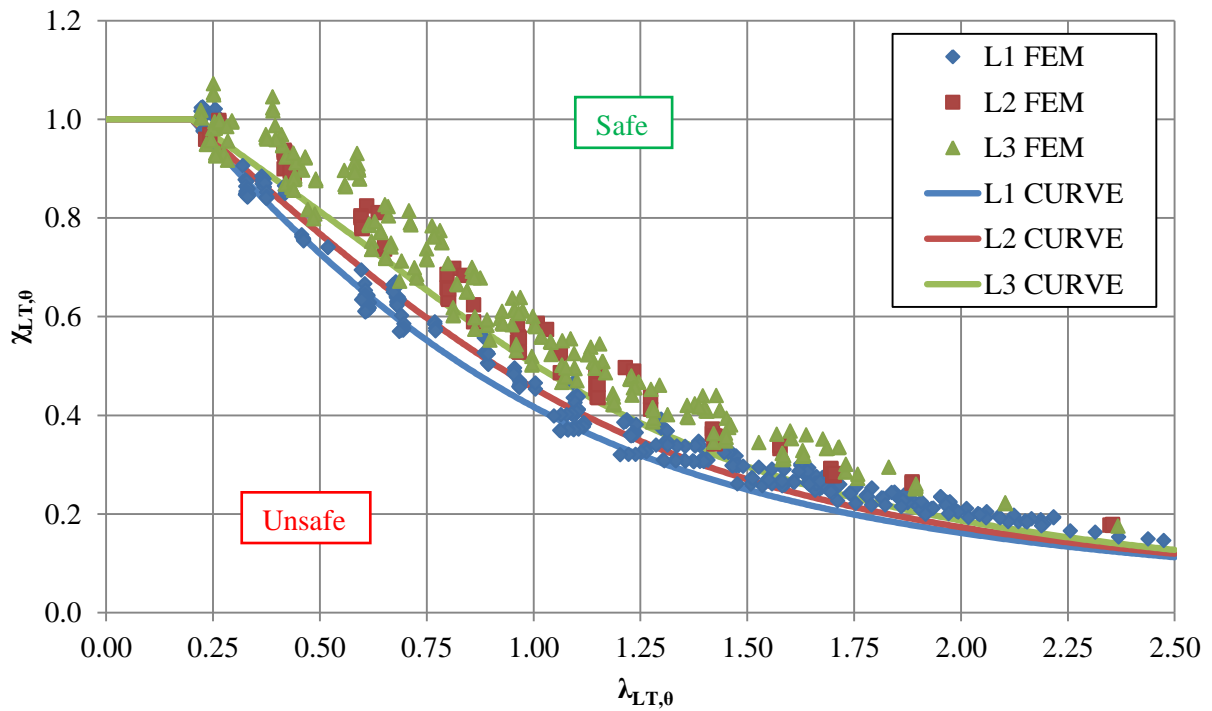


Figure 105: Comparison between the results of the parametric study and the new proposed design procedure for steel S355

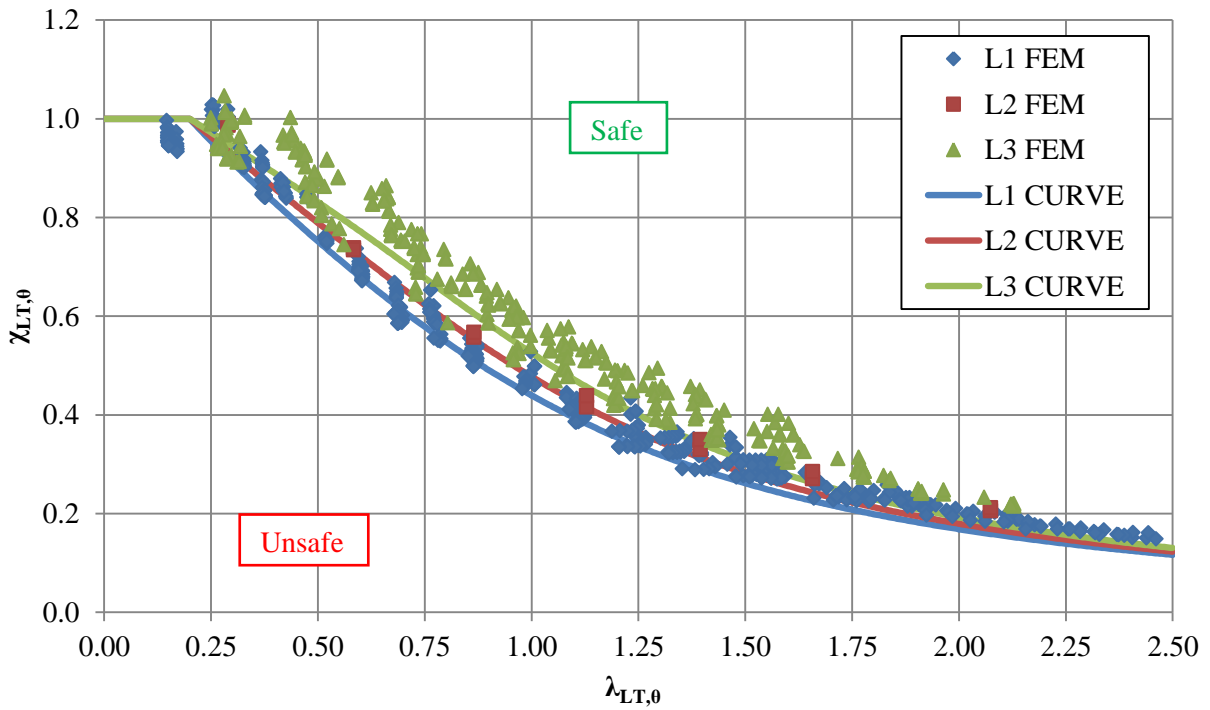


Figure 106: Comparison between the results of the parametric study and the new proposed design procedure for steel S460

All numerical results for both S355 and S460 steel grades are summarized in the following chart. The ratio of the lateral torsional buckling moment resistance, which is obtained from ABAQUS and SAFIR ($M_{b,FEM}$) and lateral torsional buckling moment resistance calculated according to new proposed design rule as described above, is illustrated:

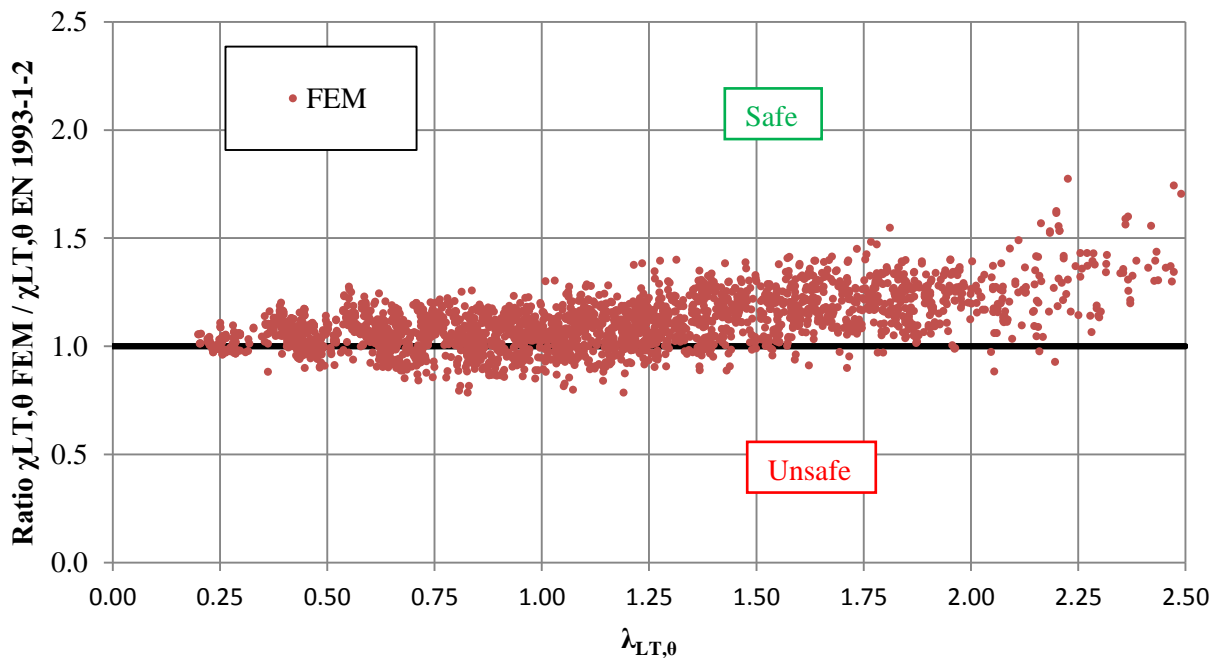


Figure 107: Comparison between the results of the parametric study and the proposed design procedure for both steel grades S355 and S460

The statistical data of the comparisons between the numerical results and the EN 1993-1-2 and between the numerical results and the new proposed design rules are given in the following table:

	EN 1993-1-2	NEW DESIGN RULES
Average ratio (design rule / FEM)	0.86	0.90
Percentage of unsafe points (%)	15.51	15.46
Percentage of safe points by more than 15% (%)	46.84	26.92

Table 36: Statistical data for the $M_{b,FEM}/M_{b,NEW}$

It is noticeable that the average ratio is improved by about 4% in the design rules compared to the EN 1993-1-2 current design curve. The most important change is for points considered as too safe points, i.e. un-economic points. Almost half of the EN 1993-1-2 design points are lower by more than 15% than the numerical simulations. This number of un-economic points decreases at less than 27% with the new design rules, while remaining in agreement with the safety ratios.

The validity of the new proposal in various cases was checked. The beams were loaded by different moment distributions and both ends of the beams are still simply supported. For these beams, other than uniform moment distribution was considered. The factor f according to the Evolution group for EN 1993-1-2 proposal in fire situation was taken into account (see previous definition). This factor is based on publication of Lopes at al.: *Numerical analysis of stainless steel beam-columns in case of fire* [4] **Erreur ! Source du renvoi introuvable.** The lower bound 0.8 of the factor f for Class 4 cross-sections was used.

The following diagrams Figure 108 to Figure 113, show numerical simulations at all defined temperatures compared with updated design method including factor f . In these simulations, the beams are loaded by non-uniform bending moment. The following figures illustrate the comparisons between the new simple design rule and the simulations for triangular bending moment and different curves from L1 to L3:

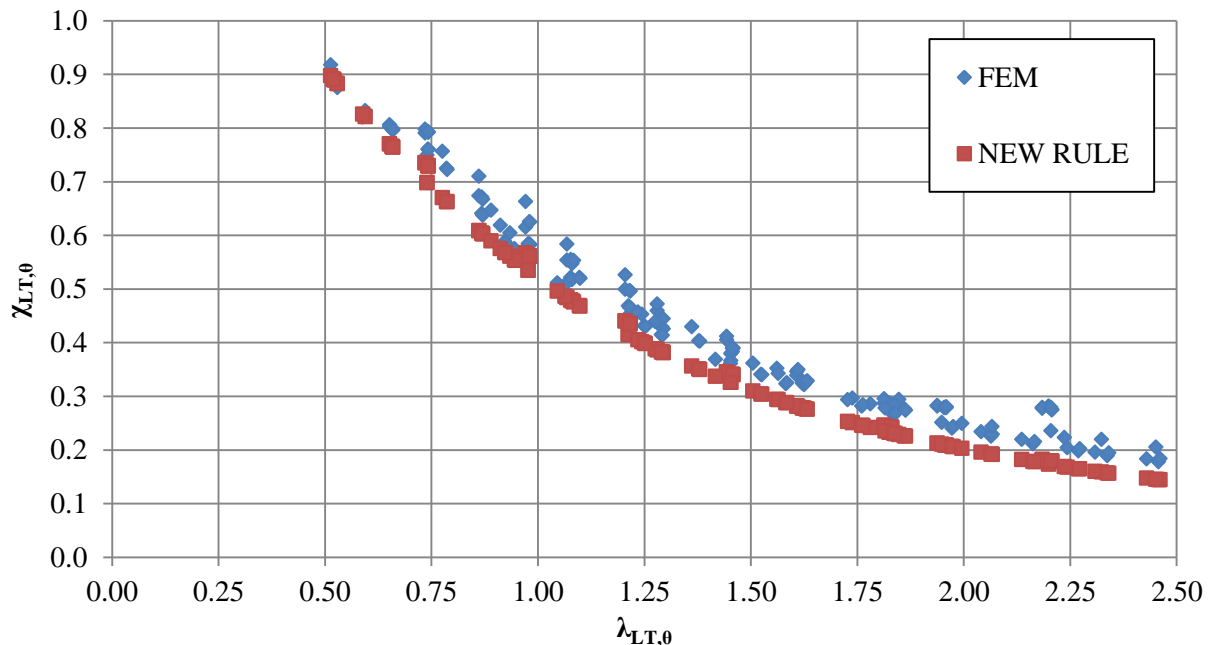


Figure 108: Comparison between the results of the parametric study and the new proposed design procedure for triangular bending moment and curve L1

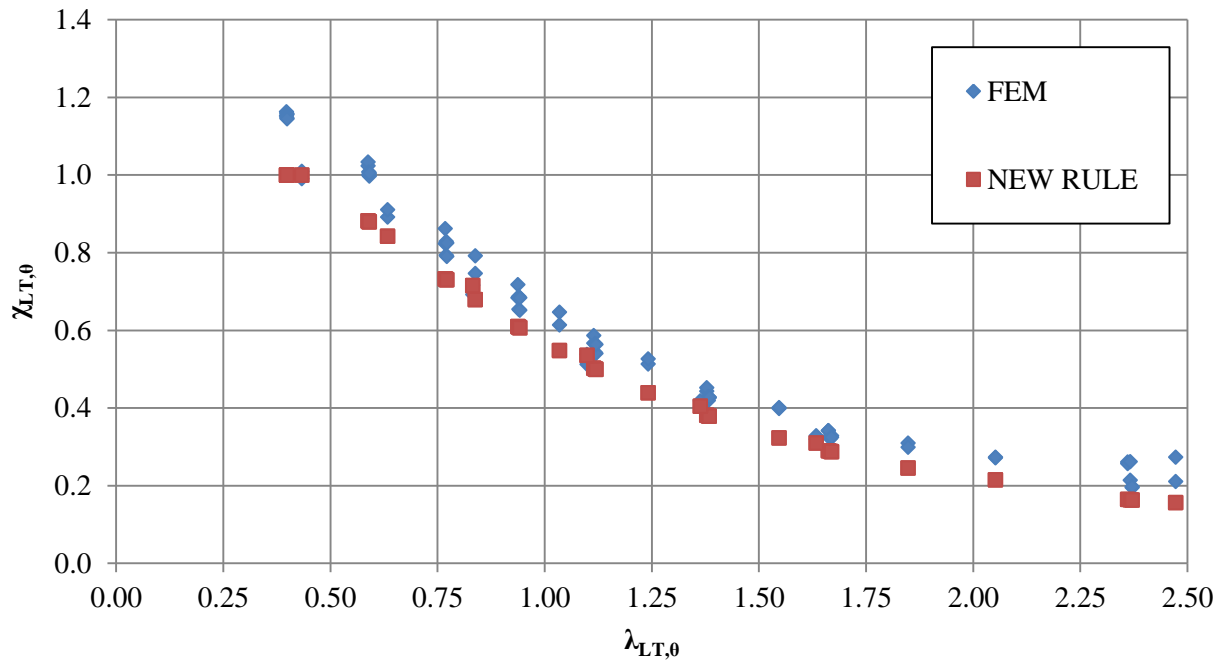


Figure 109: Comparison between the results of the parametric study and the new proposed design procedure for triangular bending moment and curve L2

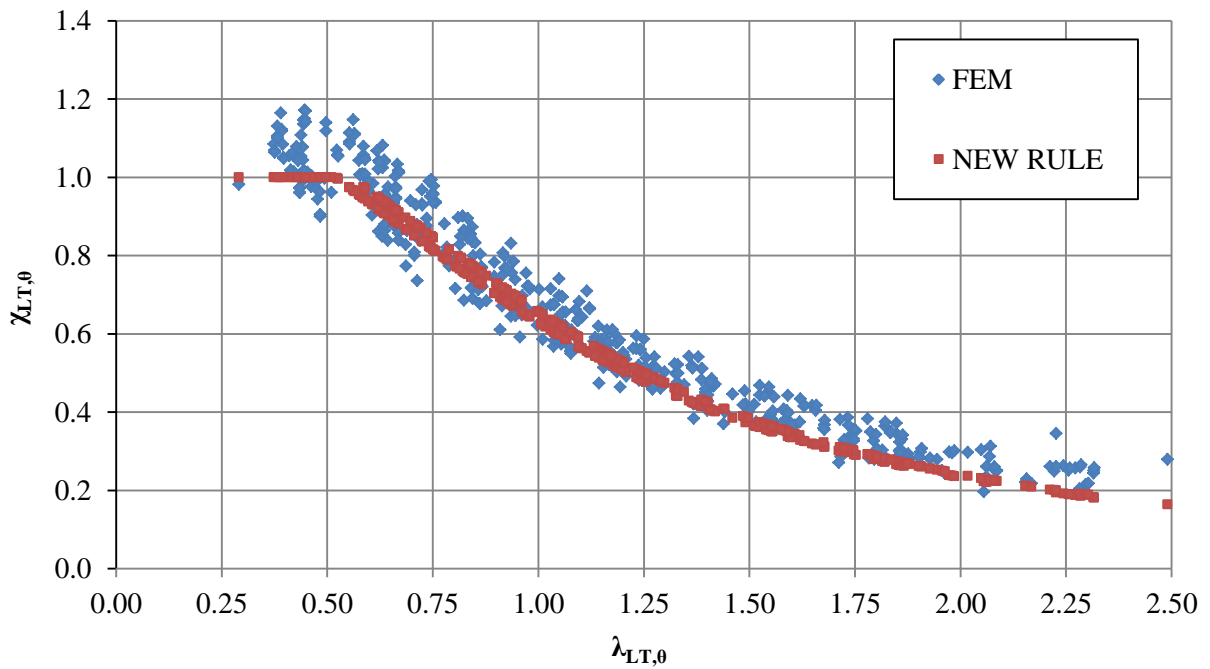


Figure 110: Comparison between the results of the parametric study and the new proposed design procedure for triangular bending moment and curve L3

The following figures illustrate the comparisons between the new simple design rule and the simulations for bi-triangular bending moment and different curves from L1 to L3:

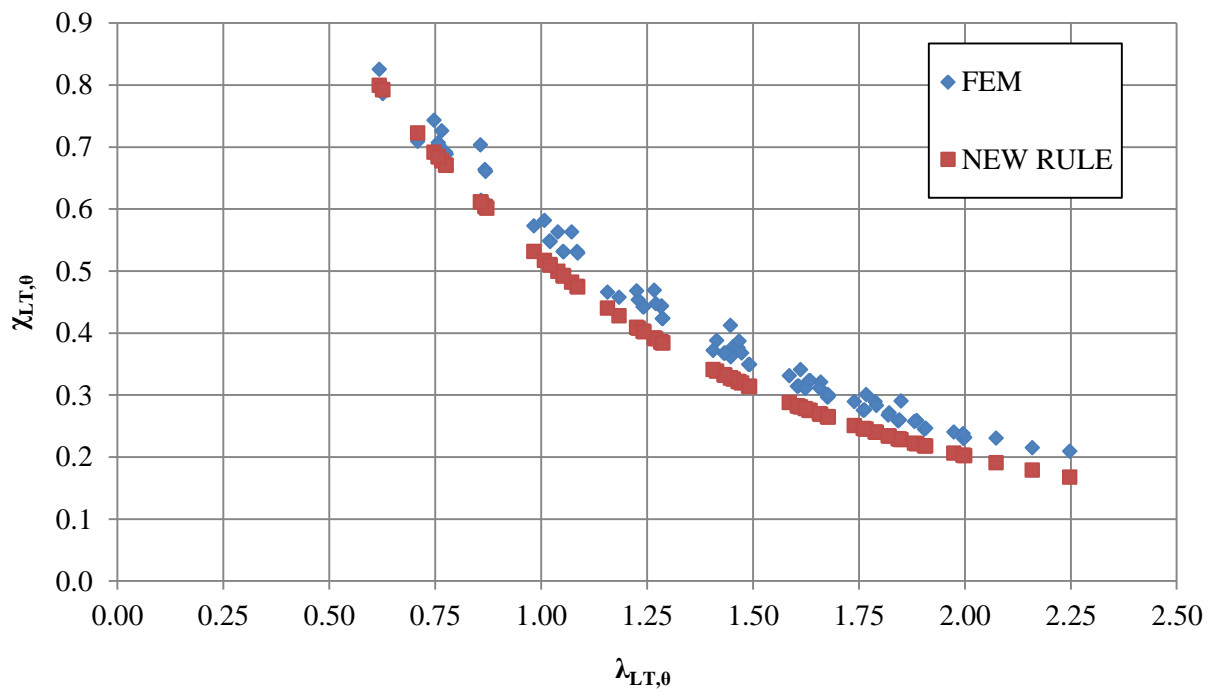


Figure 111: Comparison between the results of the parametric study and the new proposed design procedure for bi-triangular bending moment and curve L1

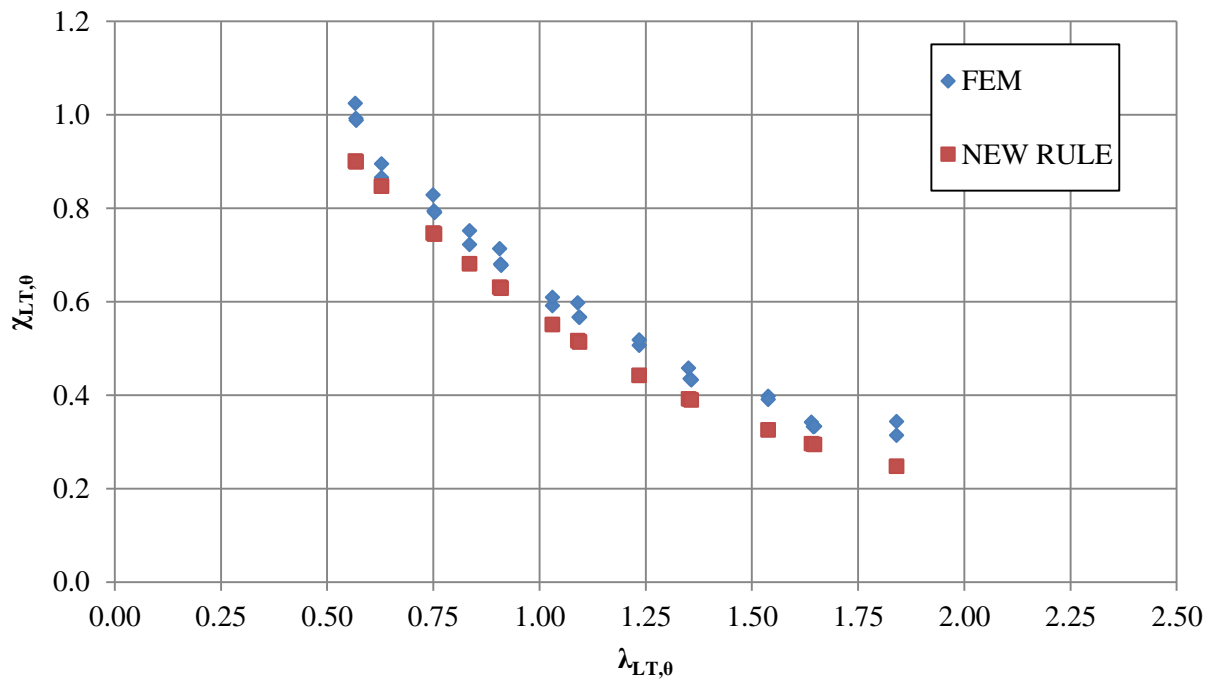


Figure 112: Comparison between the results of the parametric study and the new proposed design procedure for bi-triangular bending moment and curve L2

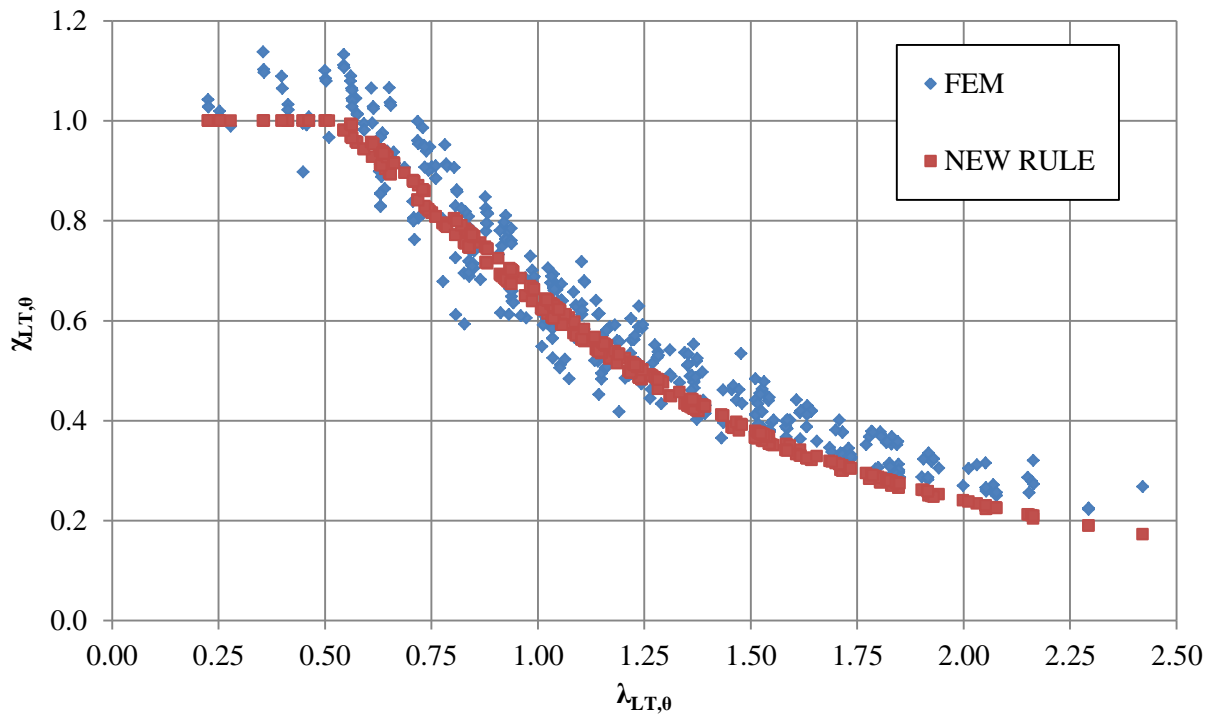


Figure 113: Comparison between the results of the parametric study and the new proposed design procedure for bi-triangular bending moment and curve L3

Tapered members are also investigated and numerical results are confronted with the new design rule taking. In these cases, the used method to evaluate the elastic moment resistant to define the L curve is the following:

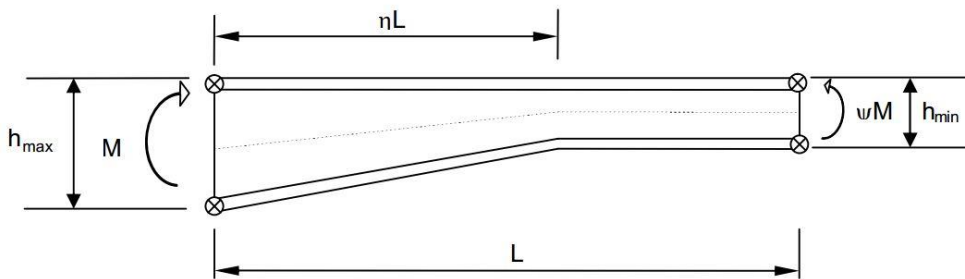


Figure 114: Scheme of general tapered member

The equation to obtain equivalent depth of the web is given with the following equation:

$$h_{eq} = h_{min} \times \left(1 - \eta + \frac{\eta^\gamma}{2} \times \left[1 + \frac{h_{max}}{h_{min}} \right] \right) \quad (23)$$

With:

$$\gamma = 1 + 0.25 \times \left(\frac{h_{max}}{h_{min}} - 1 \right) \quad (24)$$

This method is taken from the paper: *Déversement des barres à section en I bissymétrique et hauteur d'âme linéairement variable* by Y. GALEA in *Revue Construction Métallique* – 1986 [5].

The following chart illustrates the ratio between the numerical lateral torsional buckling resistance and the lateral torsional buckling resistance obtained with the new simple design rule:

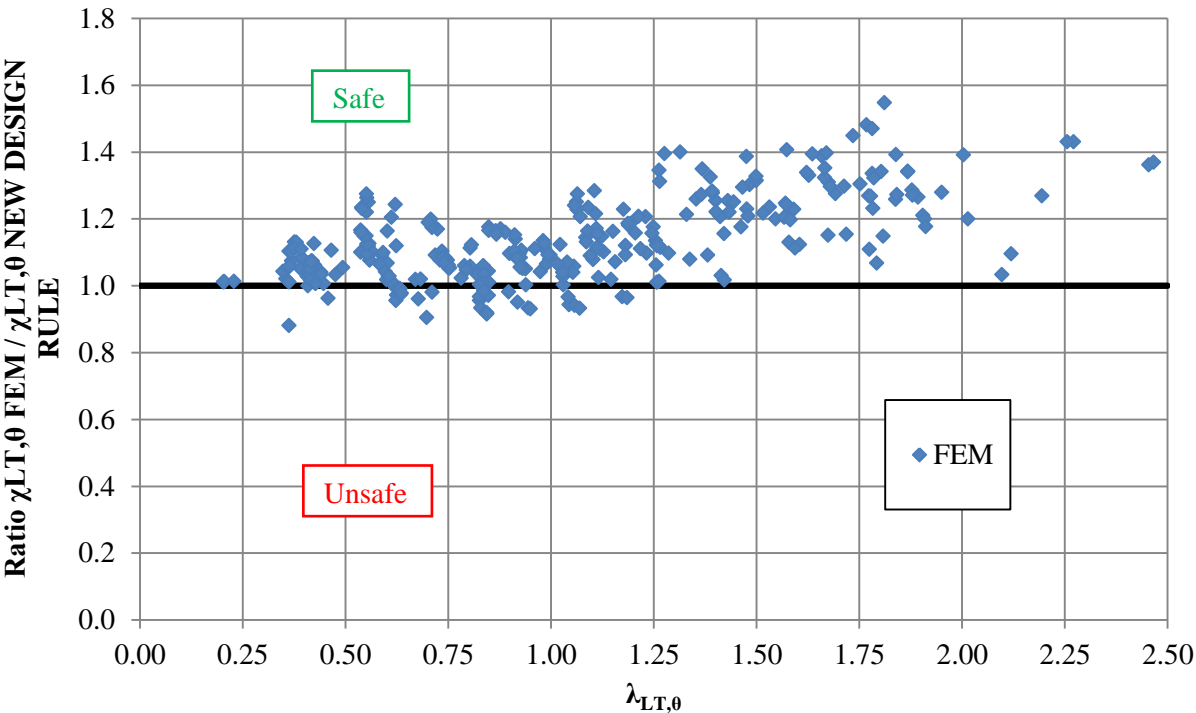


Figure 115: Tapered beams; comparison between numerical results and new design rule

Based on the numerical results, a modified approach for laterally unrestrained beam of class 4 is proposed and gives more consistent results. Different bending moment distributions are investigated in fire situation as it is described in previous chapters. It is demonstrated that the use of the developed simple design rules for constant cross-section is possible for tapered member as well.

3 Application examples

3.1 Cross-sectional resistance of a beam subjected to pure bending following new design rule

A beam subjected to a uniform bending diagram is considered heated up to 500 °C. It is S355 steel grade. It is also assumed that lateral torsional buckling is not allowed. The aim of this example is to evaluate the cross-sectional resistance of this beam following the new developed simple design rules. The dimensions of the cross-section are listed here after:

$$h = 1036 \text{ mm}$$

$$t_w = 6 \text{ mm}$$

$$b = 300 \text{ mm}$$

$$t_f = 18 \text{ mm}$$

Root fillet is assumed to be equal to zero

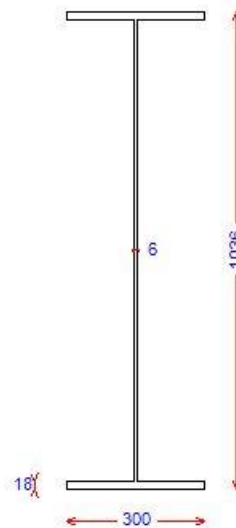


Figure 116: Dimensions of the cross-section

3.1.1 Classification of the cross-section

The following geometrical characteristics of the welded profile are relevant for the classification of the cross-section:

$$c_f = b/2 - t_w/2 = 147 \text{ mm (flange)}$$

$$c_w = h - 2t_f = 1000 \text{ mm (web)}$$

As steel grade is S355:

$$\varepsilon_\theta = 0.85\varepsilon = 0.85 \sqrt{235/f_y} = 0.692 \text{ (the class of the section is evaluated in case of fire)}$$

The class of the web, which is the internal compression part of the beam in bending about major axis is evaluated, see Figure 117:

$$c_w/t_w = 1000/6 = 166.67 > 124\varepsilon_\theta = 85.81 \rightarrow \text{Class 4 web}$$

Internal compression parts						
				Axis of bending		
				Axis of bending		
Class	Part subject to bending	Part subject to compression	Part subject to bending and compression			
Stress distribution in parts (compression positive)						
1	$c/t \leq 72\epsilon$	$c/t \leq 33\epsilon$	when $\alpha > 0,5$: $c/t \leq \frac{396\epsilon}{13\alpha - 1}$ when $\alpha \leq 0,5$: $c/t \leq \frac{36\epsilon}{\alpha}$			
2	$c/t \leq 83\epsilon$	$c/t \leq 38\epsilon$	when $\alpha > 0,5$: $c/t \leq \frac{456\epsilon}{13\alpha - 1}$ when $\alpha \leq 0,5$: $c/t \leq \frac{41,5\epsilon}{\alpha}$			
Stress distribution in parts (compression positive)						
3	$c/t \leq 124\epsilon$	$c/t \leq 42\epsilon$	when $\psi > -1$: $c/t \leq \frac{42\epsilon}{0,67 + 0,33\psi}$ when $\psi \leq -1$: $c/t \leq 62\epsilon(1 - \psi)\sqrt{-\psi}$			
$\epsilon = \sqrt{235/f_y}$	f_y	235	275	355	420	460
	ϵ	1,00	0,92	0,81	0,75	0,71

Figure 117: Classification ranges of internal compression part

The class of the compressive flange, which is the out-stand compression part of the beam in bending about major axis, is evaluated, see Figure 118:

$$c_f/t_f = 147/18 = 8.17 < 14\varepsilon_\theta = 9.69$$

→ Class 3 flange

$$c_f/t_f = 147/18 = 8.17 > 10\varepsilon_\theta = 6.92$$

Outstand flanges						
		Rolled sections		Welded sections		
Class	Part subject to compression	Part subject to bending and compression				
		Tip in compression		Tip in tension		
Stress distribution in parts (compression positive)						
1	$c/t \leq 9\varepsilon$	$c/t \leq \frac{9\varepsilon}{\alpha}$	$c/t \leq \frac{9\varepsilon}{\alpha\sqrt{\alpha}}$	$c/t \leq \frac{9\varepsilon}{\alpha\sqrt{\alpha}}$	$c/t \leq \frac{9\varepsilon}{\alpha\sqrt{\alpha}}$	$c/t \leq \frac{9\varepsilon}{\alpha\sqrt{\alpha}}$
2	$c/t \leq 10\varepsilon$	$c/t \leq \frac{10\varepsilon}{\alpha}$	$c/t \leq \frac{10\varepsilon}{\alpha\sqrt{\alpha}}$	$c/t \leq \frac{10\varepsilon}{\alpha\sqrt{\alpha}}$	$c/t \leq \frac{10\varepsilon}{\alpha\sqrt{\alpha}}$	$c/t \leq \frac{10\varepsilon}{\alpha\sqrt{\alpha}}$
Stress distribution in parts (compression positive)						
3	$c/t \leq 14\varepsilon$	$c/t \leq 21\varepsilon\sqrt{k_\sigma}$ For k_σ see EN 1993-1-5				
$\varepsilon = \sqrt{235/f_y}$	f_y	235	275	355	420	460
	ε	1,00	0,92	0,81	0,75	0,71

Figure 118: Classification ranges of outstand flanges

The cross-section of the welded profile is class 4 in pure bending about strong axis.

3.1.2 Evaluation of the effective section modulus (major axis)

The effective section modulus of the cross-section in bending about major axis is obtained using clause 4.4(3) of EN 1993-1-5: “for flanges elements of I-sections and box girders the stress ratio ψ used in Table 4.1 and Table 4.2 should be based on the properties of the gross-sectional area. For web elements the stress ratio ψ used in Table 4.1 should be obtained using a stress distribution based on the effective area of the compression flange and the gross area of the web”.

Thus, the normalised slenderness is given by:

$$\bar{\lambda}_p = \sqrt{\frac{f_y}{\sigma_{cr}}} = \frac{\bar{b}/t}{28.4 \times \varepsilon \times \sqrt{k_\sigma}}$$

For the flange under consideration:

$$\bar{b} = c_f = 147 \text{ mm}$$

$$t = t_f = 18 \text{ mm}$$

$$\varepsilon = \sqrt{235/f_y} = 0.814$$

This factor is evaluated at room temperature when it comes to the calculation of the non-dimensional slenderness of the plates.

$k_\sigma = 0.43$, see following Figure 119

Stress distribution (compression positive)		Effective ^p width b_{eff}			
		$1 > \psi \geq 0$: $b_{eff} = \rho c$			
		$\psi < 0$: $b_{eff} = \rho b_c = \rho c / (1 - \psi)$			
$\psi = \sigma_2/\sigma_1$	1	0	-1	$1 \geq \psi \geq -3$	
Buckling factor k_σ	0,43	0,57	0,85	$0,57 - 0,21\psi + 0,07\psi^2$	
		$1 > \psi \geq 0$: $b_{eff} = \rho c$			
		$\psi < 0$: $b_{eff} = \rho b_c = \rho c / (1 - \psi)$			
$\psi = \sigma_2/\sigma_1$	1	$1 > \psi > 0$	0	$0 > \psi > -1$	-1
Buckling factor k_σ	0,43	$0,578 / (\psi + 0,34)$	1,70	$1,7 - 5\psi + 17,1\psi^2$	23,8

Figure 119: Buckling factor for outstand compression elements

Then:

$$\bar{\lambda}_p = \frac{147/18}{28.4 \times 0.814 \times \sqrt{0.43}} = 0.539$$

And, according to new design rules:

$$\rho = \frac{\left(\bar{\lambda}_p + 1.1 - \frac{0.52}{\varepsilon}\right)^{1.2} - 0.188}{\left(\bar{\lambda}_p + 1.1 - \frac{0.52}{\varepsilon}\right)^{2.4}} = 0.812$$

So that the effective width of the flange, b_{eff} , is:

$$b_{eff} = \rho c_f = 0.812 \times 147 = 119.34 \text{ mm}$$

Finally, the total effective width of flange to take account for is the following:

$$b_t = 2b_{eff} + t_w = 2 \times 119.34 + 6 = 244.69 \text{ mm}$$

Considering the effective area of the flange under compression, it is necessary to evaluate the new position of the centre of gravity and the effective area of the cross-section:

$$A' = A - [(b - b_t) \times t_f] = (2 \times t_f \times b + c_w \times t_w) - [(b - b_t) \times t_f] = 16800 - (300 - 244.69) \times 18$$

$$A' = 15804.39 \text{ mm}^2$$

$$Z'_G = 1/A' \times \left(b \times t_f \times \frac{t_f}{2} + c_w \times t_w \times \frac{h}{2} + b_t \times t_f \times \left[h - \frac{t_f}{2} \right] \right)$$

$$Z'_G = 485.94 \text{ mm}$$

With these new coordinates for the centre of gravity, the stress ratio is evaluated for the web, with the help of Figure 120:

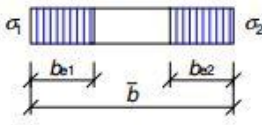
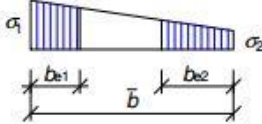
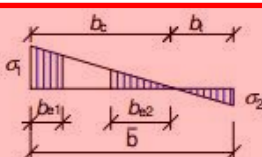
Stress distribution (compression positive)		Effective ^p width b_{eff}				
		$\psi = 1:$ $b_{eff} = \rho \bar{b}$ $b_{e1} = 0,5 b_{eff} \quad b_{e2} = 0,5 b_{eff}$				
		$1 > \psi \geq 0:$ $b_{eff} = \rho \bar{b}$ $b_{e1} = \frac{2}{5 - \psi} b_{eff} \quad b_{e2} = b_{eff} - b_{e1}$				
		$\psi < 0:$ $b_{eff} = \rho b_c = \rho \bar{b} (1 - \psi)$ $b_{e1} = 0,4 b_{eff} \quad b_{e2} = 0,6 b_{eff}$				
$\psi = \sigma_2/\sigma_1$	1	$1 > \psi > 0$	0	$0 > \psi > -1$	-1	$-1 > \psi > -3$
Buckling factor k_σ	4,0	$8,2 / (1,05 + \psi)$	7,81	$7,81 - 6,29\psi + 9,78\psi^2$	23,9	$5,98 (1 - \psi)^2$

Figure 120: Buckling factor for internal compression elements

$$\psi = -\frac{b_t}{b_c} = \frac{Z'_G - t_f}{h - Z'_G} = -0.85$$

$$k_\sigma = 7.81 - 6.29 \times \psi + 9.78 \times \psi^2 = 20.22$$

The web non-dimensional slenderness is:

$$\bar{\lambda}_p = \frac{1000/6}{28.4 \times 0.814 \times \sqrt{20.22}} = 1.60$$

And

$$\rho = \frac{\left(\bar{\lambda}_p + 0.9 - \frac{0.26}{\varepsilon} \right)^{1.5} - 0.055 \times (3 + \psi)}{\left(\bar{\lambda}_p + 0.9 - \frac{0.26}{\varepsilon} \right)^3} = 0.299$$

And the effective width of the web, b_{eff} , is:

$$b_{eff} = \rho \times c_w / (1 - \psi) = 0.299 \times 1000 / (1 - (-0.85)) = 161.62$$

$$b_{e1} = 0.4 \times b_{eff} = 64.65$$

$$b_{e2} = 0.6 \times b_{eff} = 96.97$$

The length of the non-effective area of the web is given by the following equation:

$$b_{ne} = c_w / (1 - \psi) - b_{eff} = c_w / (1 - \psi) - b_{e1} - b_{e2} = 378.92$$

The new position of the centre of gravity and the effective area of the cross-section should be evaluated a second time:

$$A'' = A' - b_{ne} \times t_w = 13530.87$$

$$Z''_G = 1/A'' \times \left(b \times t_f \times \frac{t_f}{2} + b_t \times t_f \times \left[h - \frac{t_f}{2} \right] + c_w \times t_w \times \frac{h}{2} - b_{ne} \times t_w \times \left[h - t_f - b_{e1} - \frac{b_{ne}}{2} \right] \right)$$

$$Z''_G = 439.23$$

The effective area of the cross-section under pure bending is illustrated in the following figure:

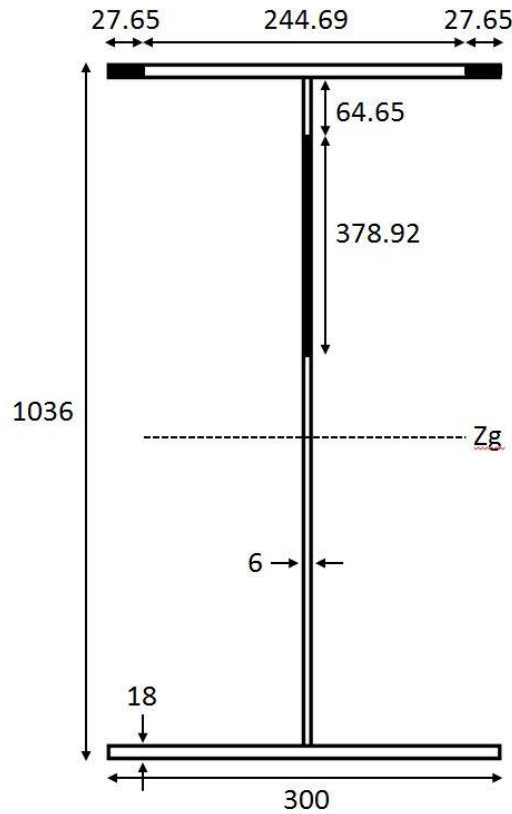


Figure 121: Dimensions and illustration of effective cross-section (mm)

The second moment of inertia of the effective cross-section is given by the following equation:

$$I_{y,eff} = I_{y,eff1} + I_{y,eff2} + I_{y,eff3} + I_{y,eff4}$$

With:

$$I_{y,eff1} = b \times \frac{t_f^3}{12} + b \times t_f \times \left(Z''_G - \frac{t_f}{2} \right)^2$$

$$I_{y,eff2} = b_t \times \frac{t_f^3}{12} + b_t \times t_f \times \left(h - Z''_G - \frac{t_f}{2} \right)^2$$

$$I_{y,eff3} = t_w \times \frac{b_{e1}^3}{12} + t_w \times b_{e1} \times \left(h - Z''_G - t_f - \frac{b_{e1}}{2} \right)^2$$

$$I_{y,eff4} = t_w \times \frac{(h - 2 \times t_f - b_{e1} - b_{ne})^3}{12} + t_w \times (h - 2 \times t_f - b_{e1} - b_{ne}) \times \left(Z''_G - \frac{[t_f + \{h - 2 \times t_f - b_{e1} - b_{ne}\}]}{2} \right)^2$$

Finally:

$$I_{y,eff} = 2800655847 \text{ mm}^4$$

The definition of the effective section modulus is given by the following formula:

$$W_{y,eff,min} = \min \left(\frac{I_{y,eff}}{Z''_G}; \frac{I_{y,eff}}{h - Z''_G} \right) = 4693023.86 \text{ mm}^4$$

The position of the centre of gravity has to be evaluated three times and the calculation of the second moment of inertia is also a bit tedious. The evaluation of the effective properties of a class 3/4 cross-section is a laborious task. This is another key point of the FIDESC4 software which is able to proceed to these calculations.

3.1.3 Calculation of the cross-sectional resistance

The cross-sectional resistance of a beam at high temperature (500°C) is given by the following equation:

$$M_{fi,Rd} = k_{y,\theta} W_{eff} f_y$$

According to Table 3.1 of EN 1993-1-2, the value of k_y at 500°C for carbon steel is the following:

$$k_y = 0.78$$

So that the final cross-section resistance is:

$$M_{fi,Rd} = 0.78 \times 4693023.86 \times 355 = 1299498306.83 \text{ N.mm}$$

As a conclusion:

$$M_{fi,Rd} = 1299.50 \text{ kN.m}$$

3.2 Lateral torsional buckling of a beam subjected to bending

An unrestrained beam subjected to a triangular bending diagram is considered heated up to 500°C. It is S355 steel grade. Lateral restraints are placed in the supports. Warping is not prevented. The aim of this example is to evaluate the lateral torsional buckling resistance of this beam following the new developed simple design rules. The same cross-section as in the previous case was considered. The static scheme is shown here after. The dimensions are those of 3.1:

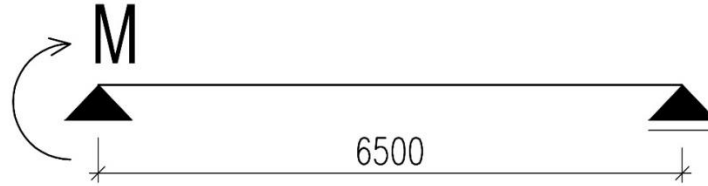


Figure 122: Static scheme

3.2.1 Evaluation of the non-dimensional slenderness

The non-dimensional slenderness for lateral torsional buckling at high temperature (500 °C) is obtained using clause 4.2.3.3(5), equation (4.15) of EN 1993-1-2.

$$\bar{\lambda}_{LT,\theta} = \bar{\lambda}_{LT} [k_{y,\theta} / k_{E,\theta}]^{0.5}$$

The non-dimensional slenderness for lateral torsional buckling at room temperature is obtained using clause 6.3.2.2(1) of EN 1993-1-1.

$$\bar{\lambda}_{LT} = \sqrt{\frac{W_{y,eff} f_y}{M_{cr}}} = \sqrt{\frac{4693023.86 \times 355}{3936600000}} = 0.65$$

The elastic critical moment $M_{cr} = 3936.6$ kNm was obtained from LTBeam program. Boundary conditions at both ends were set: Kv and $K\theta$ were fixed (lateral and torsional restraint); Kv' and $K\theta'$ were free (weak axis rotation and warping free).

According to Table 3.1 of EN 1993-1-2, the value of $k_{y,\theta}$ and $k_{E,\theta}$ at 500°C for carbon steel is the following:

$$k_{y,\theta} = 0.78; k_{E,\theta} = 0.60$$

So that the slenderness is equal to:

$$\bar{\lambda}_{LT,\theta} = 0.65 \times [0.78/0.60]^{0.5} = 0.74$$

3.2.2 Calculation of the reduction factor for LTB

The reduction factor for lateral-torsional buckling in the fire design situation is given by:

$$\chi_{LT,fi} = \frac{1/f}{\phi_{LT,\theta} + \sqrt{\phi_{LT,\theta}^2 - \lambda_{LT,\theta}^2}}$$

With (according to new proposed design rules):

$$\phi_{LT,\theta} = 0.5 \times (1 + \alpha_{LT} \times (\bar{\lambda}_{LT,\theta} - 0.2)) + \bar{\lambda}_{LT,\theta}^2$$

$$\phi_{LT,\theta} = 0.5 \times (1 + 0.69 \times (0.74 - 0.2) + 0.74^2) = 0.96$$

The imperfection factor α_{LT} depends on effective section factor (s), see Table 21:

$$s = \frac{W_{y,eff}}{W_{y,el}} = \frac{4693023.86}{6367502.70} = 0.73$$

Then:

$$\alpha_{LT} = 0.75 \times \varepsilon = 0.75 \times \sqrt{\frac{235}{355}} = 0.61$$

So that the reduction factor for lateral-torsional buckling in the fire design situation equal to:

$$\chi_{LT,fi} = \frac{1/f}{0.96 + \sqrt{0.96^2 - 0.74^2}}$$

For taking into account the moment distribution between the lateral restraints of the beam, the evaluation of the factor f is necessary:

$$\chi_{LT,fi,mod} \leq 1.0 \text{ and } \chi_{LT,fi} \leq \frac{1}{\lambda_{LT}^2}$$

with

$$f = 1 - 0.5 \times (1 - k_c) \text{ but } f \geq 0.8$$

With k_c is a correction factor according to Table 35.

Then:

$$k_c = 0.6 + 0.3 \times 0.0 + 0.15 \times 0.0^2 = 0.6$$

$$f = 1 - 0.5 \times (1 - 0.6) = 0.80$$

3.2.3 Evaluation of the lateral torsional buckling resistance

Finally:

$$\chi_{LT,fi} = \frac{1/0.8}{0.96 + \sqrt{0.96^2 - 0.74^2}} = 0.7954$$

The lateral torsional buckling resistance moment of a beam at elevated temperature (500°C) is given by the following equation:

$$M_{b,fi,Rd} = \chi_{LT,fi} k_{y,\theta} W_{y,eff} f_y = 0.7954 \times 0.78 \times 4693023.86 \times 355 = 1033620953 \text{ N.mm}$$

As a conclusion:

$$M_{b,fi,Rd} = 1033.62 \text{ kN.m}$$

4 List of references

- [1] EN 1993-1-2, Eurocode 3, Design of Steel Structures – Part 1-2: General rules Structural fire design, 2005
- [2] EN 1993-1-5, Eurocode 3, Design of Steel Structures – Part 1-5: Plated structural elements, 2006
- [3] C. Couto, P. Vila Real, N. Lopes, B. Zhao; *Effective width method to account for the local buckling of steel thin plates at elevated temperatures*, 2013
- [4] Lopes N., Real P. V., da Silva L. S., Franssen J. M., *Numerical Modelling of Thin Walled Stainless Steel Structural Elements in Case of Fire*, Fire Technology, vol. 46, pp. 91-108, Jan 2010
- [5] Galéa Y.; *Déversement des barres à section en I bissymétrique et hauteur d'âme linéairement variable*, Revue Construction Métallique, 1986